Alma Mater Studiorum – University of Bologna

SCHOOL OF SCIENCE
Department of Industrial Chemistry "Toso Montanari"

Second cycle degree in

Low Carbon Technologies and Sustainable Chemistry

Classe LM-71 - Scienze e Tecnologie della Chimica Industriale

Aqueous Phase Reforming of maltose mediated by bimetallic nanostructured catalysts

Experimental degree thesis

CANDIDATE

Andrea Lucente

SUPERVISOR

Chiar.mo Prof. Nikolaos Dimitratos

CO-SUPERVISOR

Atul Bansode

Stefano Scurti

Michele Offidani

Academic Year 2021-2022

Abstract

Hydrogen is currently derived from nonrenewable natural gas and petroleum, but it could be generated from renewable resources such as biomass or water. Many manufacturing industries, such as breweries, have large waste streams which are mainly conditioned and returned to the environment, in fact, the beer production process generates from three to ten liters of wastewater per liter of beer. In this research the Aqueous Phase Reforming (APR) was studied as an approach to enhance H_2 production from brewery wastewater, where maltose, a disaccharide made of two glucose molecules, constitutes most of the sugar made on the malting stage of the beer production and therefore it is one of the principal components of the wastewater. Aqueous phase reforming (APR) is the catalytic conversion at mild conditions of feedstock with organic compounds (e.g., biomass derived compounds) into valuable gaseous species from which H_2 stands out. This reaction is mainly performed using monometallic and bimetallic catalysts made of nanoparticles. The preparation of metal nanoparticles could be a bit tricky due to the presence of some operating parameters which can modify the quality of the final product; for this reason, it's fundamental to have a good geometry and morphology control of these system and, consequently, that’s why it is the most treated topic in the chemical catalysis to obtain the desired material. In particular, in this research, the sol-immobilization method is used to synthetize nanostructured catalysts having metallic nanoparticles as active site, stabilized by polymers and deposited on a support. Then, the catalyst obtained are tested to perform the Aqueous Phase Reforming of Maltose, to see which one works better for the production of Hydrogen.

Index

1. Introduction

1.1 Nanomaterials

Nanomaterials are nanoscale systems of particular interest because normally, properties like, electrical conductivity or magnetism for bulk amounts do not depend on size but, when the size of a particle falls below a certain limit, 100 nm, these properties become size dependent.[1] The history of nanomaterials begins with the discovery of the electron by J.J. Thomson in 1897. This discovery allowed for an understanding of the nature and properties of materials at the atomic and molecular level. In the 1950s, physicists Richard Feynman and Enrico Fermi suggested the idea of using nanotechnology to build machines and devices on an atomic scale. In the 1980s, chemist Eric Drexler introduced the concept of molecular nanotechnology, which envisioned the construction of molecular machines by assembling atoms and molecules. Meanwhile, physicists had begun discovering new nanoscale materials such as gold, silver, and silica particles.[2]

In the 1990s, carbon-based nanotechnologies such as carbon nanotubes and graphene were discovered, which sparked enormous interest for their mechanical, thermal, and electrical properties. Since then, research on nanomaterials has grown rapidly, leading to the discovery of many other nanoscale materials such as quantum dots, fullerenes, magnetic nanoparticles, and porous nanostructures.

The size difference between nanoscale and bulk materials can confer different chemical and physical properties to the material itself. At the nanoscale level, materials have a high surface area relative to their volume. This means that, for the same mass, a nanoscale material has many more exposed atoms on its surface than a bulk system. This can influence the chemical and physical properties of the material.[3]

---

[1] Emil Roduner, 'Physics And Chemistry Of Nanostructures: Why Nano Is Different', *Size Matters:Why Nanomaterials Are Different*, 2006, 39–336.
[2] https://www.nano.gov/nanotech-101/what/history
[3] 'Nanoparticles_and_their_potential_application_as_a.Pdf', n.d.

For example, the optical properties of nanoscale materials can be different from those of larger materials. The size of nanomaterials can affect the frequency and wavelength of the light that is absorbed or emitted by the material, making the nanomaterial a different color than the bulk material.[4] Additionally, the size of nanomaterials can affect their chemical reactivity and their ability to form bonds with other molecules. Nanomaterials can exhibit high catalytic activity, or the ability to accelerate chemical reactions, due to their high surface area and crystalline structure.[5] In summary, the size of nanomaterials can influence their chemical and physical properties, making them very different from bulk counterpart. However, it is important to note that the properties of nanomaterials also depend on many other factors, such as their composition, shape, crystalline structure, surface area, and purity.

The peculiar properties observed derive from the combination of the *surface effects* and *quantum effects.* For what concerns the surface effect, in general, the surface of an object becomes increasingly important as its size decreases and, in nanoparticles, most atoms reside on their surface. The surface atoms differ from the bulk atoms. For example, a surface atom has unsatisfied bond that make it very reactive it means that the chemical activity of a material increases drastically as its size reaches few nm. The second effect is a quantum-size effect that is the consequence of quantum mechanics and of the particle wave duality.[6] The consequences of these two are that many properties of materials can be tuned by adjusting the particle size. A key example is the one of gold, which is not catalytically active at the surface of the bulk metal, but in the form of nanoparticles gold works well in catalysis.

1.1.1 The surface effect

The reduction in size implies that as the diameter of the material decreases, there is an increase in the ratio between the surface area and volume, resulting in an increase in chemical reactivity. This phenomenon is due to a greater number of atoms on the surface, which show less coordination between metallic nuclei, making them energetically unstable and therefore more likely to react with other substrates. The increase in atoms on the surface generates an increase

[4] K. Lance Kelly et al., 'The Optical Properties of Metal Nanoparticles: The Influence of Size, Shape, and Dielectric Environment', *The Journal of Physical Chemistry B* 107, no. 3 (1 January 2003): 668–77, https://doi.org/10.1021/jp026731y.
[5] L Zhang et al., 'Nanoparticles in Medicine: Therapeutic Applications and Developments', *Clinical Pharmacology & Therapeutics* 83, no. 5 (May 2008): 761–69, https://doi.org/10.1038/sj.clpt.6100400.
[6] Roduner, 'Physics And Chemistry Of Nanostructures: Why Nano Is Different'.

in structural defects, resulting in greater catalytic activity of nanomaterials compared to bulk materials.[7]

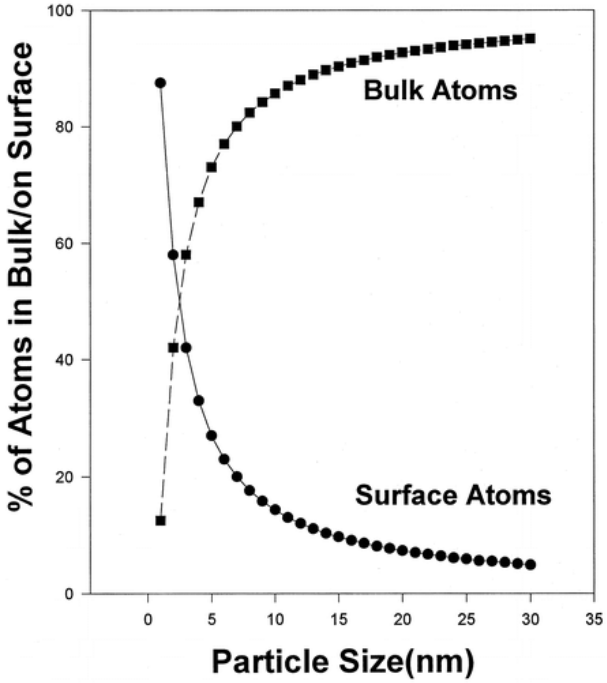

Figure 1. Relationship between particle size and the percentage of atoms present in the material.

The dependence of material properties on their dimensions can be expressed by the relationship:

$$\frac{E_t}{V} = E_i + \left(\frac{A}{V}\right) E_s$$

Where, E_t is the total energy per unit of volume; E_i is the internal energy per unit of volume; E_s is the superficial energy per unit of volume; V is the volume of the solid and A is its surface. The ratio *A/V,* it's the dispersion F which represents the fraction of dispersed atoms on the surface, respect to the total number of atoms present in the sample.[8]

As the dispersion increases, surface energy becomes increasingly relevant. The energetic contribution affects some physical properties, such as the melting temperature of nanomaterials. In fact, a solid-phase system, being subject to lattice constraints, has high surface energy, which is increased by dimensional effects. The material is energetically unstable and tends to undergo

[7] Jin S Yoo, 'Selective Gas-Phase Oxidation at Oxide Nanoparticles on Microporous Materials', *Catalysis Today* 41, no. 4 (June 1998): 409–32, https://doi.org/10.1016/S0920-5861(98)00028-5.

[8] Karuna Kar Nanda, 'Size-Dependent Density of Nanoparticles and Nanostructured Materials', *Physics Letters A* 376, no. 45 (October 2012): 3301–2, https://doi.org/10.1016/j.physleta.2012.10.001.

phase transitions at lower melting temperatures than macroscopic materials, to achieve a state of greater equilibrium.

Also, the increase in surface area causes a change in the density of the material. The explanation for this phenomenon is due to the presence of two factors: the cohesive forces between atoms described as a set of short-range electrostatic forces that are generated between molecules of the same substance, and the volume of the unit cells of the crystalline lattice. The change in density is described by the following equation:

$$\rho = \frac{m_a}{v} - \frac{a_v\left(1 - \frac{3h}{2d}\right)}{c^2 v}$$

Where m_a is the atomic mass; v is the atomic volume; a_v it's the cohesive energy of the material; h it's the atomic diameter, d is the nanoparticle diameter and c it's the speed of the light. When the dimensions of a system decrease, its density tends to increase according to a general trend, but this phenomenon does not always occur. For example, the term for cohesive forces usually decreases as the dimensions decrease, but in some situations, the sample geometry may influence lattice parameters. In the case of nanoparticles, which have spherical symmetry, the lattice undergoes isotropic contraction, meaning uniform in all directions, resulting in a decrease in bond lengths and a density increase. However, for nanostructured materials, which undergo anisotropic, non-uniform dimension reduction, the lattice tends to expand due to the deformation of bonds along the grain boundaries of the material. Therefore, when analyzing these systems, the density may decrease with dimension instead of increasing as would be expected based on the general trend.[9]

1.1.2 The quantum effect

When the dimensions of a material are reduced to the nanoscale, the electronic structure of the material changes, resulting in a phenomenon known as quantum confinement. This is due to the collapse of the electronic energy bands observed in bulk materials, leading to the formation

[9] Nanda.

of discrete energy states that are similar to those of individual atoms. In these confined systems, the wavelength of electrons becomes comparable to the size of the particles, which further alters the electronic properties of the material.

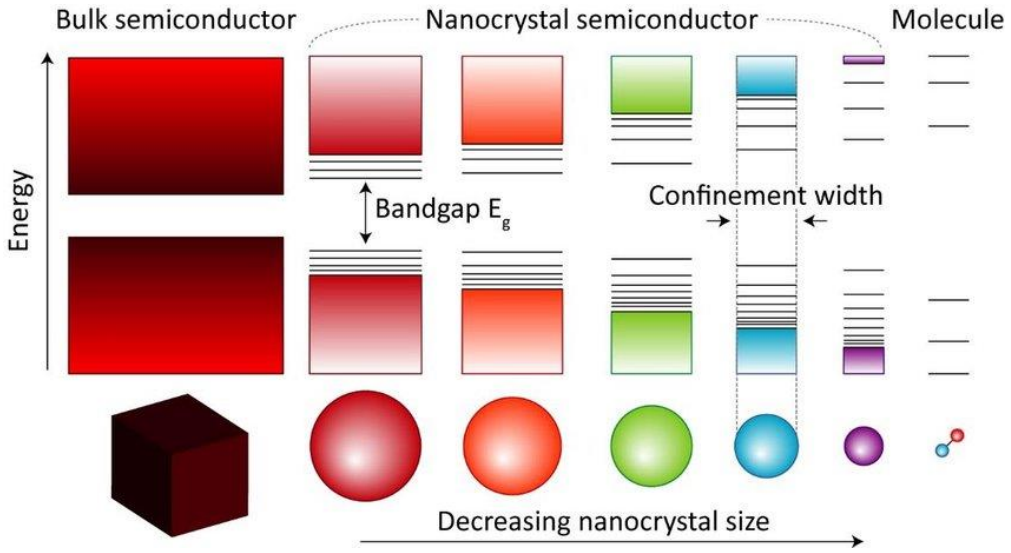

Figure 2. Quantum Confinement Effect.

In general, as the number of atoms in a system decreases, the density of electronic states becomes increasingly sparse, and the distance between them becomes larger. This means that the energy required to excite electrons in these systems becomes larger, and absorption and emission of energy become more limited.

When the number of atoms is reduced to a few tens, one can observe the effect of quantum confinement, in which the density of states becomes even more sparse, and the electrons can be considered confined in a system of finite energy.

In summary, the evolution of the density of states in systems with decreasing numbers of atoms depends on their size and level of quantum confinement.

The critical threshold at which confinement is detected is linked to the radius of the Bohr exciton.

$$\alpha_B = \varepsilon \frac{m}{m^*} \alpha_0$$

Where, ε is the dielectric constant of the material, m^* it's the particle mass, m is the mass of the electron, α_0 it's the Bohr radius in the H_2 atom.

When the system's dimensions approach this value, there is an uptick in the band gap energy between states.
The band gap, which refers to the energy difference between the highest occupied level and the lowest unoccupied level, can be mathematically modeled using the Kubo equation.

$$\delta = \frac{4E_f}{3n}$$

Where, E_f it's the Fermi's energy of the material; n is the total number of valence electron, δ is the average electronic level spacing.[10]

The value of δ for a bulk metal is typically quite low, as the number of electrons that can move around freely within the material's band structure is roughly equal to the number of atoms that make up the material's mass. As a result, any observed energy gap can only be observed at very low temperatures. For nanomaterials, the number of free charges is usually lower than it is for bulk materials. Additionally, because of quantum confinement, any energy gap that is observed is typically much wider. As the dimensions of the material are reduced, the valence and conduction bands shift apart from each other, leading to a transition from metallic to non-metallic properties. [11]

It's possible to determine a material's behavior by comparing the Kubo gap with the thermal energy kT of the system at room temperature. If the value of δ is less than kT, the material can be considered metallic; on the contrary, for lower temperatures and larger energy gaps, the values are related to non-metallic properties. These differences in behavior can result in variations in the material's electrical conductivity and magnetic susceptibility.
Moreover, with photoemission spectroscopy technique it was demonstrated that the nanometric systems the atoms are bonded with Van Der Waals forces. [12]
It means that, from an electronic point of view: the increase in size causes the atomic levels to spread out, forming bands with the transition from insulating to conductive behavior. On the other hand, from catalytic point of view, the reduced number of atoms involved in the formation

[10] Y. Volokitin et al., 'Quantum-Size Effects in the Thermodynamic Properties of Metallic Nanoparticles', *Nature* 384, no. 6610 (December 1996): 621–23, https://doi.org/10.1038/384621a0.
[11] D. A. B. Miller et al., 'Band-Edge Electroabsorption in Quantum Well Structures: The Quantum-Confined Stark Effect', *Physical Review Letters* 53, no. 22 (26 November 1984): 2173–76, https://doi.org/10.1103/PhysRevLett.53.2173.
[12] V De Gouveia et al., 'Electronic Effect Induced by Variation of Size for Pd Clusters in 1,3-Butadiene Hydrogenation', n.d.

of the bands leads to a greater localization of the electrons with a decrease in the width of the valence band, this electronic structure variation increases the reactivity of the surface towards the adsorbates.[13]

1.1.3 Methods of Synthesis

Nanomaterial fabrication has matured year by year, and there's today a very good control over the size, shape and thus over the properties of the material. There two main different methodologies to obtain nanomaterials are the *Top-down approach* and the *Bottom-up approach.* The first approach is related to the transformation of large and organized systems in nano-sized particles. It is simple to use but, the difficulty in obtaining and controlling proper particle size and shape is the main downside of this approach. In the second approach, the smaller components of atomic or molecular dimensions self-assemble, naturally or by applying an external driving force, to form larger and more organized systems. Nanomaterials with well-defined shape, size, and chemical composition are formed with this method.[14]

[13] Gouveia et al.
[14] Dr V M Arole and S V Munde, 'FABRICATION OF NANOMATERIALS BY TOP-DOWN AND BOTTOM-UP APPROACHES – AN OVERVIEW' 1, no. 2 (2014).

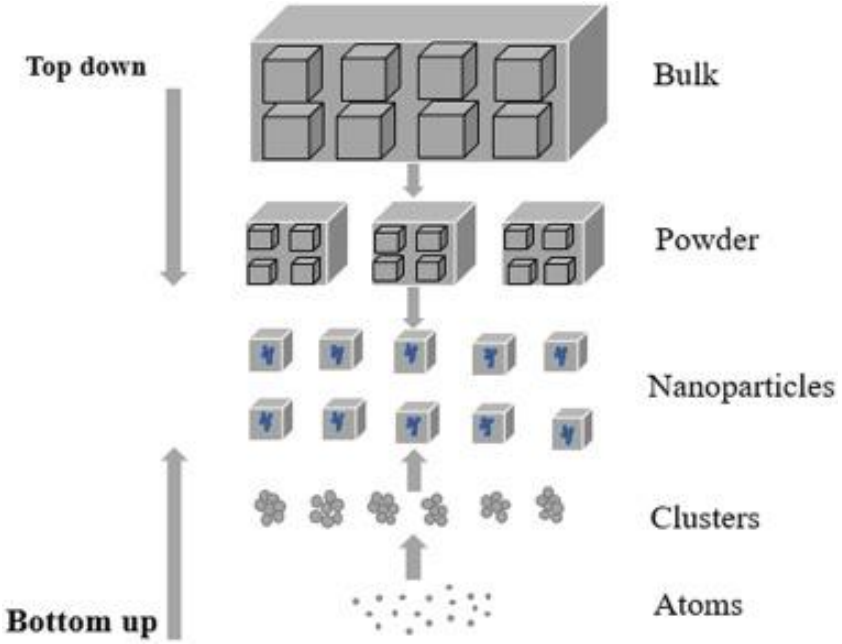

Figure 3. Top-down approach and Bottom-up approach.[15]

Each of these approaches comprises the utilization of different techniques.

- Top-down approach main techniques: *Mechanical milling or ball milling process; thermal evaporation.*
- Bottom-up approach main techniques*: chemical vapor deposition, hydrothermal method, co-precipitation method and sol-gel method.*

Synthesis methods are chosen bases on available primary materials, facilities, their potential application and on environmental and economic restriction.[16]

1.2 Nanoparticles

[15] Namra Abid et al., 'Synthesis of Nanomaterials Using Various Top-down and Bottom-up Approaches, Influencing Factors, Advantages, and Disadvantages: A Review', *Advances in Colloid and Interface Science* 300 (February 2022): 102597, https://doi.org/10.1016/j.cis.2021.102597.
[16] Abid et al.

Nanoparticles are defined as materials with at least one dimension that is less than 100nm, it means that they can be placed in a similar size domain of ultrafine particles and in a sub-set of colloidal particles.

A colloidal system is a two-phase system:

1) Dispersed medium
2) Dispersing medium.[17]

Specifically, a colloidal system is a heterogeneous mixture containing solid particles dispersed in a liquid medium. The definition is valid only if the solid phase is larger than atomic dimensions, but small enough to guarantee Brownian motion inside the fluid.

Chemically, nanoparticles can be metallic or non-metallic particles in their elemental state, but also inorganic and organic substances created by their combination. The reason why nanoparticles are of great scientific interest is because they represent a bridge between bulk substances and their molecular or atomic structure.[18]

The behavior of the nanoparticles can be different, and it depends on the different components of the material. A nanoparticle is usually constituted by:

1) A surface, that may be often functionalized.
2) A shell material, that can be intentionally added, and it is a layer of chemically different material from the core material.
3) The core material, the center of the nanoparticle and usually used to refer to the nanoparticle itself.[19]

1.2.1 Optical properties

[17] P. Christian et al., 'Nanoparticles: Structure, Properties, Preparation and Behaviour in Environmental Media', *Ecotoxicology* 17, no. 5 (July 2008): 326–43, https://doi.org/10.1007/s10646-008-0213-1.
[18] Nicolae Strambeanu et al., 'Nanoparticles: Definition, Classification and General Physical Properties', in *Nanoparticles' Promises and Risks*, ed. Mihai Lungu et al. (Cham: Springer International Publishing, 2015), 3–8, https://doi.org/10.1007/978-3-319-11728-7_1.
[19] Christian et al., 'Nanoparticles'.

The study of optical phenomena of metals is related to the interactions between electromagnetic radiations and matter, characterized by the presence of free electrons inside the material and the possibility of observing inter-band excitations, if the energy of the photons allows to overcome the energy gap. Some nanomaterials display very different optical properties, like the colour and the transparency, compared to the bulk materials. For what concerns the colour, it is well known that it is given by the interaction of the light with the material, only reflected wavelengths reach our eyes and are the ones that allow the material to appear with a certain colour.

In general, light (I) incident on a material, can be transmitted (T), absorbed (A) or reflected (R). As the size of the material is reduced, the scattering (S) of the light can also contribute to its colour or to the transparency.

$$I = T + A + R.$$

This formula still holds if the scattering occurs because it simply contributes to the reflection (back scattering) and transmission parts of the equation. Of course, light that has been absorbed cannot be scattered.

Nanomaterials can have peculiar optical properties depending on the way in which the light interacts with their fine nanostructure. The colour is based on the constructive interference of light wavelengths as they interact with the nanomaterial and, the phenomena observed are:

- Scattering
- Surface plasmon
- Quantum fluorescence

In the scattering, the colours arise from the fact that different particle sizes scatter different wavelengths. This phenomenon can be easily seen in colloids. The surface plasmon, instead, is a peculiar effect found in metal-nanoparticles, so in metal-colloids and it is responsible for their vivid colours. Concerning the last effect, the quantum confinement in nanomaterials leads to discrete energy levels from which energy can be emitted, after being absorbed by the semiconductor. The quantum fluorescence is typical of semiconductor quantum dots.

The most interesting phenomena in the case of this study, is the surface plasmons. This phenomenon is due to the scattering of nanoparticles with a diameter smaller than the light

wavelength, with the incident waves and it is called, more precisely, localised surface plasmon resonance. Basically, when light hits a metal surface some of the wave propagates along the metal surface, creating the "surface plasmon" which is a group of surface conduction electrons, that propagate in a direction parallel to the metal/dielectric interface. When a plasmon is generated in a bulk material, electrons can move freely in the material without registering any type of effect. In the case of nanoparticles, the surface plasmon localized in space, so it oscillates in a small space and the effect is called localise surface plasmon resonance (LSPR).

The energy of LSPR is sensitive to the dielectric function of the material and the surroundings and to the shape and the size of the nanoparticles. One of the consequences, of the LSPR effect in metal nanoparticles is that they have very strong visible adsorption due to the resonant coherent oscillation of the plasmons. As result, colloids of metal nanoparticles can display colours which are not found in their bulk form, depending on the shape, size and surrounding media as shown in Figure 4 for Au nanoparticles.

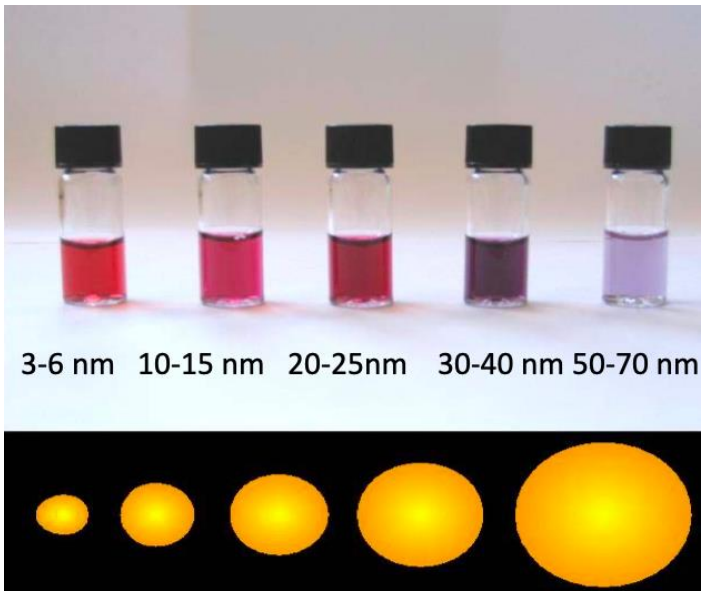

Figure 4. Suspension of gold nanoparticles of various size.

Moreover, also the variation of the dielectric constant (ε_d) affects the optical response: the particles are dispersed in a dense medium and the local electric field differs from the external excitation due to the polarization of the medium. The particles themselves are sources of electric

fields, which in turn change the surrounding environment and their local field. At high values of ε_d, the resonance shifts to longer wavelengths.[20]

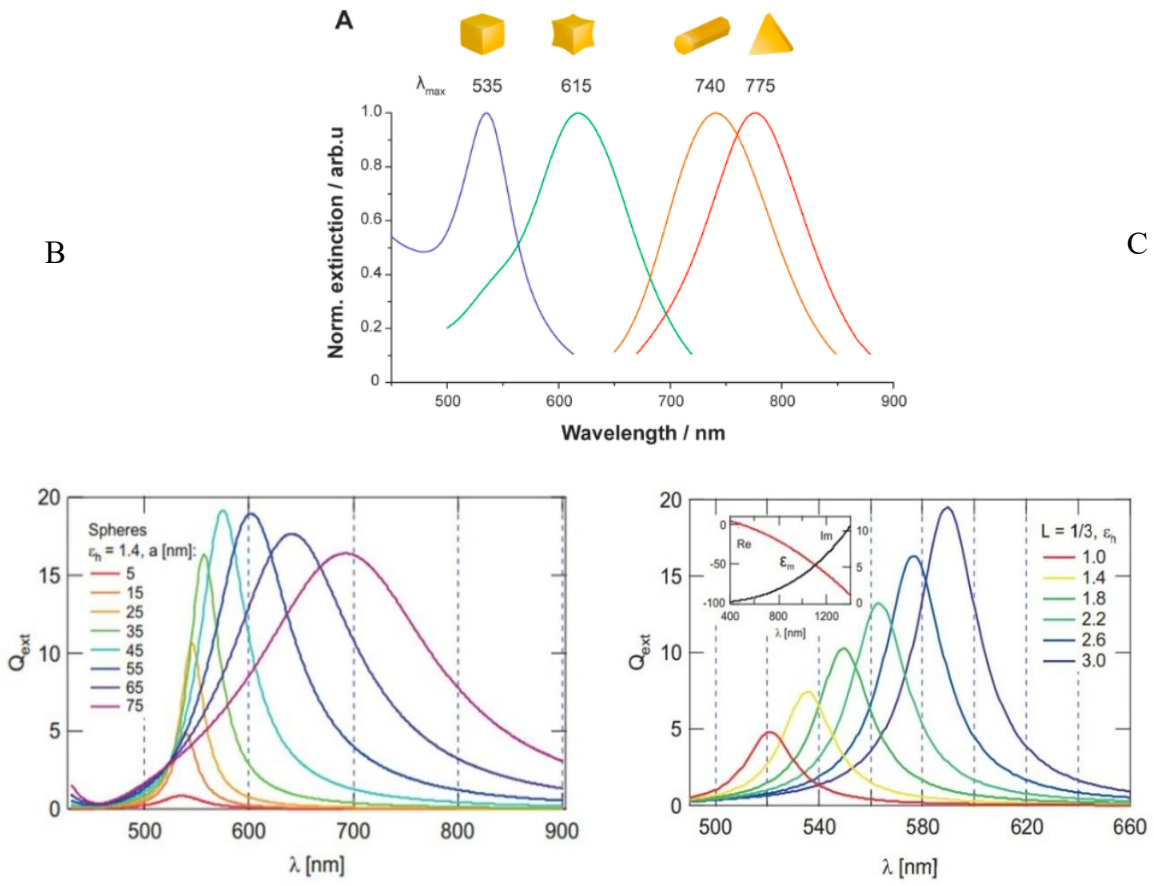

Figure 5. Variation of the plasmonic peak extinction efficiency due to the shape of the nanoparticles (A)[21] ; of their dimensions (B)[22] and of the dielectric constant of the medium in which they are dispersed (C). [23]

The optical response of a nanoparticle characterized by a dielectric function is obtained by solving the Maxwell equations in matter, which describe how electric and magnetic field are generated by charges, current and changes of the fields. The effects of an electromagnetic wave on nanoparticles can be expressed by the Mie theory, which is the exact solution of Maxwell's

[20] Cecilia Noguez, 'Surface Plasmons on Metal Nanoparticles: The Influence of Shape and Physical Environment', *The Journal of Physical Chemistry C* 111, no. 10 (1 March 2007): 3806–19, https://doi.org/10.1021/jp066539m.
[21] Erik Martinsson et al., 'Influence of Surfactant Bilayers on the Refractive Index Sensitivity and Catalytic Properties of Anisotropic Gold Nanoparticles', *Small* 12, no. 3 (January 2016): 330–42, https://doi.org/10.1002/smll.201502449.
[22] 'Absorption and Scattering by a Sphere'.
[23] Michael Quinten, *Optical Properties of Nanoparticle Systems: Mie and Beyond*, 1st ed. (Wiley, 2011), https://doi.org/10.1002/9783527633135.

problem for spherically symmetric objects and allows to describe the optical phenomena in a colloidal solution where the nanoparticles can be approximated to have spherical geometry.[24]

The Mie theory for the scattering and absorption of light by spherically symmetric nanoparticles can explain the reasons for the colours observed in colloidal samples. Metallic nanoparticles exhibit localised plasmons that show deviations from the free electron model, which are due to quantum effects in small materials. The band gap created between the valence and conduction states alters the contribution of the inter-band transitions from the *(n-1)d* electrons to the *nsp* hybrid bands, affecting the position of the surface plasmons. The resonance peaks carry characteristic colours for the particles: red for Cu and Au, yellow for Ag.[25] The colour changes are due to the positions of the peaks and directly related to the size of the nanoparticles.

1.2.2 Stability of colloidal solution

A solution is defined colloidal if contain two phases in which one substance is dispersed in the other. Colloidal systems usually are not true solution but homogenous mixture of two or more substances, it means that they're not stable in time so, the maintenance of the stability is crucial. A dispersion of colloids is stable if the particles in the dispersion continue to exist as individual units. So, the stabilization of colloids is all related to how prevent particles aggregation and/or flocculation.[26]

The stability of these system can be described by the Derjaguin, Landau, Verwey and Overbeek theory (DLVO) which characterizes stability by the interaction energy of the particles in solution. The addition of different substances and the influence of other factor like the concentration, ionic strength and pH can change the total potential energy of interactions.[27]

There are different types of stability.

---

[24] Kelly et al., 'The Optical Properties of Metal Nanoparticles'.
[25] Quinten, *Optical Properties of Nanoparticle Systems*.
[26] Jakub Matusiak and Elżbieta Grządka, 'Stability of Colloidal Systems - a Review of the Stability Measurements Methods', *Annales Universitatis Mariae Curie-Sklodowska, Sectio AA – Chemia* 72, no. 1 (8 December 2017): 33, https://doi.org/10.17951/aa.2017.72.1.33.
[27] 'Derjaguin-Landau-Verwey-Overbeek-Theory (DLVO Theory).Pdf', n.d.

1) Electrostatic stabilization: this stabilization is the consequence of electrostatic repulsion forces. If the particles suspended in the liquid possess the same electrostatic charge on its surface, they don't attract each other, increasing the stability (short-term stability).
2) Steric stabilization: it is obtained by the addition of macromolecules (surfactants or polymers) to the system changing its interphase properties. These long-chain molecules are anchored on the surface of the particles creating a thin shell around them.
3) Depletion stabilization: involves the addition of non-ionic polymers to colloidal dispersion. The difference from the steric stabilization is that, in this case, the polymers are not adsorbed on the particle surface so, they're free to move.[28]

The opposite of stabilization is the flocculation, which occurs when the sum of the attraction forces is higher than that of repulsion ones. There are two types of flocculation caused by the polymer: the bridging, occurs when two or more colloidal particles are linked using polymer chains adsorbed on the solid surface, which results in the system aggregation and the depletion, and the depletion flocculation caused by the aggregation of solid particles influenced by some free unabsorbed macromolecules.[29]

1.2.3 DLVO Theory

The DLVO theory is based on the balance between van der Waals attraction forces and repulsion electric double layer forces. The degree of stability of the suspension is quantified through the calculation of the interaction potential between two electrostatically charged surfaces immersed in a fluid.[30] Conventionally, when the potential is positive, there is a repulsion between the two surfaces. Conversely, when the potential takes on negative value, attractive interaction forces prevail. If the sum of the repulsion forces is higher than the sum of the attractive ones, the system can be considered stable.[31]

---

[28] Matusiak and Grządka, 'Stability of Colloidal Systems - a Review of the Stability Measurements Methods'.
[29] A. N. Semenov and A. A. Shvets, 'Theory of Colloid Depletion Stabilization by Unattached and Adsorbed Polymers', *Soft Matter* 11, no. 45 (2015): 8863–78, https://doi.org/10.1039/C5SM01365H.
[30] Hiroyuki Ohshima, 'The Derjaguin-Landau-Verwey-Overbeek (DLVO) Theory of Colloid Stability', in *Electrical Phenomena at Interfaces and Biointerfaces*, ed. Hiroyuki Ohshima (Hoboken, NJ, USA: John Wiley & Sons, Inc., 2012), 27–34, https://doi.org/10.1002/9781118135440.ch3.
[31] Matusiak and Grządka, 'Stability of Colloidal Systems - a Review of the Stability Measurements Methods'.

Orientation interaction, dipole interactions and dispersion interactions are collectively called, van der Waals forces and are responsible for intramolecular reactions.

In this section, the DLVO theory will be describe taking in consideration the attractive potential for macroscopic systems and for spherical particles.

The attractive potential for *macroscopic* systems is described by Hamacker theory where Van der Waals forces acting between particles due to the attractive forces between the molecules present in each particle. So, this theory sums the interaction between bodies with defined geometry neglecting the electrostatic response of the medium. For solid systems, the van der Waals forcers are expressed by the following equation:

$$u_{VdW} = -\frac{A_H f}{D^n}$$

Where A_H is the Hamacker constant; *f* expresses the dependence on the geometry of the system and *D* is the distance.[32,33]

In the case of *spherical particles*, the Derjaguin approximation it's fundamental to not consider the geometry dependence. This approximation assumes that the distance between two spherical particles is narrower than the radius: the van der Waals force between particles becomes weaker as the distance between them increases and, becomes stronger as the size of the particles increases.[34]
To describe what happens in the case of spherical particles the Electric Double Layer (EDL) must be considered and the most suitable model to explain the phenomenon is the Gouy-Chapman-Stern. Louis Georges Gouy and David Chapman hypothesized that the fall of electrical potential in the double layer had an exponential trend.[35]

The Electric double layer is divided in two regions:

[32] Ian W. Hamley, *Introduction to Soft Matter– Revised Edition* (Chichester, UK: John Wiley & Sons, Ltd, 2007), https://doi.org/10.1002/9780470517338.
[33] 'Isdraelachvili - Chapter 4', n.d.
[34] Hamley, *Introduction to Soft Matter– Revised Edition*.
[35] Hamley.

1) *The Stern layer:* in which the charged surface and the adsorbed counter-ions are located. In this region, the electric potential of the surface decreases linearly with increasing distance.
2) *The Gouy layer (or diffusion layer):* where solvated ions can be found. In this region, the electric potential has lower values and decreases exponentially, until it coincides with that of the solution.

According to this model the electric potential ψ decreases linearly with distance.[36]

Inside the diffusion layer, there's a *shear plane* which separates the potentially mobile fluid, because of external fields, from the superficial one. The value of ψ measured on the shear plane is called zeta potential (ζ) and responds inversely proportionally to the increase in electrolytes in solution. The overall trend of the potential in the diffuse layer follows an exponential decay.

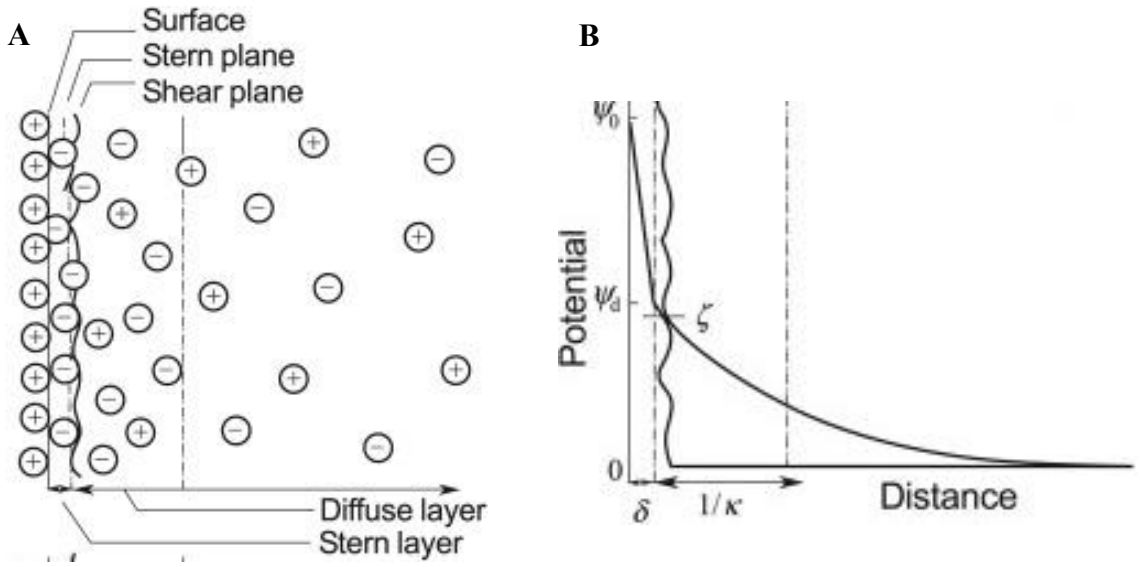

Figure 6. Schematic representation of the electric double layer of Gouy-Chapman-Stern (A); correlation of the potential ψ with the distance from the surface (B).

The interaction between charged surfaces (EDL) leads to the formation of repulsive forces and the resulting energy is geometry dependent. In the case of spherical nanoparticles, assuming the symmetry of the material as a planar surface, the contribution is described by the equation:

$$u_{EDL} = 64 k_B T C_0 tanh^2 \left(\frac{e\psi_0}{4k_B T}\right) e^{-\frac{\delta}{\lambda_D}}$$

[36] André H. B. Dourado, 'Electric Double Layer: The Good, the Bad, and the Beauty', *Electrochem* 3, no. 4 (2 December 2022): 789–808, https://doi.org/10.3390/electrochem3040052.

Where: C_0 is the concentration of the electrolyte in bulk phase; λ_D it is the length of Debye (distance at which the attractive effects of the surface do not affect the behavior of the ions); ψ_0 is the potential of the surface charge; δ is the distance that separates the two electrical layers.

When the electrical double layers are far away, the interaction between them is weak and the total potential, deriving from the DLVO theory, can be written as the sum of Van der Waals and EDL interactions:

$$u_{DLVO} = u_{EDL} + u_{VdW} = 64k_BTC_0\lambda_D tanh^2\left(\frac{e\psi_0}{4k_BT}\right)e^{-\frac{\delta}{\lambda_D}} - \frac{A_H}{12\,\pi D^2}$$

This equation is the mean through which it's possible to rationalize the stability of the nanoparticles present in solution.[37]

Representing the resultant potential V_{tot} as function of the distance,

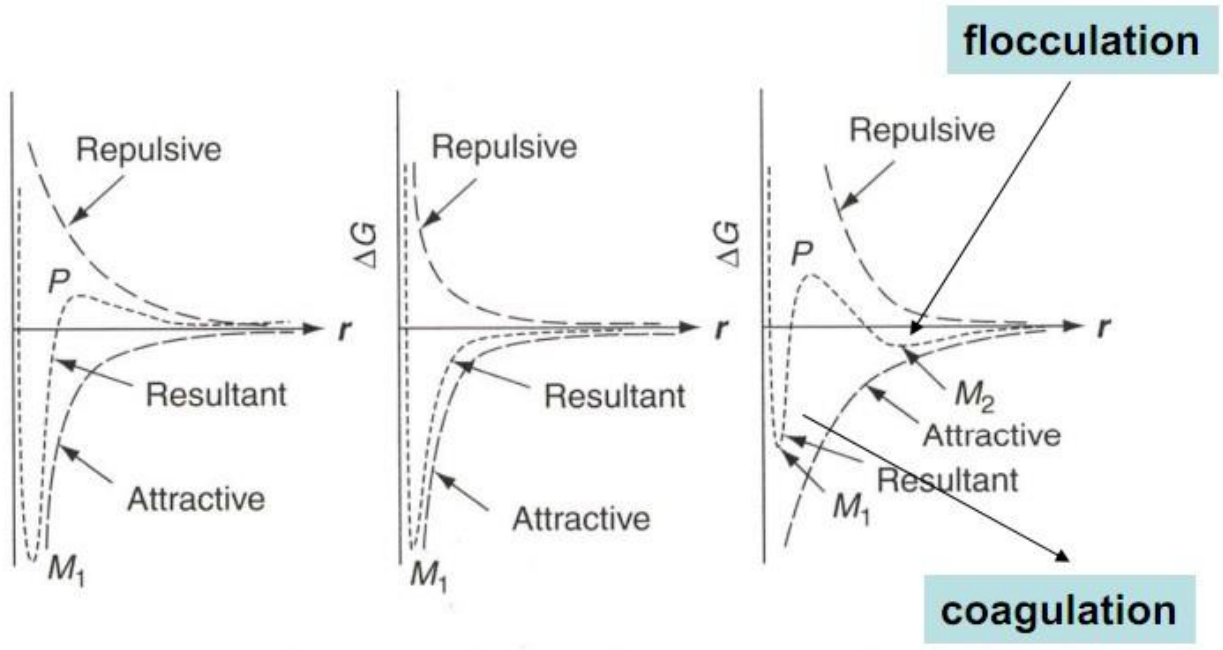

Figure 7. DLVO's Potential Energy Profile as function of the distance.

the energy profile shows that:

1. The energy profile shows a deep primary minimum when the distance is so small that the Van Der Waals forces prevail. Here, the resultant is negative, attraction forces

[37] Ohshima, 'The Derjaguin-Landau-Verwey-Overbeek (DLVO) Theory of Colloid Stability'.

prevail with consequent particle attraction and coagulation occurs. The colloidal system is not stable.

2. If the repulsion forces are greater than those of attraction, the resultant has a maximum corresponding to an energy barrier, due to repulsive forces, that prevents the particles from aggregating and the colloidal system is stable. The curve then, fall again in a minimum (secondary minimum). In this case, the stabilizing effect is called "flocculation", a reversible effect due to the little depth of the minimum in fact heating or shaking the system will bring it back to the colloidal phase.[38]

The DLVO theory can account for the stability of colloidal suspensions, or whether coagulation or flocculation occur. The stability of the system is described by the height of the barrier. The coagulation (or flocculation) happens when the energy of the barrier is lower than the energy of the particles. [39]

1.3 Supported metal nanoparticles

The problem related to the unsupported metal nanoparticles is linked to the phenomena by which the nanoparticles undergo due to low thermal stability, absence of support and metal-support interaction and therefore the possibility of aggregation, particles size increases, and the deactivation and loss of the catalytic activity happen. For this reason, it's fundamental the control of the size, shape, and dispersity of the nanoparticles to obtain a selective and enhanced activity. This high control can be achieved using porous supports and these materials, are called "supported metal nanoparticles". The fusion between porous materials and nanoparticles increases the green of the process with high selectivity, conversion, yield, and catalyst recovery providing perfect bases for catalysis application.

Metal nanoparticles have a large surface-to-volume ratio as compared to their bulk equivalents making them very attractive for catalytic application. As the size of a material decreases to the nanoscale, the percentage of atoms at its surface becomes relevant. The increase of the surface-to-volume ratio influences the properties related to the surface. Other interesting properties are related to the high zeta potential, that avoids the aggregation of nanoclusters in solution and to

[38] Semenov and Shvets, 'Theory of Colloid Depletion Stabilization by Unattached and Adsorbed Polymers'.
[39] Hamley, *Introduction to Soft Matter– Revised Edition*.

the recyclability of these materials, reducing the catalyst contamination. The reason why is preferable to have nanoparticles anchored onto solid support is because of the small size and the solubility of the nanoparticle in solution. Porous supports are the most used. Generally, a porous material is a solid characterized of a network of inter-connected porous and morphology, textural and physical properties depend on its constituents. The use of these kinds of material as supports for nanoparticles allows the generation of specific adsorption sites, also allows the inhibition of particle growth, reducing their aggregation. The activity of any metal-supported nano-catalysts depends on the metal loading and on its dispersion on the support, also considering that the size of the metal particles is a key factor. The control of the particle size and shape allows to optimize the geometry of the particles, providing important surface properties for specific reactions. Moreover, decreasing the particle size increases the available surface of the system which, again, determined the efficacy of these kind of nanoparticles in catalytic applications.[40] As it has been already said, the smaller are the nanoparticles, the larger is the fraction of exposed surface atoms but, the small NPs can easily aggregate to form larger ones. The formation of larger particles is explained by the Ostwald ripening principle, according to which thermodynamically stable larger particles are more favored than smaller ones: the system lowers its energy by releasing atoms from the small particle surface that diffuse, through the solution, and then attach to the larger particle surface. To avoid the agglomeration stabilizers such as polymers, surfactants, and ligands, that act as protective layer, are required.[41]

1.3.1 Preparation routes for supported metal nanoparticles

The preparation of supported metal nanoparticles happens taking always in consideration the sustainability of the process. In fact, the system should be prepared using the less toxic precursor, the less toxic solvents, using the least number of reagents with reaction temperature close to the room temperature. Moreover, it's also necessary to use as few synthetic steps as possible to minimize the quantities of by-products and wastes that can be generated. The nanoparticles also must be well dispersed on the support surface and highly active in catalytic

[40] Matumuene Joe Ndolomingo, Ndzondelelo Bingwa, and Reinout Meijboom, 'Review of Supported Metal Nanoparticles: Synthesis Methodologies, Advantages and Application as Catalysts', *Journal of Materials Science* 55, no. 15 (May 2020): 6195–6241, https://doi.org/10.1007/s10853-020-04415-x.
[41] Jingyue Jimmy Liu, 'Advanced Electron Microscopy of Metal-Support Interactions in Supported Metal Catalysts', *ChemCatChem* 3, no. 6 (14 June 2011): 934–48, https://doi.org/10.1002/cctc.201100090.

applications. The preparation routes can be physical or chemical, in this study we will focus only on the chemical ones.[42]

The classical chemical methods used for the synthesis of supported metal nanoparticles are impregnation, deposition-precipitation, and sol-immobilization.

Impregnation

Among the many methods to prepare supported metal catalysts, impregnation is the simplest and most widespread method used. It consists of the dispersion of the metallic precursor in an aqueous solution on a support, followed by drying and calcination phases. Using an amount of the precursor solution above the pore volume of the support, yielding a thin slurry is termed wet impregnation (WI). Limiting the solution amount to just fill the pore volume is called dry or incipient wetness impregnation (DI or IWI). Various metal oxides can be used as a support. The advantages are that there is no need to adjust the pH to promote the interaction between metal and support, and that it is a relatively simple and inexpensive method. However, the major weakness of the impregnation method is the lack of size control of metal particles except when the porous substrate has a narrow pore size distribution.[43]

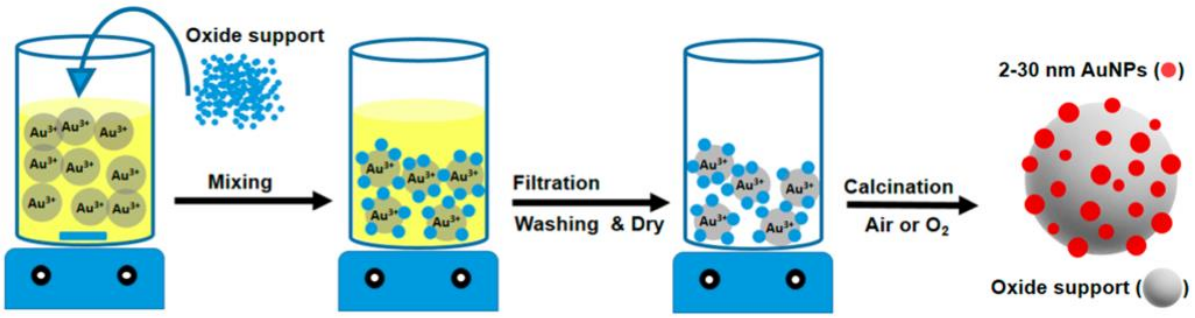

Figure 8. Scheme of impregnation method to synthetize supported gold nanoparticles.[44]

Deposition-precipitation

[42] Ndolomingo, Bingwa, and Meijboom, 'Review of Supported Metal Nanoparticles'.
[43] Ki-Joong Kim and Ho-Geun Ahn, 'Complete Oxidation of Toluene over Bimetallic Pt–Au Catalysts Supported on ZnO/Al2O3', *Applied Catalysis B: Environmental* 91, no. 1–2 (September 2009): 308–18, https://doi.org/10.1016/j.apcatb.2009.05.037.
[44] Alshammari, 'Heterogeneous Gold Catalysis: From Discovery to Applications', *Catalysts* 9, no. 5 (29 April 2019): 402, https://doi.org/10.3390/catal9050402.

The deposition-precipitation (DP) method involves the conversion of a highly soluble metal salt precursor into a less-soluble substance that precipitates only on the support and not in solution. Typically, this process is achieved by a change in solution pH, the addition of a precipitating agent, the addition of a reducing agent, or change in the concentration of a complexation agent. Two main conditions that must be fulfilled to make sure that the precipitation occurs only on the support instead of in solution: (1) strong interaction between the soluble metal precursor and the surface of the support and (2) controlled concentrations of the precursor in solution to avoid spontaneous precipitation.[45] Usually, in the presence of a support, the solubility limit shifts to a lower concentration compared to the solubility limit in solution to help deposition on the support. This technique consists of stirring the support powder in a solution containing the metal precursor, a hydroxide, or a hydrated oxide. By adding a precipitating agent as a base, the precursor of the metal becomes insoluble by increasing the pH and precipitates on the support. In this case, the pH is an important parameter that can influence and control the nanoparticles formed, like the dimension or the metal loading.[46]

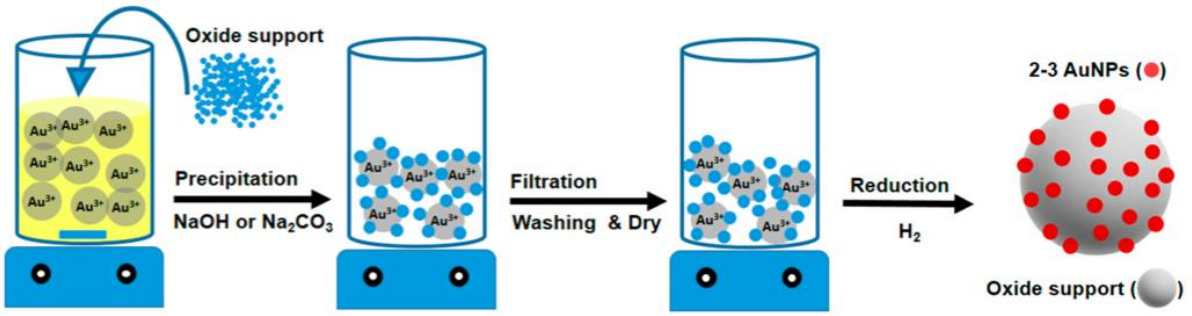

Figure 9. Scheme of deposition-precipitation method to synthetize supported gold nanoparticles. [47]

Sol-Immobilization

Sol-immobilization technique is a colloidal method that allows the synthesis of nanoparticles directly in solution. The metal precursor is reduced, and the nanoparticles are formed. It is fundamental the use of surfactants or stabilizing agent to avoid the metal nanoparticles

[45] Michela Signoretto et al., 'Effects of Support and Synthetic Procedure for Sol-Immobilized Au Nanoparticles', *Catalysts* 6, no. 6 (20 June 2016): 87, https://doi.org/10.3390/catal6060087.
[46] Nasrallah M Deraz, 'The Comparative Jurisprudence of Catalysts Preparation Methods: II. Deposition-Precipitation and Adsorption Methods.' 2, no. 2 (2018).
[47] Alshammari, 'Heterogeneous Gold Catalysis'.

aggregation. Also in this case, the pH of the solution plays an important role in the synthesis, for example in the synthesis of gold nanoparticles, the addition of NaOH enhances the power of the reducing agent leading to the formation of smaller nanoparticles.[48] The main advantage of this technique is the possibility to control the particle size, in fact, depending on the concentration of the reducing agent, the size can be tuned before having the deposition of the nanoparticles onto the support. High concentrations of reducing agent leads to the formation of a greater number of nuclei, and consequently to smaller nanoparticles. Apart from the concentration, also the type of the reducing agent has a great influence on the morphology of the nanoparticles and the most used one is sodium borohydride ($NaBH_4$) as a strong reducing agent. Concerning instead the immobilization step, it can happen because of two types of interaction: steric or electrostatic. In the case of the electrostatic stabilization, anions and cations from the starting materials interact with the nanoparticles forming an electric double layer that avoids aggregation; the steric stabilization is due to the possible adsorption of polymers or macromolecules on the surface of the dispersed particles. Usually, to have a better stabilization, both the interactions are chosen. Some examples of polymer stabilizers are the PVA (polyvinyl alcohol) and PVP (polyvinyl pyrrolidone) which are commonly used because they're non-toxic and soluble in water.[49]

Figure 10. Scheme of Sol-Immobilization method to synthetize supported metal nanoparticles.

1.4 Catalyst Design

[48] Signoretto et al., 'Effects of Support and Synthetic Procedure for Sol-Immobilized Au Nanoparticles'.
[49] Ndolomingo, Bingwa, and Meijboom, 'Review of Supported Metal Nanoparticles'; Signoretto et al., 'Effects of Support and Synthetic Procedure for Sol-Immobilized Au Nanoparticles'.

The catalytic activity plays an important role in the Aqueous Phase Reforming reaction focusing mainly on the production of hydrogen. In this section the general concepts related to the homogenous and heterogenous catalysis are be discussed.

1.4.1 Catalysis.

The term "catalysis" was coined by Berzelius over 150 years ago when he has noticed changes in substances when they were brought in contact with small amounts of certain species called "ferments". Many years later, in 1895, Ostwald came up with the definition that we use until today: *"A catalyst is a substance that changes the rate of a chemical reaction without itself appearing into the products"*. To be more precise *"a catalyst is a substance which increase the rate at which a chemical reaction approaches the equilibrium without becoming permanently involves"*.

Catalysts are substances that can increase the reaction rate of a chemical reaction, without being consumed in the process. The catalyzed pathway has a lower Activation Energy E_a but the net change in the energy of the reaction (difference between the energy of reactants and products) is not affected by the presence of the catalyst.

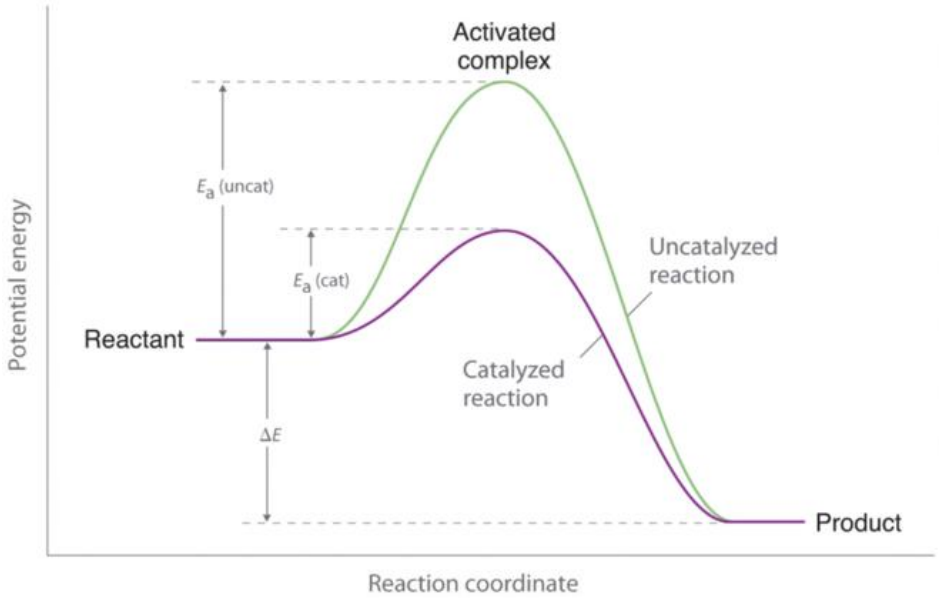

Figure 11. Activation Energy of a catalyzed reaction.

The catalyst decreases the height of the energy barrier, increasing the rate of both the direct and reverse reactions in fact, because of lower E_a, the reaction rate of the catalyzed reaction is higher than the reaction rate of the uncatalyzed reaction at the same temperature. However, catalysts

do not reduce the activation energy of the uncatalyzed reaction. Rather, they provide a different route to the products an alternative reaction mechanism with lower activation energy.

The fundamental aspects of catalysis are first, the collision between particles and, second the number of successful collisions. Collisions happen only if the particles interact with a certain minimum energy, the activation energy but, to increase the rate of the reaction, the number of successful collisions must increase. To do that, the only way is to provide an alternative pathway for the reaction to happen and this pathway must have a lower activation energy. This situation is the result of adding a catalyst in a reaction.

All molecules possess a certain amount of energy, this energy can be kinetic energy or potential energy. When molecules collide, their kinetic energy can be used to stretch, bend and to break the bonds, which leads to a chemical reaction. if molecules move too slowly or collide without the proper orientation, they cannot react, whereas, if they move fast enough and have the right orientation in a way in which the kinetic energy upon collision is higher than the minimum energy barrier, the reaction can occur. The minimum energy required to have the reaction is the activation energy, E_a. The activation energy is the energy difference between the reactants and the activated complex, also called transition state which is defined as the highest-energy state of the system. If the molecules in the reactants collide with enough kinetic energy and this energy is bigger than the transition state energy, the reaction occurs, and the products are formed.

These words can be expressed mathematically:

In thermodynamic, the change in Gibbs Free energy, ΔG is defined as:

$$\Delta G = \Delta H - T\Delta S$$

Where, ΔG is the change in Gibbs free energy of the reaction; ΔH is the change in enthalpy and ΔS change in entropy.

ΔG° is the change in the Gibbs energy when the reaction happens at standard state (1 atm, 298 K, pH 7). Taking in consideration a reaction that doesn't happen at standard state, the Gibbs free energy equation can be written as:

$$\Delta G = \Delta G^\circ + RT \ln K$$

Where, $\Delta G°$ is the standard Gibbs free energy; R is the ideal gas constant and K is the equilibrium constant.

When the reaction is at equilibrium, $\Delta G = 0$, the equation becomes:

$$\Delta G° = -RT \ln K$$

In the transition state theory, the Gibbs energy of activation, $\Delta G^{‡}$ is defined as

$$\Delta G^{‡} = -RT \ln K^{‡}$$

And,

$$\Delta G^{‡} = \Delta H^{‡} - T\Delta S^{‡}$$

Where, $\Delta G^{‡}$ is the Gibbs energy of activation, $\Delta H^{‡}$ is the enthalpy of activation, and $\Delta S^{‡}$ is the entropy of activation.

Combining the last two equations, solving it for the $\ln K^{‡}$, the Eyring equation is obtained:

$$\ln K^{‡} = -\frac{\Delta H^{‡}}{RT} + \frac{\Delta S^{‡}}{R}$$

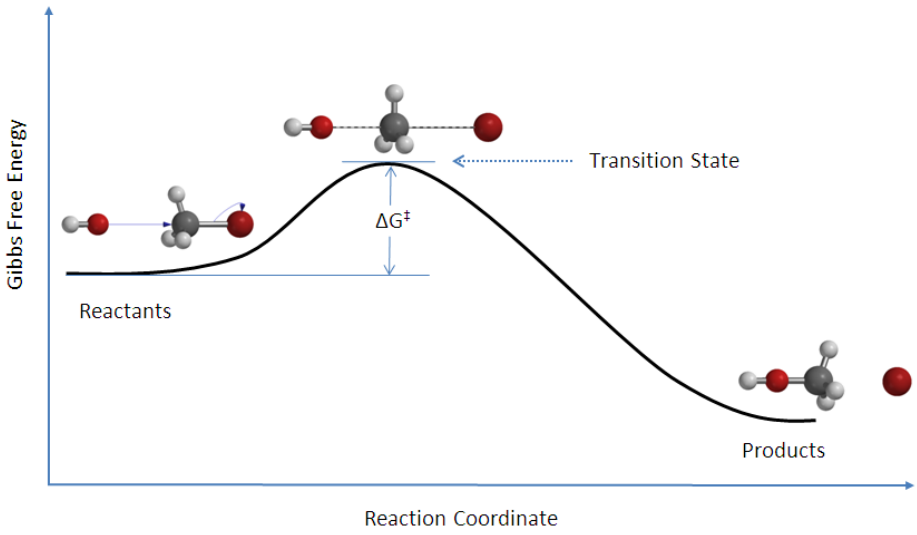

Reaction: $HO^- + CH_3Br \rightarrow [HO{-}{-}{-}CH_3{-}{-}{-}Br]^{‡} \rightarrow CH_3OH + Br^-$

As shown in the graph, the activation enthalpy is the difference in energy between the ground state and the transition state in a chemical reaction. Higher is the activation enthalpy, the more is the energy required to obtain the products. This activation enthalpy is equal to the activation energy when comparing the Arrhenius Equation with the Eyring equation:

$$E_a = \Delta H^{\ddagger} + RT$$

In overall, a reaction proceeds faster if E_a and $\Delta H^{\ddagger}$ are small. On the contrary, if these two quantities are large, the reaction rate is slow.[50]

1.4.2 Homogeneous Catalysis

Homogeneous Catalysis, by definition, refers to the situation in which the substrates involved in the reaction and the catalysts are brought together in one phase, often the liquid phase. Examples of such catalytic systems are:

1. Acid and base catalysis
2. Lewis's acids as catalysts
3. Organic Catalysts
4. Enzymatic processes
5. Coordination complexes.

Ligand effects are extremely important in homogeneous catalysis by metal complexes because one metal can give a variety of products from one single substrate by changing the ligands present around the metal center.

The mass transfer is the net movement of mass from one phase to another, so the process that drives the contact between the reagent and the catalyst. However, in the case of homogeneous catalyst, when the reagent is in the gas phase, it presents a limitation.

Taking as an example the hydrogenation process, our reagent is the hydrogen that must reach the catalyst. The step that the hydrogen should follow are:

[50] 'Chemistry - The Central Science', n.d.

- H_2 diffusion towards the liquid phase interphase,
- H_2 diffusion into the liquid
- Interaction with the catalyst (chemical step).

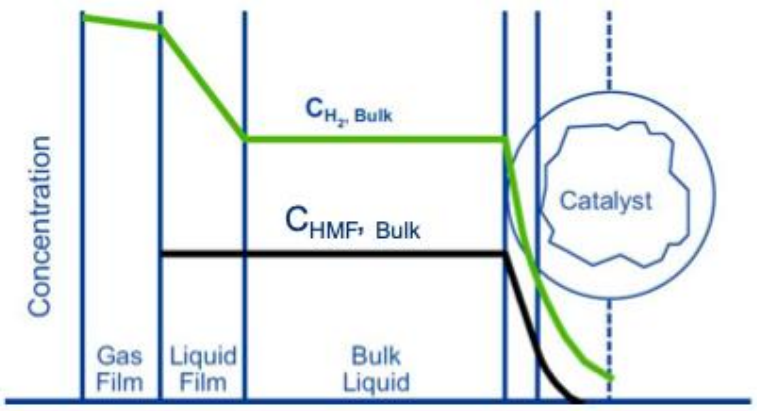

Figure 12. Mass Transfer in Homogeneous Catalysis.

The drawback is related to the fact that hydrogen has low solubility in liquid phase.

To increase the mass transfer, increasing the pressure, changing the solvent or modify the type of the reactor could be good strategies.

Homogenous catalysts are characterized of some advantages, in fact they're highly selective and it's easy the control of the temperature. However, they also present a lot of disadvantages:

- Bad recovery of the catalyst since products and catalyst will be in the same phase at the end of the reaction.
- Contamination of the product from the catalyst.
- Inefficient reusability.
- Corrosivity and toxicity.
- Mass transfer issues with gaseous reagents.

1.4.2.1 *Hydrogenation: the most popular homogeneous catalyst application*

A large part of today's general knowledge on homogeneous catalysis has been derived from the early studies on hydrogenation. The most popular homogenous catalyst used for this reaction is the Wilkinson's catalyst, $RhCl(PPh_3)_3$, discovered in the sixties.[51]

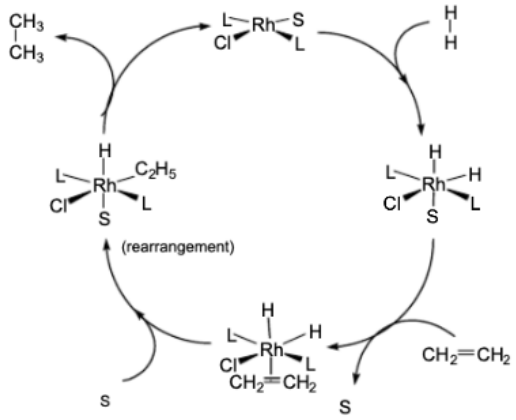

Figure 13. Wilkinson's hydrogenation cycle.

In the scheme, L stands for triaryl phosphines and S for solvent (e.g., ethanol or toluene) whereas the alkene is ethene. The first step in this sequence is the dissociation of one ligand L which is replaced by a solvent molecule. For simplicity it has been chosen the Wilkinson's complex as the starting point of the cycle, but several alternatives have been found involving, for example the formation of dimers from unsaturated species. The number of valence electrons switches during the cycle, in this case the valence electron counts switch between 16 and 18.

After ligand dissociation an oxidative addition reaction of dihydrogen takes place. This occurs in cis-position and can be promoted by the substitution of more electron-rich phosphines on the rhodium complex.

The next step is the migration of the hydride forming the ethyl group, then the reductive elimination of ethane completes the cycle. The rate of this step can be increased by employing electron withdrawing ligands. Strong donor ligands, however, stabilize the trivalent rhodium chloro-dihydride to such an extent that the complexes are no longer active.

The degree of substitution on the olefin substrate is the key factor in terms of rates of hydrogenation, since the rate-limiting step in this mechanism is the insertion into the olefine

---

[51] Jardine, F. H.; Osborn, J. A.; Wilkinson, G.; Young, J. F. Chem. Ind. (London) 1965, 560; J. Chem. Soc. (A) 1966, 1711.

which is limited by the severe steric hindrance around the metal center. In fact, terminal and substituted alkenes are good substrate but more hindered alkenes are slower to hydrogenate.[52]

1.4.3 Heterogeneous Catalysis.

Many catalytic processes are known in which the catalyst and the reactants are not present in the same phase. These are known as heterogeneous catalytic reactions. Usually, there are only two phases, solid-liquid or solid-gas but, it's possible to have also solid-liquid-gas phase together. Examples of such catalytic systems are:

- Metals
- Oxide
- Sulfides
- Chlorides
- Carbonaceous materials
- Zeolite
- Bimetallic catalysts.

Also in this case, the mass transfer drives the process and now it follows very precise steps, to obtain the products. In fact, during an overall catalytic reaction, the reactants and products undergo a series of steps over the catalyst, including:

1) Diffusion of the reactants through a boundary layer surrounding the catalyst particles.
2) Interparticle diffusion of the reactants into the catalyst pores to the active site.
3) Adsorption of the reactants onto active sites.
4) Surface reactions involving formation or conversion of various absorbed intermediates, possibly including surface diffusion steps.
5) Desorption of products from catalyst sites.
6) Interparticle diffusion of the products through the catalyst pores.

[52] Kevin Burgess, Wilfred van der Donk, Chul-Ho Jun, Young Jun Park, "Chlorotris(triphenylphosphine)-rhodium(I)" Encyclopedia of Reagents for Organic Synthesis 2005 John Wiley & Sons

7) Diffusion of the products across the boundary layer surrounding the catalyst particles.

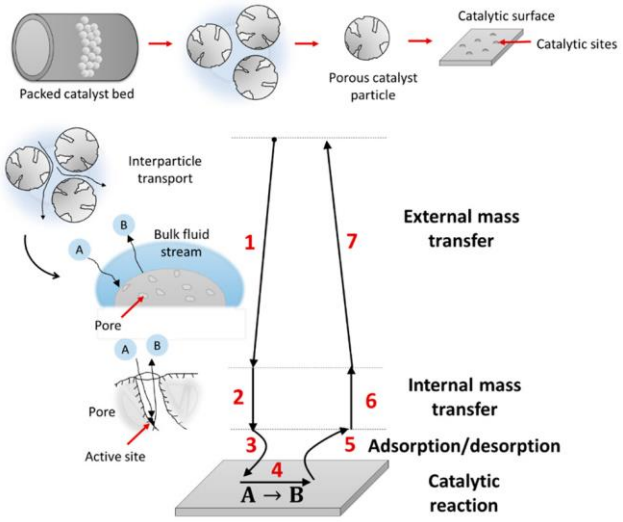

Figure 14. Scheme for illustrating the kinetic steps in heterogeneous catalysis reactions.[53]

There are different regimes of catalytic rate control:

- Film diffusion control: in the first and in the last step.
- Pore diffusion control: in the second and in the sixth step.
- Intrinsic reaction kinetic control of catalyst performance: third and fifth steps.

Heat transfer effect can also occur in heterogenous catalysis for highly exothermic and endothermic reactions.

To increase the mass transfer in heterogenous catalysis, the key is to make easier the process by which reactants arrive to the active sites just modifying the surface area and the pore's size. Increasing the flow rate, the external diffusion increases and decreasing the particle size (making larger the pores), the internal diffusion increases.

The advantages of heterogenous catalysts are:

- They're easily to separate.

[53] Julieth T. García-Sánchez et al., 'Calculation of Mass Transfer Limitations for a Gas-Phase Reaction in an Isothermal Fixed Bed Reactor: Tutorial and Sensitivity Analysis', *ACS Catalysis*, 5 May 2023, 6905–18, https://doi.org/10.1021/acscatal.3c01282.

- There are no corrosion issues.
- No harmful wastes from the catalysts are obtain.

However, there are also many drawbacks:

- Internal and external mass transfer limitation.
- Difficult control of the temperature.[54]

1.4.4 Reaction Mechanism in Heterogeneous Catalysis.

Considering a solid catalyst and gaseous reactants there are three mechanisms in heterogenous catalysis.

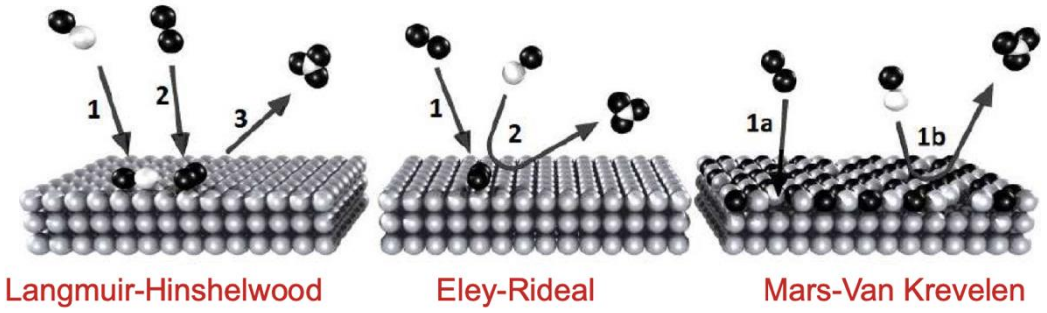

Figure 15. Reaction Mechanisms in Heterogenous Catalysis.

Langmuir was the first to describe how a bimolecular reaction takes place at the surface of the catalyst.

[54] Moisés R. Cesário et al., 'Understanding Heterogeneous Catalysis: A Brief Study on Performance Parameters', in *Heterogeneous Catalysis* (Elsevier, 2022), 1–18, https://doi.org/10.1016/B978-0-323-85612-6.00001-2.

Langmuir-Hinshelwood mechanism

In this mechanism the interaction involved is between two molecules or atoms that are absorbed at adjacent sites on the surface. So, both reactants are adsorbed on the surface of the catalyst, after the rection between the two, the product desorb from the surface of the catalyst.

Eley-Rideal mechanism

In this mechanism the interaction takes place as result of the collision between the gas molecules of one of the reactants and the adsorbed molecules of the other. So, a molecule adsorbs onto the surface and another molecule interacts with the adsorbed one, until a product is formed and desorbs from the surface.

Mars-Van Krevelen mechanism

There's also another mechanism proposed by Mars and van Krevelen and, according to this mechanism, it involves two consecutive steps.

In this mechanism one of the reagents is absorbed onto the surface of the catalyst becoming part of the catalyst surface. So, the surface becomes an active part in the reaction. The other molecule reacts directly from the gas phase with the catalyst surface, the product is formed and then desorbed.[55]

1.5 Aqueous Phase Reforming

The Aqueous Phase Reforming it's a catalytic reaction of biomass-derived oxygenated compounds in aqueous solution leading mainly Hydrogen and a range of organic compounds such as alkene production.[56] It has been a research area of interest due to its sustainable operations, in fact, under relatively mild reaction conditions (200 – 250 °C and 20 – 45 bar) it

[55] Yoo, 'Selective Gas-Phase Oxidation at Oxide Nanoparticles on Microporous Materials'.
[56] R D Cortright, R R Davda, and J A Dumesic, 'Hydrogen from Catalytic Reforming of Biomass-Derived Hydrocarbons in Liquid Water' 418 (2002): 4.

is obtained a successful catalytic conversion of highly diluted hydrocarbon streams into hydrogen and other valuable species.[57]

In the APR, the drying of the biomass or of the waste stream is not necessary for the valorization and, since drying process is one of the most energy intensive in the biomass conversion, it makes the process an efficient and cost-effective technique. There are also other advantages of the APR: first, it is preferred over other types of biomass-based Hydrogen production technologies (gasification, fermentation, etc.) due to its high H_2 selectivity at specific conditions; second, it is a highly adaptable process since the reaction conditions and the setup can be tuned to achieve specific goals and the key is the identification of the proper aspects as desired. [58] An example is through the catalyst design. So, in overall, the Aqueous Phase Reforming is a highly sustainable process.

The hydrogen production is not considered as exclusive because there are several competing reactions, like CO_2 methanation, alkenes and alcohols production.[59] Even though the formation of these by-products lowers the H_2 selectivity, it is not seen as a drawback but as an alternative to the Hydrogen production since these products can be used as fuels, as a base for other chemicals or even as a means of transport for H_2 itself.

The main drawback of the Aqueous Phase Reforming is the catalyst deactivation caused mainly by the carbonaceous deposit.[60] Therefore, the goal of the present work is to overcome this challenge, taking in consideration the use of bimetallic catalysts.

A reductive study of the reactions occurring in the APR it's necessary to better understand the proves. The two main reactions considered in this work are the same ones reported by Oliveira et al.[61] which are adapted to the production of hydrogen through the Aqueous Phase Reforming

---

[57] A.S. Oliveira et al., 'Continuous Aqueous Phase Reforming of a Synthetic Brewery Wastewater with Pt/C and PtRe/C Catalysts for Biohydrogen Production', *Chemosphere* 281 (October 2021): 130885, https://doi.org/10.1016/j.chemosphere.2021.130885.
[58] Yi Wei et al., 'Renewable Hydrogen Produced from Different Renewable Feedstock by Aqueous-Phase Reforming Process', *Journal of Sustainable Bioenergy Systems* 04, no. 02 (2014): 113–27, https://doi.org/10.4236/jsbs.2014.42011.
[59] Fasolini et al., 'A Short Overview on the Hydrogen Production Via Aqueous Phase Reforming (APR) of Cellulose, C6-C5 Sugars and Polyols', *Catalysts* 9, no. 11 (3 November 2019): 917, https://doi.org/10.3390/catal9110917.
[60] Oliveira et al., 'Continuous Aqueous Phase Reforming of a Synthetic Brewery Wastewater with Pt/C and PtRe/C Catalysts for Biohydrogen Production'.
[61] Oliveira et al.

of Maltose Monohydrate (MM) solution and the Water Gas Shift (WGS) reaction shown by the equations below.

$$C_{12}H_{24}O_{12} + 12\,H_2O \leftrightharpoons CO_2 + 24\,H_2$$

$$CO + H_2O \leftrightharpoons CO_2 + H_2$$

Concerning the formation of by-products (hydrocarbons mostly), H_2 and CO_2 react instantly (especially at low temperatures) forming alkenes and water.[62]

The Aqueous Phase Reforming reaction pathway can be summarized in the following steps:

1. Maltose Monohydrate is dehydrogenated on the active metal surface giving as result intermediate products before the C-C and C-O bonds' cleavage.
   1.1 Cleavage of C-C bond with the formation of H_2 and CO.
   1.2 H_2 and CO reacts through the WGS to produce CO_2 and H_2O.
   1.3 The CO left and the CO_2 produced react with H_2 to produce Hydrocarbons (mainly alkanes) and water through the Fischer-Tropsch reactions.
2. Dehydration reactions that lead to the C-O bond cleavage producing alcohols, catalyzed by the active metal catalyst.
3. Direct Hydrogenation/Dehydration of Maltose Monohydrate forming organic acids which, through the catalyst, produce alkanes.

To give a better representation on what has been described, in *Figure 14* the overall pathway is illustrated.

[62] Cortright, Davda, and Dumesic, 'Hydrogen from Catalytic Reforming of Biomass-Derived Hydrocarbons in Liquid Water'.

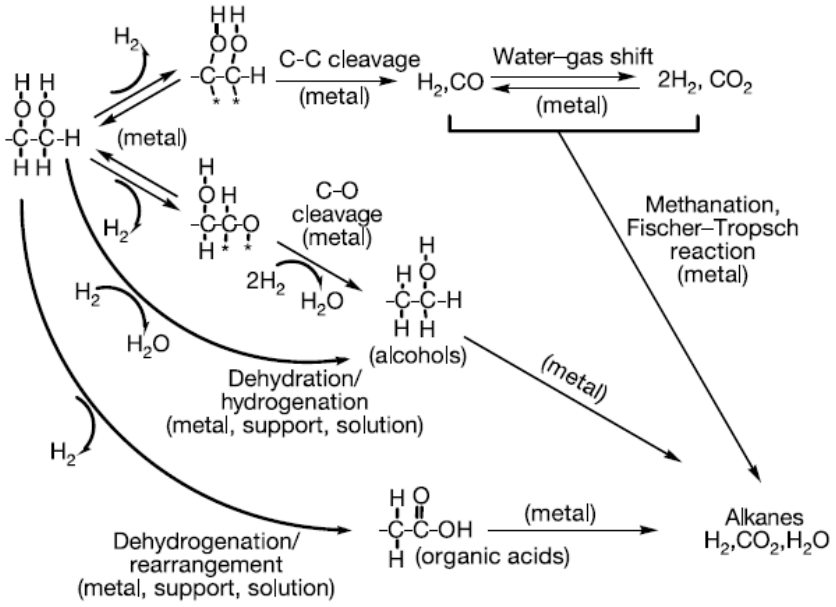

Figure 16. Reaction pathways for production of H_2 by reactions of oxygenated hydrocarbons with water. (Asterisk represents a surface metal site).

These are reforming reactions, endothermic reactions that require energy to be conducted.[63] An interesting correlation is that, increasing the temperature the dehydrogenation reactions are promoted and it delays the hydrogenation of CO_2 and other chemicals. However, if taken too far, this could enhance the C-C and C-O bond cleavage, promoting the alkenes formation.

1.5.1 Main Investigated Catalysts in APR

The catalytic activity plays a key role in the APR process. The catalyst should enhance the reforming reaction of the starting biomass and the water gas shift reaction, avoiding hydrogenation reactions of carbon oxides. In literature, the catalysts used for Methanol aqueous phase reforming are based on noble metals, like Platinum and Ruthenium, but also on non-noble metals such as Copper and Nickel. In general, the most used ones are Pt-based catalysts, in fact Platinum is very active and presents high selectivity towards hydrogen. However, it shows lower C-C cleavage compared to other noble metals like Ruthenium, for example. Metals like copper, instead, show high activity for the WGS reaction but no activity for breaking C-C

[63] Cortright, Davda, and Dumesic.

bond.[64] Probably, the use of bimetallic catalyst, rather than monometallic ones, would be the best choice since they're characterized of synergistic behavior that makes these catalysts superior to either monometallic component.

1.5.2 Monometallic Systems

Platinum is the most studied metal for APR reaction, it is the perfect combination between high activity and moderate selectivity. Davda et al. studied the C-C and C-O bond cleavages of ethanol by DFT on Pt and they report that (1) Pt-C bonds are more stable than Pt-O bonds and (2) the C-C cleavage should be faster than C-O cleavage because the energy for the transition state of the C-C bonds is one order of magnitude lower than C-O bonds so, the C-C cleavage is more favored than the C-O bond breaking. The authors also observed that the level of hydrogenation of intermediates also influence the breaking of the just mentioned bonds because of geometric and electronic effects and, also in agreement with other studies, the C-C breaking is favorable on Pt after several dehydrogenation steps and it's easier than the C-O cleavage. On Ruthenium, the activation energy for C-C cleavage is lower than on platinum, so it is more sensitive to the first dehydrogenation steps.[65] However, it is far more active towards methanation than Pt, decreasing the hydrogen selectivity.[66]

The decomposition of glycerol has been explored on Pt, Pd, Rh, Cu through the hydroxyl groups focusing on dehydrogenation, C-C and C-O cleavage and it has been reported that C-C breaking is favorable on Pt after several dehydrogenation steps, and it is easier than C-O breaking. The pathway is similar on Pd, but the lowest C-C scission transition state energy is higher than on Pt, suggesting that Pt is more active. Despite dehydrogenation is always necessary, the situation is different on Rh and Ni, where the energies between C-C and C-O are more comparable. Moreover, the transition states are quite low in terms of activation energy, explaining the

[64] R.R. Davda et al., 'A Review of Catalytic Issues and Process Conditions for Renewable Hydrogen and Alkanes by Aqueous-Phase Reforming of Oxygenated Hydrocarbons over Supported Metal Catalysts', *Applied Catalysis B: Environmental* 56, no. 1–2 (March 2005): 171–86, https://doi.org/10.1016/j.apcatb.2004.04.027.
[65] Cheng-chau Chiu, Alexander Genest, and Notker Rösch, 'Decomposition of Ethanol Over Ru(0001): A DFT Study', *Topics in Catalysis* 56, no. 11 (August 2013): 874–84, https://doi.org/10.1007/s11244-013-0051-0.
[66] M.A. Vannice.'The Catalytic Synthesis of Hydrocarbons from H2/CO Mixtures over the Group VIII Metals'. Journal Of Catalysis 50, 228-2236 (1977)'.

experimentally known high activity of Ni despites its low selectivity. Finally, on Cu the transition states show high activation energy, highlighting the low Cu activity.[67]

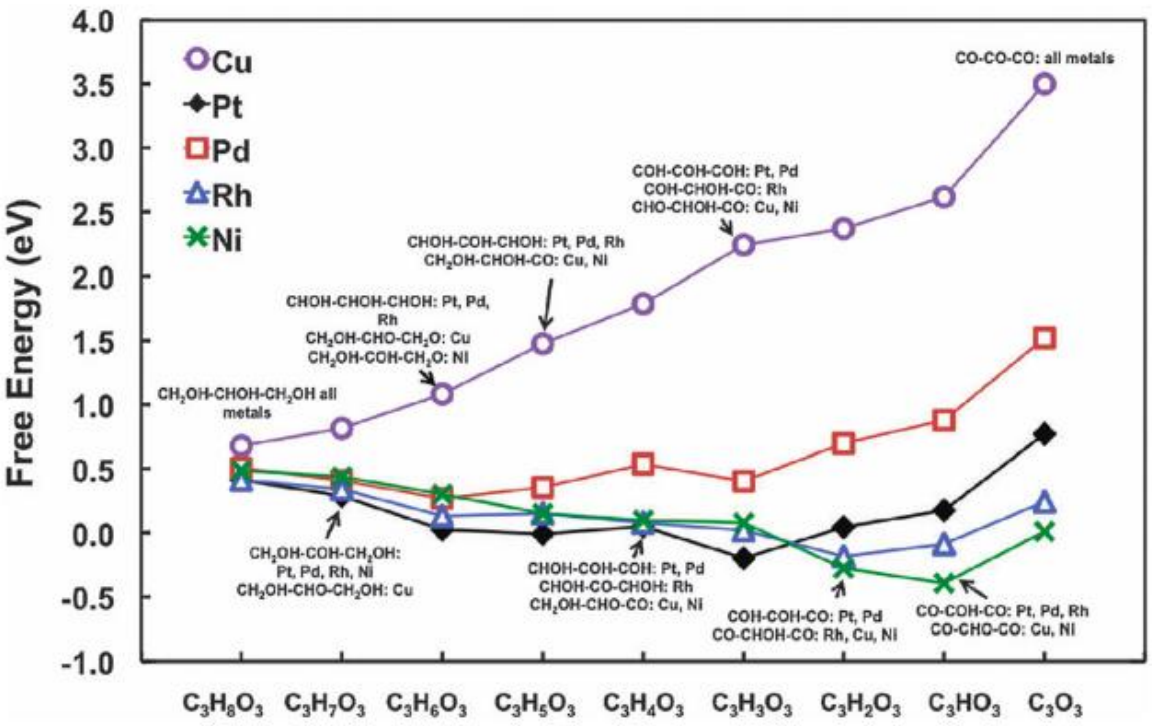

Figure 17. Free energies of glycerol dehydrogenation on Pt (black diamonds), Pd (brown squares), Rh (blue triangles), Cu (purple circles) and Ni (green crosses).

Davda et al. also investigated the performances of Ni, Ru, Rh and Pd supported on silica for ethylene glycol APR and promising ability for Pt to produce hydrogen are reported, while Pd showed low activity but highest selectivity. Concerning the non-noble metals, Nickel was comparable to Pd, but suffered from low selectivity, that means high alkene production, so it was more prone to deactivation. The use of cheap material, such as Ni, would increase the cost-effectiveness of the process. However, its low stability and H_2 TOF, which is much lower than Pt, would impede its utilization in a larger scale context.[68]

[67] Bin Liu and Jeffrey Greeley, 'A Density Functional Theory Analysis of Trends in Glycerol Decomposition on Close-Packed Transition Metal Surfaces', *Physical Chemistry Chemical Physics* 15, no. 17 (2013): 6475, https://doi.org/10.1039/c3cp44088e.

[68] R.R. Davda et al., 'Aqueous-Phase Reforming of Ethylene Glycol on Silica-Supported Metal Catalysts', *Applied Catalysis B: Environmental* 43, no. 1 (June 2003): 13–26, https://doi.org/10.1016/S0926-3373(02)00277-1.

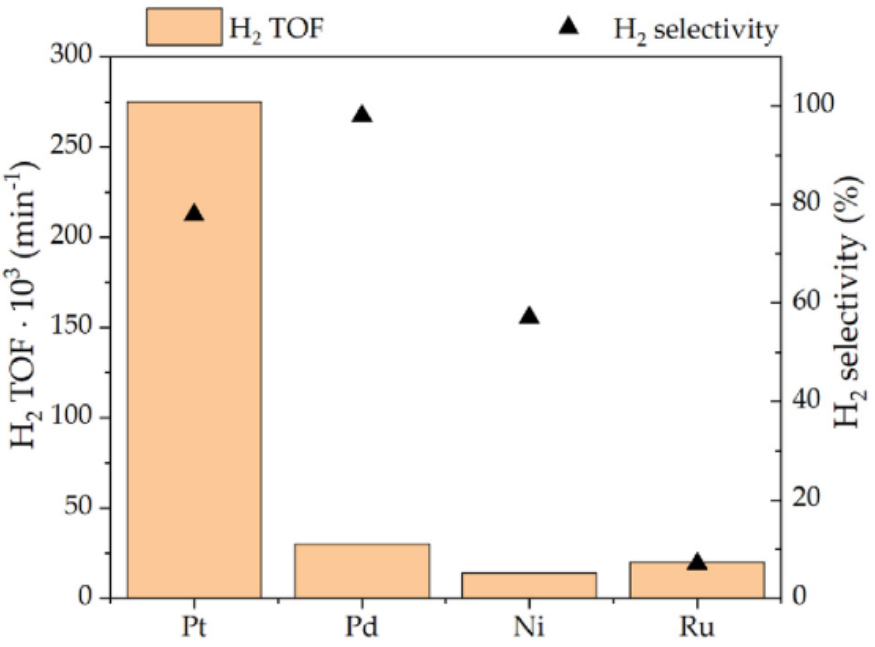

Figure 18. APR of ethylene glycol. (Reaction conditions: 225 °C 22 bar, 10 wt% ethylene glycol solution, 0.06 mL/min.) [69]

1.5.3 Bimetallic Systems

Bimetallic catalysts perform better than monometallic in many fields and APR is part of them. Since Pt and Pd showed the best performance in monometallic systems a lot of Pt and Pd bimetallic catalysts were screened in APR of different biomass.

Godina et al. investigated the APR of xylitol over mono and bimetallic catalysts. Among the Pt-based bimetallic ones, Pt-Re showed the highest conversion at each weight hourly space velocity (WHSV) investigated. This outcome was related to the higher WGS, promoted by Re. low amount of erythritol was found in the liquid phase, suggesting that C-O cleavage was favored over C-C, while Pt-Re mostly led to butane and propane. Because of the lower hydrogen selectivity of the bimetallic system than the monometallic one, the hydrogen turnover frequency of the former, 23 min^{-1}, was lower than the latter, 26 min^{-1} at WHSV 9.5 h^{-1}.[70]

[69] Davda et al.
[70] Lidia I. Godina et al., 'Sibunit-Supported Mono- and Bimetallic Catalysts Used in Aqueous-Phase Reforming of Xylitol', *Industrial & Engineering Chemistry Research* 57, no. 6 (14 February 2018): 2050–67, https://doi.org/10.1021/acs.iecr.7b04937.

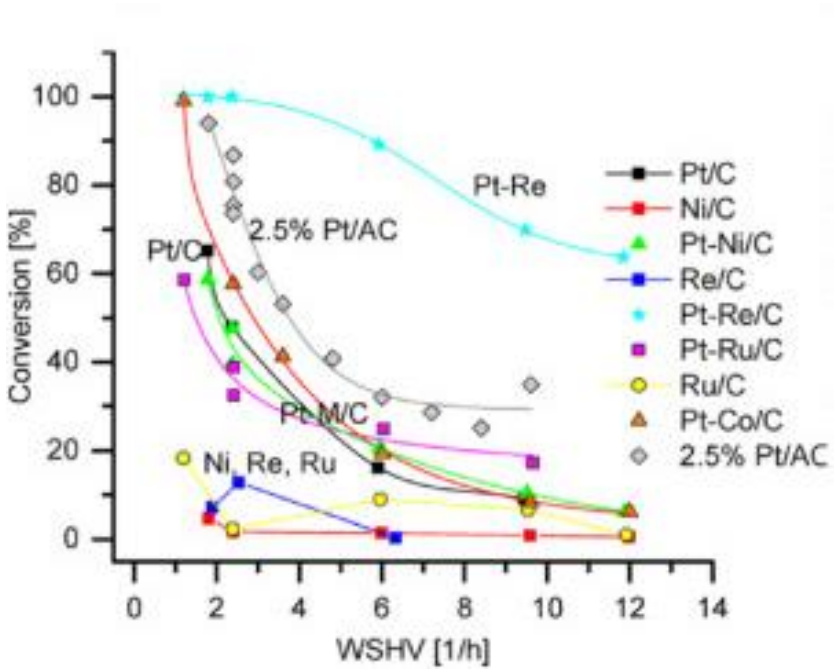

Figure 19. Conversion of xylitol in APR carbon-supported catalysts as function of WHSV. Xylitol concentration 100 g/L; T=498 K; P=29.7 bar; catalyst mass 0.5 g.[71]

Guo et al. investigated the APR of glycerol on different Pt-based catalysts supported on γ-Al_2O_3 and the promoters were Ni, Co, Fe and Cu. Iron showed the highest carbon conversion to gas and hydrogen yield with 1:1 atomic ratio, this metal promoted the water activation producing OH groups that can react with the CO adsorbate on Pt. These results were confirmed by WGS tests that shows consistent results with the APR tests and it leads to the understanding of how the WGS has a strong influence of the overall results.[72]

Dosso et al. studied bimetallic Pt based catalysts promoted with Ni or Co for APR of polyols derived from glucose degradation. Pt and Ni are completely miscible, and this occurrence affected the electronic properties of Pt reducing the binding of adsorbate. X-ray photoelectron spectroscopy showed that Pt was mainly in the oxidized state, likely because of the donation of electrons (Fig.20 A). The interaction of Pt with Co and Ni was suggested by the presence of a broad peak in the H_2-TPR as depicted in Figure 20 B. Pt-Ni showed higher yield than Pt-Co and, being the Ni not active for WGS, a high selectivity towards CO was observed. Moreover, it was found a higher presence of coke on Pt-Ni compared to Pt-Co, not directly explained sue

[71] Godina et al.
[72] Yong Guo, Xiaohui Liu, and Yanqin Wang, 'Catalytic and DRIFTS Studies of Pt-Based Bimetallic Alloy Catalysts in Aqueous-Phase Reforming of Glycerol', *Industrial & Engineering Chemistry Research* 58, no. 8 (27 February 2019): 2749–58, https://doi.org/10.1021/acs.iecr.8b05774.

to its limited higher activity. No direct comparison with the monometallic could be performed because the authors used different preparation techniques.[73]

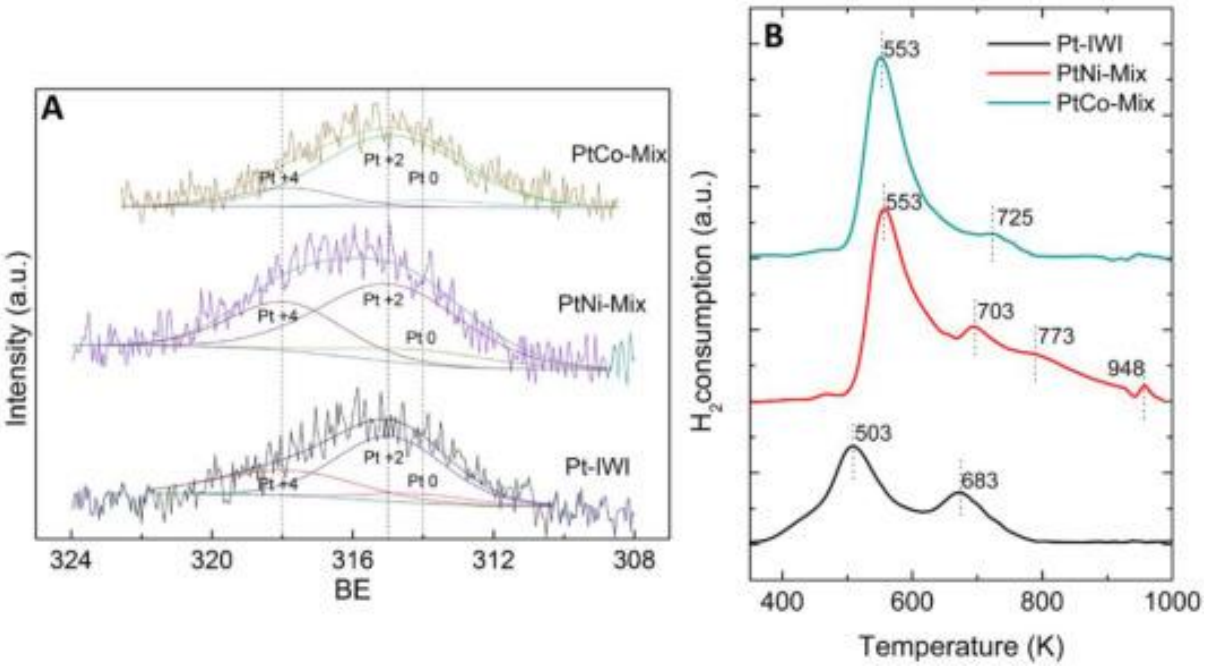

Figure 20. A: XPS spectrum; B: H2-TPR of the reduced catalysts.[74]

Larimi et al. investigated other promoters, with particular attention on Pt-Rh supported on γ-Al_2O_3. In this case, while the conversion was approximately constant, the hydrogen selectivity was minimum for monometallic Pt and maximum for Pt-Rh. It was suggested that Rh helped the WGS, increasing, at the same time, the mobility, and the reactivity of surface oxygen atoms.[75] The addition of Rh can have different effects on different supports. When added to Pt/α-alumina both the hydrogen yield and the stability increases, by preventing the coke formation. On the other hand, Pt/γ-alumina's performance was negatively influenced by Rh, with a slight decrease of the hydrogen yield.[76]

[73] Liza A. Dosso, Carlos R. Vera, and Javier M. Grau, 'Aqueous Phase Reforming of Polyols from Glucose Degradation by Reaction over Pt/Alumina Catalysts Modified by Ni or Co', *International Journal of Hydrogen Energy* 42, no. 30 (July 2017): 18853–64, https://doi.org/10.1016/j.ijhydene.2017.06.100.
[74] Dosso, Vera, and Grau.
[75] Afsanehsadat Larimi and Farhad Khorasheh, 'Renewable Hydrogen Production over Pt/Al_2O_3 Nano-Catalysts: Effect of M-Promoting (M=Pd, Rh, Re, Ru, Ir, Cr)', *International Journal of Hydrogen Energy* 44, no. 16 (March 2019): 8243–51, https://doi.org/10.1016/j.ijhydene.2019.01.251.
[76] Éder V. Oliveira, Ana C. M. Seixas, and Elizabete Jordão, 'Performance of Pt and Pt-Rh Catalyst in the Hydrogen Production from Glycerol', *The Canadian Journal of Chemical Engineering* 95, no. 10 (October 2017): 2018–23, https://doi.org/10.1002/cjce.22826.

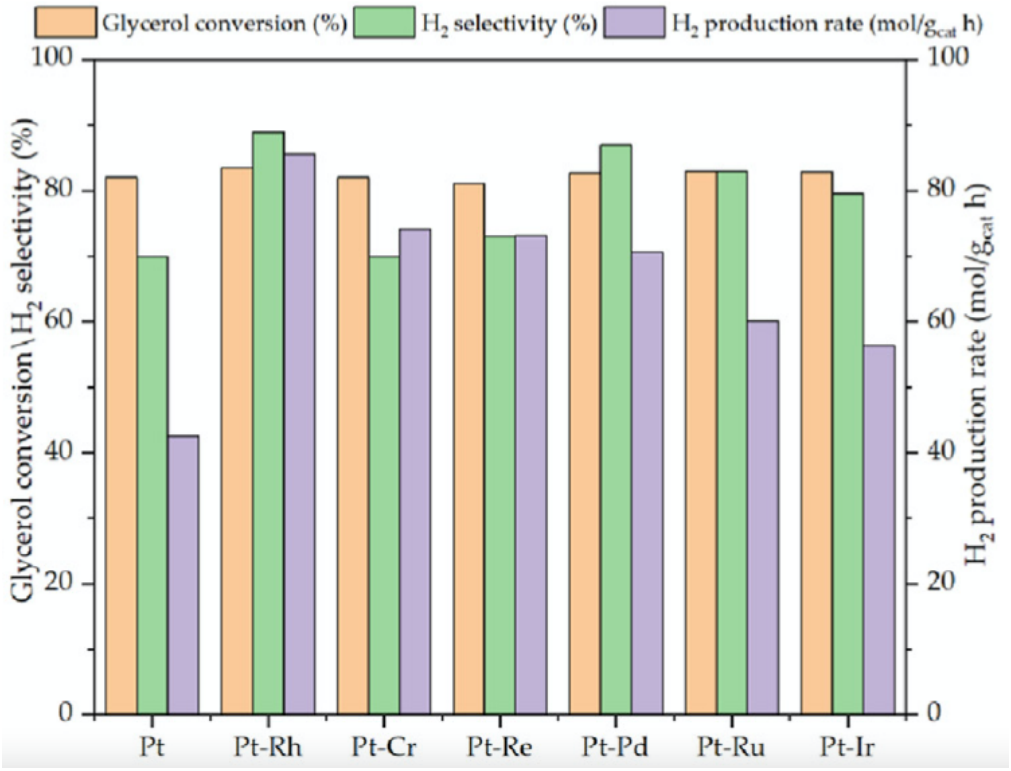

Figure 21. Performance of Pt-based catalyst with different promoters. (Reaction conditions: 250°C/50 bar, 0.25 g catalyst, WHSV 2.45 h^{-1}) [77]

As last example, Lei et al. used atomic layer deposition to modify Pt/alumina catalysts by ZnO promotion. Higher hydrogen production was obtained when Pt was deposited before than Zn. This is because it took advantage of the two interfaces Pt-ZnO and Pt-Al2O3. Thanks to X.ray adsorption near edge structure (XANES) spectroscopy, the authors suggested that the significant charge transfer from Zn to Pt promoted the H_2 selectivity. Moreover, the bimetallic system showed only limited sintering, the particle size increased from 0.9 nm to 1.2 nm, contrarily to the monometallic catalyst which was affected by an increase of particle size from 1 nm to 2.4 nm.[78]

In overall, the positive impact is commonly associated to the promotion of the water gas shift reaction while, the typical drawback is that the increase of conversion is partially counterbalance by a decrease of hydrogen selectivity, since methanation is promoted as well.[79]

[77] Larimi and Khorasheh, 'Renewable Hydrogen Production over Pt/Al_2O_3 Nano-Catalysts'.
[78] Yu Lei et al., 'Combining Electronic and Geometric Effects of ZnO-Promoted Pt Nanocatalysts for Aqueous Phase Reforming of 1-Propanol', *ACS Catalysis* 6, no. 6 (3 June 2016): 3457–60, https://doi.org/10.1021/acscatal.6b00963.
[79] Giuseppe Pipitone et al., 'A Critical Review on Catalyst Design for Aqueous Phase Reforming', *International Journal of Hydrogen Energy* 47, no. 1 (January 2022): 151–80, https://doi.org/10.1016/j.ijhydene.2021.09.206.

The support effect and metal particle size effect, which are often intertwined, are two critical factors influencing the activity of a supported metal catalyst. The interaction between metals and support are known to be very sensitive to the particle size of the metal as well.

1.5.4 Influence of the particle of size

The size effect is often seen in the range of 1-10 nm, where the fraction of surface atoms with low coordination number increases drastically increasing the size.[80] Increasing the particle size implies that the number of face atoms increases, while the number of edges and corner atoms decreases. In the APR field there are not so much information related to if small or big nanoparticles influence the amount of hydrogen produced.[81] The first dependence was reported by Lehnert and Claus: increasing the particle size, the hydrogen selectivity increases, without affecting the conversion. It means that higher amount of face atoms allows favorable adsorption of oxygenated compound for the C-C cleavage.[82]

[80] Yong-Xiao Tuo et al., 'Insight into the Support Effect on the Particle Size Effect of Pt/C Catalysts in Dehydrogenation', *Journal of Catalysis* 360 (April 2018): 175–86, https://doi.org/10.1016/j.jcat.2018.02.001.
[81] Pipitone et al., 'A Critical Review on Catalyst Design for Aqueous Phase Reforming'.
[82] Kerstin Lehnert and Peter Claus, 'Influence of Pt Particle Size and Support Type on the Aqueous-Phase Reforming of Glycerol', *Catalysis Communications* 9, no. 15 (September 2008): 2543–46, https://doi.org/10.1016/j.catcom.2008.07.002.

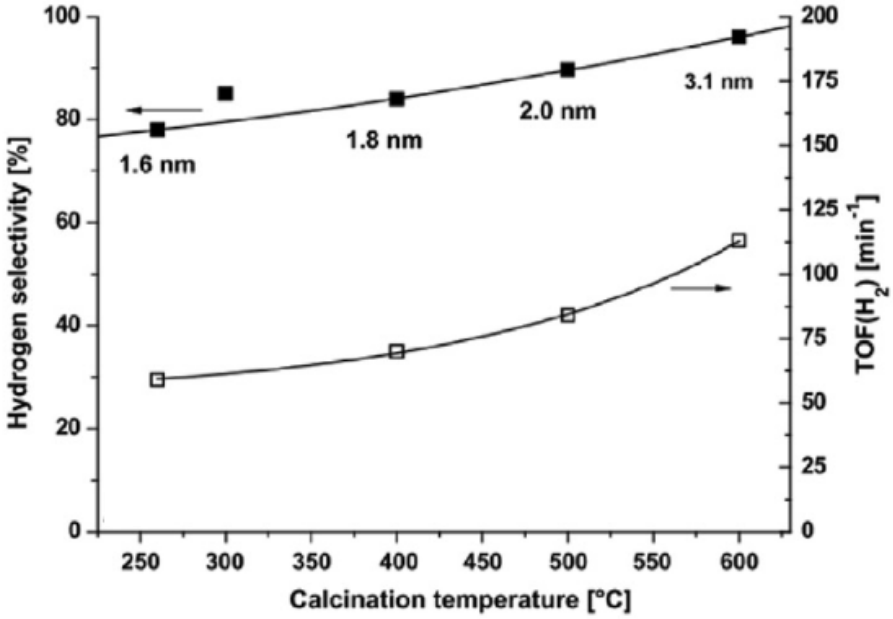

Figure 22. Influence of particle size on APR performance. Blank squares TOF for hydrogen production, full squares TOF for hydrogen selectivity.[83]

However, Wawrzets et al., being still in agreement on the fact that the conversion was slightly affected by the particle size, they report that the hydrogen selectivity is higher for smaller particles: having smaller particles means highly coordinatively unsaturated metal atoms and, as consequence, higher concentration of metal atoms at support-metal boundary.[84]

[83] Lehnert and Claus.

[84] A. Wawrzetz et al., 'Towards Understanding the Bifunctional Hydrodeoxygenation and Aqueous Phase Reforming of Glycerol', *Journal of Catalysis* 269, no. 2 (5 February 2010): 411–20, https://doi.org/10.1016/j.jcat.2009.11.027.

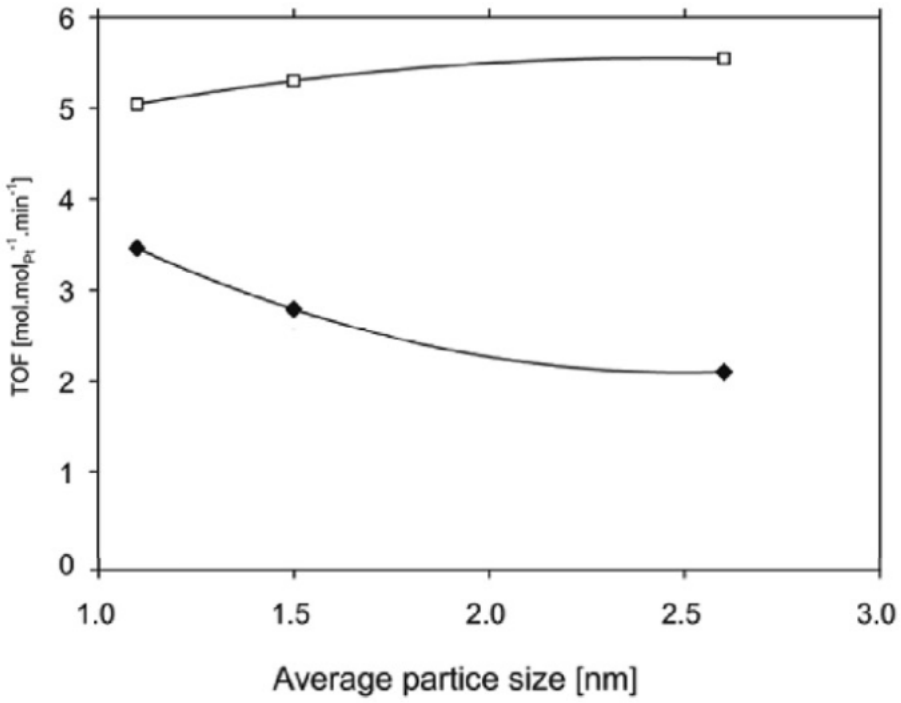

Figure 23. Influence of particle size on APR performance. Blank squares TOF for glycerol conversion, full squares TOF for hydrogen production.[85]

Effect of the support

Supports can not only afford a huge surface to disperse active metal particles but also interact substantially with the metal particles deposited onto it, therefore it provides stronger metal-support interaction. In the case of APR reaction, the nature of the support is considered a mean for tuning the H_2 production. The support, in fact can affect the hydrogenation sites due to its electronegativity, because of its acid-base properties. Shabaker et al. analyzed different supports for Pt-based catalyst, and it emerged that the ranking at 225°C was:

$$TiO_2 > Carbon > Al_2O_3 > ZrO_2 > CeO_2, ZnO, SiO_2$$

With Al_2O_3, ZrO_2 and TiO_2 showing the highest hydrogen selectivity.[86]

[85] Wawrzetz et al.
[86] J W Shabaker et al., 'Aqueous-Phase Reforming of Ethylene Glycol Over Supported Platinum Catalysts', n.d.

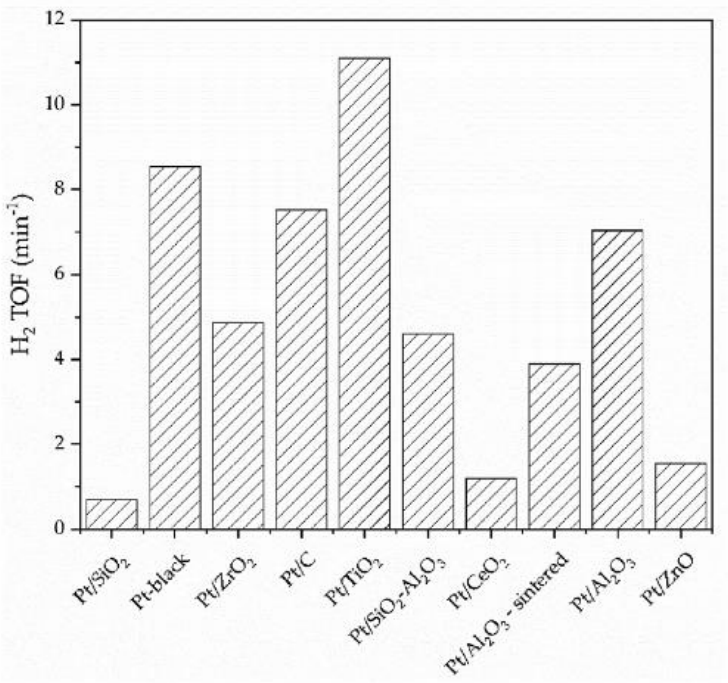

Figure 24. Influence of the support on APR of ethylene glycol.[87]

In other studies, Zirconia was explored alone in the APR the result was higher production of coke than Pt-based catalysts, indicating that the metal plays an important role in preventing the deactivation of the catalyst.[88] In overall, the acid-base properties and the reducibility were mostly investigated since they're directly involved in the WGS which is a key step to promote the hydrogen yield.

[87] Shabaker et al.

[88] Kamila Koichumanova et al., 'In Situ ATR-IR Studies in Aqueous Phase Reforming of Hydroxyacetone on Pt/ZrO2 and Pt/AlO(OH) Catalysts: The Role of Aldol Condensation', *Applied Catalysis B: Environmental* 232 (September 2018): 454–63, https://doi.org/10.1016/j.apcatb.2018.03.090.

2. Scope

Although APR may be considered more suitable for processing dilute side streams than gasification, there are few studies using this type of streams as feedstock. For this reason, in different research brewery wastewater has been proposed as feedstock for treatment through the APR.

In 2019, the first paper concerning the APR of a brewery wastewater was published. Platinum catalysts supported on different carbon materials, have been tested at temperatures of 473 and 498 K with the aim of evaluating the effects of the supports and the organic load of the wastewater. With Pt/C catalysts tested, APR led to high TOC and COD removal with significant differences between the catalysts depending on the carbon support used. The highest values of gas production were obtained using as support a non-microporous commercial carbon black at 498 K, probably because of the basic character and the mesoporous texture of the support. The organic load expressed as COD of the starting wastewater has a significant influence on the catalytic performance and results of APR in fact, at the lowest wastewater concentration TOC and COD removal values up to 99% were obtained, while at the highest concentration, these values were reduced dramatically to 51%. This indicates that APR can be a promising technology for biomass-derived wastewater through the production of H2 and alkanes.[89]
For this reason, Oliveira et al., the same group research, in 2021 investigated continuous APR of synthetic brewery wastewater with Pt/C and PtRe/C catalysts to produce biohydrogen, using 228 °C and 28 bar as temperature and pressure, respectively, and argon as carrier gas. The main scope of this study is to optimize the reaction conditions, based also on the previous work done in the same field. In fact, in this case, the influence of the weight hourly space velocity and the superficial Ar gas flow velocity were assessed and the hydrogen production was found to be higher using the bimetallic catalyst at the lowest WHSV ($0.03 h^{-1}$) and at the highest V_{Ar} (0.8 cm s^{-1}). The maximum of H_2 production increased with decreasing WHSV and increasing $V_{Ar.}$ The catalysts showed deactivation, attributed to the deposition of solids on the catalyst surface.[90] Later, hydrogenation of maltose has been evaluated as an approach to increase the suitability of brewery wastewater as feedstocks for APR and H_2 production. This strategy was

[89] A.S. Oliveira et al., 'Production of Hydrogen from Brewery Wastewater by Aqueous Phase Reforming with Pt/C Catalysts', *Applied Catalysis B: Environmental* 245 (May 2019): 367–75, https://doi.org/10.1016/j.apcatb.2018.12.061.
[90] Oliveira et al., 'Continuous Aqueous Phase Reforming of a Synthetic Brewery Wastewater with Pt/C and PtRe/C Catalysts for Biohydrogen Production'.

chosen because lower H2 yields amd selectivity have been reported in the APR of sugars. In the hydrogenation stage, sugars can be converted to more reduced compounds which react more selectively to H_2 and CO_2 in the APR stage. So, the combination of the hydrogenation and APR could improve the hydrogen production in sugar-based feedstocks. In the APR of maltose, after 48 h TOS and at 225°C, a significant catalysts deactivation and increase of pressure was observed, probably due to the formation of carbonaceous deposits on the catalyst surface and on the reactor's walls. In contrast, in the APR of maltiol, lower deactivation was observed meaning that undesirable reactions in the liquid phase are less favored. Conversion of the initial feedstock to gas phase was higher in the APR of maltose, however, higher H_2 selectivity, yield and TOF were achieved in the combined hydrogenation and APR than the APR of maltose. So, the overall process can be considered efficient because an increase in H_2 production compensated for the consumption in hydrogenation, also achieving the increase of the catalyst durability.[91]

Industries producing large volumes of wastewater, like the brewing plants, are interesting candidates for the treatment of wastewater by APR. The brewing industry generates 3 to 10 L of wastewater per liter of beer produced that needs to be disposed-off or safely treated for reuse which is often costly and problematic for most breweries. Due to the wide variety of techniques and ingredients used by breweries, as well as the process itself, the composition of the brewery is not constant and even small factors like equipment, cleaning products or additives can have an influence. For this reason, is better to focus on the characteristic of the stream rather than on the composition. The main characteristic of the waste stream is the higher oxygen chemical demand (COD), which describes the amount of oxygen required to breakdown the contaminating agents from a chemical perspective, than the biological chemical demand (BOD), the amount of oxygen required to breakdown the organic pollutants via biological ways. This means that, opposite to what might have been expected, since brewery wastewater (SBW) is a by-product of the beverage process, chemical processes are more efficient than any other biological mean, to remove these pollutants. The components of the SBW are Maltose extract, yeast extract, peptone, maltose, ammonium sulphate, ethanol, sodium sulphate and disodium

[91] A.S. Oliveira et al., 'Enhanced H2 Production in the Aqueous-Phase Reforming of Maltose by Feedstock Pre-Hydrogenation', *Applied Catalysis B: Environmental* 281 (February 2021): 119469, https://doi.org/10.1016/j.apcatb.2020.119469.

sulphate.[92] Maltose has been chosen as feedstock for the aqueous phase reforming reaction, since it is the main component of the brewery wastewater.

The goal of the present work is to investigate the main challenges hindering the optimal operation of the APR reaction applied to a biomass-based waste stream, such as the maltose-based wastewater. As already evaluated in the paragraph 1.5.1 (Main catalysts used in the APR reaction) the most relevant obstacles are connected to the catalytic activity. The most used catalysts have been monometallic ones, supported on different types of support like silica, titania, zirconia or activated carbon but, all of them present deactivation issues, mainly due to the blockage of the active sites. As suggested by the last research, the alternative way to perform this kind of reaction, in order to have a balance between high hydrogen production and good catalytic activity, may be the use of bimetallic catalysts, again, using supports which showed the optimal synergistic effect with the metal nanoparticles.

So, following this line, also according to the primary research done in this area by Oliveira et al,[93] the main objectives of the thesis concern first, the design and the synthesis of the catalyst. The preparation of the heterogeneous catalysts used in this research activity takes place by *sol immobilization* in aqueous solution, the system thus obtained takes the name of nanostructured catalyst. Monometallic catalysts are widely used in APR due to their high hydrogen selectivity shown, however, bimetallic catalysts have been found to achieve better activity than monometallic ones.[94] [95] Therefore, in this work also bimetallic systems were synthetized, with the same method and with different ratios between the metals. The aim is to compare the catalytic activity between the different systems depending on the production of hydrogen.

Besides the Hydrogen selectivity, also the alkene selectivity is evaluated through HPLC analysis. The liquid phase resulting from APR was analyzed to identify the main reaction products which are mainly C-C_8 alkenes. Considering the reaction pathway (*figure 14*) and based on what has been reported in literature, alkene selectivity can be favored and controlled by promoting the C-O cleavage and hydrogenation reactions.[96] However, it must be taken in

---

[92] Adhena Ayaliew Werkneh, Hayelom Dargo Beyene, and Abduljeleel A. Osunkunle, 'Recent Advances in Brewery Wastewater Treatment; Approaches for Water Reuse and Energy Recovery: A Review', *Environmental Sustainability* 2, no. 2 (June 2019): 199–209, https://doi.org/10.1007/s42398-019-00056-2.

[93] Oliveira et al., 'Enhanced H2 Production in the Aqueous-Phase Reforming of Maltose by Feedstock Pre-Hydrogenation'.

[94] Davda et al., 'Aqueous-Phase Reforming of Ethylene Glycol on Silica-Supported Metal Catalysts'.

[95] Godina et al., 'Sibunit-Supported Mono- and Bimetallic Catalysts Used in Aqueous-Phase Reforming of Xylitol'.

[96] Oliveira et al., 'Continuous Aqueous Phase Reforming of a Synthetic Brewery Wastewater with Pt/C and PtRe/C Catalysts for Biohydrogen Production'; Cortright, Davda, and Dumesic, 'Hydrogen from Catalytic Reforming of Biomass-Derived Hydrocarbons in Liquid Water'.

consideration that both mentioned routes are hydrogen-consuming reactions, and this would lower the H_2 production considerably. Therefore, this should be considered a short-term sustainable solution for biomass conversion.

In overall, the purpose of this work is to prepare and to characterize Platinum, Palladium and Copper-based nanostructured catalysts monometallic and bimetallic, with different metal ratio, supported on TiO_2. The as-prepared materials were tested in the APR reaction of Maltose employing a continuous flow reactor to evaluate the catalytic activity in terms of Hydrogen production (gas phase analysis with GC apparatus) and the formation of by-products in liquid phase (HPLC analysis). Moreover, the reaction setup was improved to guarantee the constant presence of aqueous phase on the fixed bed reactor and therefore better evaluate the obtained results outcome.

3. Experimental Section

The entire research was conducted at the Industrial Catalysis Laboratory of the TU Delft.

3.1 Solvents and Reagents

For APR reaction and for catalysts' synthesis the following materials have been used: Maltose Monohydrate ($C_{12}H_{22}O_{11} \cdot H_2O$), Sodium Borohydride ($NaBH_4$), Titanium Dioxide P25 (TiO_2), Hexachloroplatinic(IV) acid hexahydrate ($H_2PtCl_6 \cdot 6\,H_2O$), Copper(II) nitrate hemi(pentahydrate) ($Cu(NO_3)_2 \cdot 2.5\,H_2O$), Potassium hexachloropalladate (IV) (K_2PdCl_6), Polyvinyl alcohol (PVA).
For HPLC analysis, according to Oliveira et al., the expected products are Glucose ($C_6H_{12}O_6$), Sorbitol ($C_6H_{14}O_6$), 1-2 Propanediol ($C_3H_8O_2$), Ethanol (C_2H_6O), Propanol (C_3H_8O), Ethylene Glycol ($C_2H_6O_2$), Formaldehyde (CH_2O), Acetaldehyde (C_2H_4O), DL-Lactic Acid($C_3H_6O_3$), Acetic Acid ($C_2H_4O_2$).

3.2 Aqueous Phase Reforming setup and operating procedure

The APR setup is in Box 7 of the Industrial Catalysis Lab of TU Delft. The setup consists of three independent fixed bed reactors which can operate at their own pressure and temperature, but only one of the three reactor is used for the analysis. The experiments are conducted at 225°C and, the best performing catalysts are also tested at 175 °C and at 200 °C. The reactors are heated externally, and the operating temperature is monitored through a thermocouple located outside the stainless-steel reactor tube, but in close contact to it. A constant operating pressure of 44 bar was set based on what is explained on section 1.5. A constant feed of 0.060 ml/min of 1% maltose monohydrate solution is chosen as liquid phase flow for each experiment. Based on the conclusions of similar research experiments, 25 ml/min of N_2 was feed with the liquid phase, operating as inert gas carrier. A simplified version of the flow diagram is shown in Figure 25, supported by Table 1, which provides the list of the equipment and instrumentation, with its corresponding abbreviation.

Equipment			*Instrumentation*		
Abbreviation	Equipment	Control	Abbreviation	Valve	Control
FT1	Feedstock tank	Manual	**GV1**	[N_2] gas valve	Automatic
FP1	Feedstock pump	Automatic	**GV2**	[H_2] gas valve	Automatic
R1	Reactor 1	Automatic	**GV R1**	R1 gas control valve	Automatic
R2	Reactor 2	Automatic	**GV R2**	R2 gas control valve	Automatic
R3	Reactor 3	Automatic	**GV R3**	Reactor 3 gas control valve	Automatic
C1	Condenser	Manual	**GPV1**	Gas pressure valve	Automatic
LBB1	Liquid by-product beaker	Manual	**BV1**	By-pass valve	Automatic
WC1	Water cooler	Manual	**SPV**	Liquid Pressure valve	Manual
GC	Gas Chromatograph	Automatic	**LV R1**	R1 liquid control valve	Automatic
-	Hot Box	Automatic	**LV R2**	R2 liquid control valve	Automatic
			LV R3	R3 liquid control valve	Automatic
			BPR1	Back pressure regulator 1	Manual
			BPR2	Back pressure regulator 2	Manual
			BPR3	Back pressure regulator 3	Manual
			VS	Valve switch	Automatic

Table 1. Equipment and Instrumentation

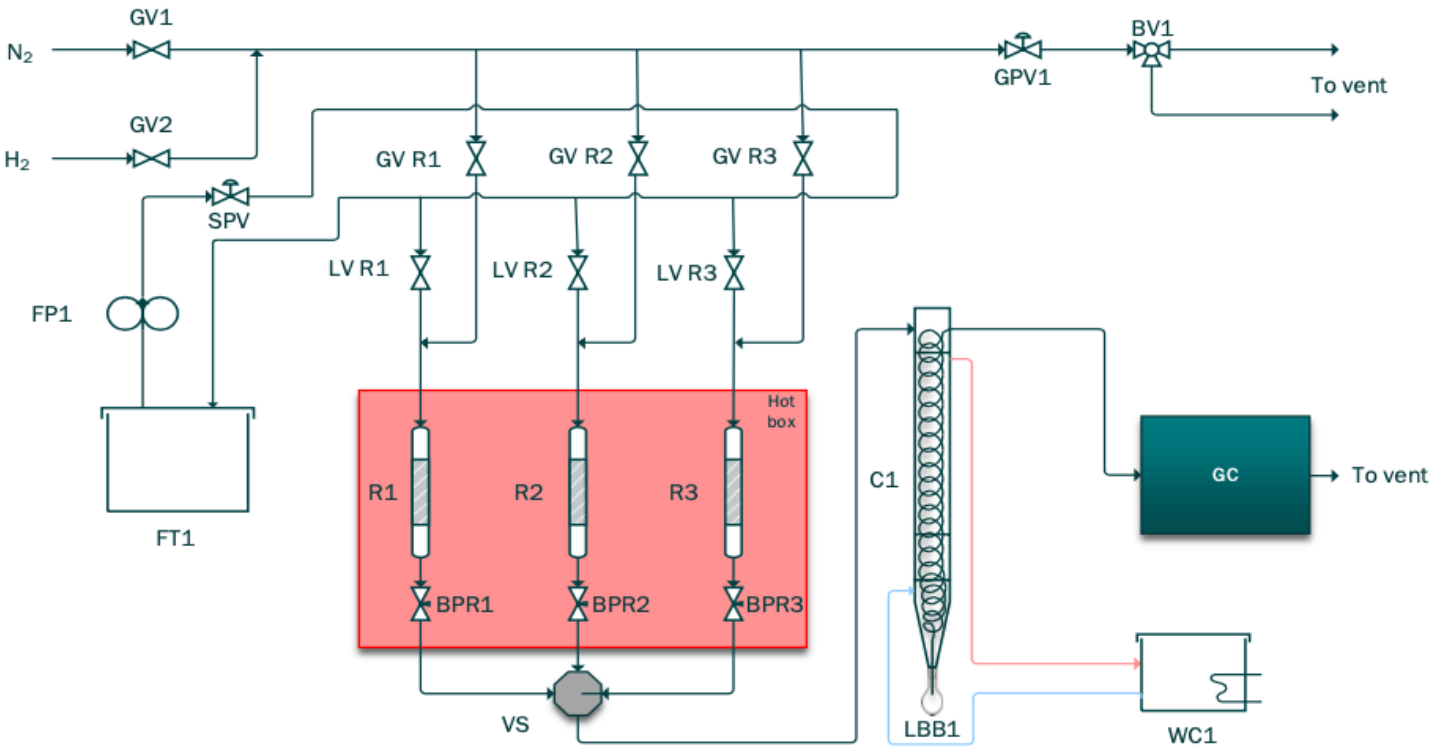

Figure 25. APR Setup.

Each experiment consists of four main stages which are, catalyst loading, in-situ reduction, aqueous phase reforming reaction and catalyst recovery.

1) ***Catalyst loading***: The stainless-steel tube reactor (length 29.6 cm, internal diameter 0.4 cm) is filled with a steel string for support, quartz wool and 200 mg of catalyst reduced in pellets. Then, GV1 is open and set at 900 ml/min of N_2, followed by opening and setting GV R3 with 300 ml/min flow. At this point, a leak test is performed using snoop liquid leak detector at all tube connections. In case any leaks are found, the connections are tightened and checked again.
2) ***In-situ reduction***: N_2 flow is shut down by setting GV1 to zero and H_2 flow is enable by setting GV2 to 30 ml/min followed by setting the pressure of the gas feed to 2 bar through the GPV1. The catalyst reduction is conducted by heating the reactor tubes at 300°C, setting GV R3 to 25ml/min. These conditions are kept for 2 hours. Once the reduction is finished, the temperature on the reactor is set to 0°C letting the system cool down.
3) ***Post-reduction***: After the reduction and cooling to room temperature the H_2 flow and the pressure of the gas feed are set back to zero. Then, the N_2 flow valve is opened and

set at 330 ml/min and, after a minute also the pressure of the gas feed is set to 47.5 bar. 300 ml/min is set on GV R3 and the steel handle needle valve, placed at the back pressure regulator, is closed. When the reactor reaches the pressure 44 bar, the N_2 flow and the GV R3 are set to 10 ml/min. Here, another leak test at the inlet and the outlet of the reactor is performed.

4) ***APR reaction***: If there are no leaks, the flow rate of N_2 is maintained to 10 ml/min while a setpoint of zero is given to GV R3. The system is then depressurized slowly using the steel handle needle valve on the BPR. The feedstock is ready to enter in the reactor, so the valve of the liquid injection system is opened, and the pump (FP1) is set to 1 ml/min. To pressurize the reactor with the liquid phase, the steel handle needle valve is closed. Once the pressure of 44 bar in the reactor is reached, the liquid flow rate is lowered at 0.060 ml/min and the GV R3 is set to 10 ml/min. After the stabilization of the system, the desired temperature is applied, and the GC sequence can start. During the reaction, the switched valve (SV) enables the samples to be fed to the condenser (C1) which is constantly cooled by a recirculating flow of water at 2°C-5°C cooled by a water cooler (WC1). The role of the condenser is to behave as a water trap to prevent it from getting into the GC. The water is collected inside a round bottom flask (LBB1).
5) ***Post-reaction***: The separated products and by-products are analyzed by a Gas Chromatograph with FID and TCD online detectors, programmed to continuously measure and store the results from the reaction. The liquid products present in the round bottom flask are stored to perform HPLC analysis. The system is then cooled down to room temperature, the liquid flow is set to zero and the inert gas flow is increased to 50 ml/min to clean the pipelines and the reactor. After one hour, the reactor tubes are removed and kept in an oven at 100°C overnight to dry the catalyst as much as possible. The following day the catalyst is carefully removed from the tube and stored for post-reaction analysis.

3.3 Synthesis of Supported Metal Nanoparticles

The catalysts prepared with 1% wt as metal loading, for the research, are:

- Cu/TiO_2
- Pd/TiO_2
- $Pd:Cu\ (1:1)/TiO_2$
- $Pd:Cu\ (1:3)/TiO_2$
- $Pd:Cu\ (3:1)/TiO_2$
- Pt/TiO_2
- $Pt:Cu\ (1:1)/TiO_2$
- $Pt:Cu\ (1:3)/TiO_2$
- $Pt:Cu\ (3:1)/TiO_2$

They were all prepared with sol-immobilization method. The solution of the metal precursor was made solubilizing the metal salt in water, to obtain 0.0078 M as concentration.
Taking Cu/TiO_2 synthesis as reference, the following experimental protocol was used: 20 ml of Cu-solution were diluted in 786 ml of H_2O then, 0.65 ml of PVA, obtained solubilizing 101 mg of polymer in 10 ml of water, were added.
After 3 minutes, a fresh $NaBH_4$ solution was added. The solution contained 0.029 g of reducing agent dissolved in 7.8 ml of H_2O. After 30 minutes, to support metal nanoparticles, 0.99 g of TiO_2 was added. The entire procedure was done under N_2 flux to avoid the oxidation of copper from Cu to Cu^{2+}. The colloidal solution was left under stirring for one hour then it was filtered and washed with distilled H_2O, until the neutrality of the compound was restored. The solid product was left to air dry overnight and dry in the oven at 80 °C, the day after, for 4 hours.
The same procedure was applied to $Pt/\ TiO_2$ and to $Pd/\ TiO_2$ without using the N_2 flux. Concerning instead the bimetallic catalysts' synthesis, the procedure was still the same, but two solutions of the two metal precursors were added, using the N_2 flux since there were still copper as second metal. The amount of support used was calculated to obtain 1% metal loading.
The synthesized catalysts were analyzed at TEM and at the XPS to check the metal loading, the dispersion, and the distribution of the metal NPs.

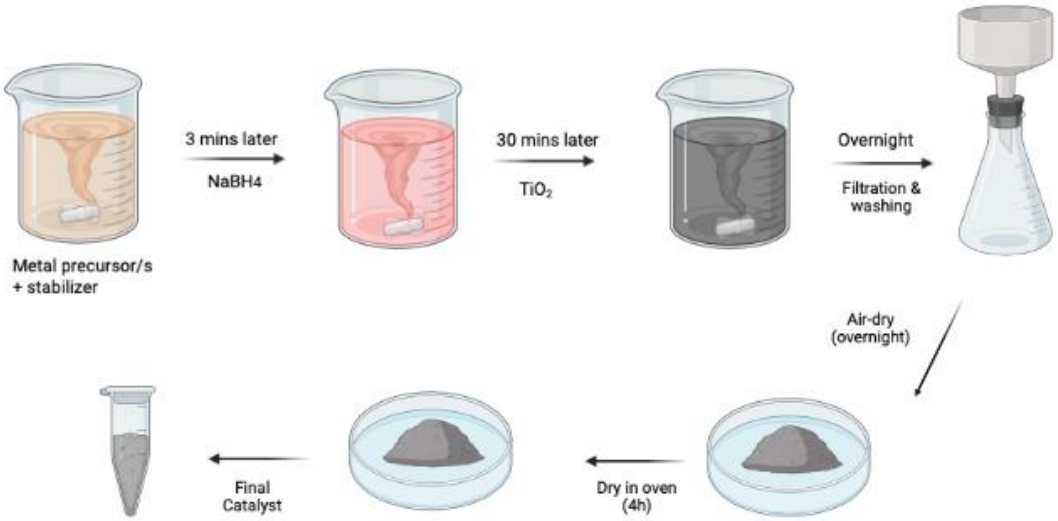

Figure 26. Synthesis of Metal Nanoparticles supported on TiO_2

3.4 Characterization Techniques

Transmission Electron Microscopy (TEM) and X-Ray Photoelectron Spectroscopy (XPS) are the techniques used to characterize the catalyst before and after the reaction, while HPLC (High Performance Liquid Chromatography) and GC (Gas Chromatography) are the analytical techniques used to analyse and quantify the liquid and the gas products of the reaction. These analyses were performed in the Applied Science department of TU Delft.

3.4.1 TEM

Transmission Electron Microscopy is an analytical technique used for characterizing surfaces obtained by the transmission of electrons through the sample. The electrons are formed through a tungsten filament and are then, accelerated by an electric potential (100 – 300 keV), collimated and finally focused on the sample thanks to the use of special lenses. This analysis requires vacuum condition to occur in fact, it was observed that the generated electrons interact with the surface of the sample and part of them is transmitted without interacting with the sample. This fraction of electrons is captured by a fluorescent screen on which is obtained a zoomed image of the sample. The TEM instrument was used to evaluate the size and the distribution of the metal nanoparticles of the catalysts before and after the reaction and were performed using “Jeol JEM-1400 plus TEM” which works at 120 kV. Samples are prepared by

suspending a little amount of the powder in ethanol, a drop of this suspension is placed on specific TEM grids. The grid is placed on the sample holder and the latter is insert in the TEM instrument.

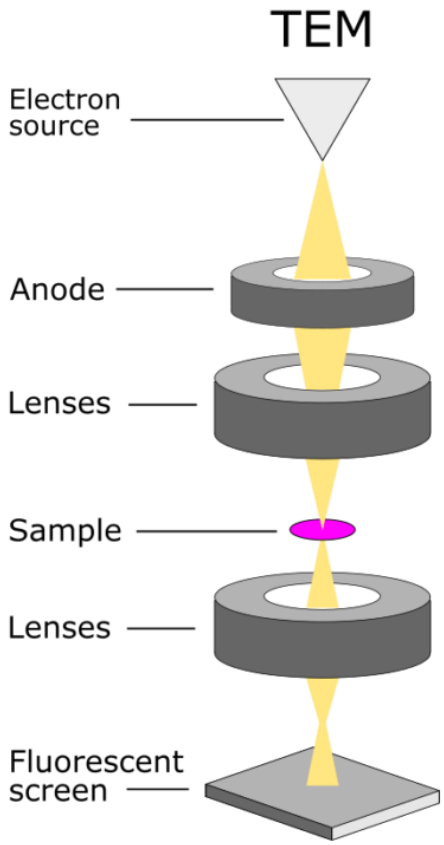

Figure 27. Scheme of the TEM

3.4.2 XPS

X-ray Photoelectron Spectroscopy is an analytical technique useful to obtain information concerning the chemical composition and oxidation states of the elements. It is based on the irradiation of the sample's surface with high energy photons. The energy of the radiation is higher than the bonding energy of electrons present in the atoms and that's why the electrons of the analyzed sample leave the latter with a kinetic energy that is equal to the excess energy of the photon linked to the binding energy. Thanks to that, it is possible to identify and quantify the atoms present on the surface of the sample through the proportionality between the atomic intensity and the intensity measured by the XPS. The experiments were conducted using a K-alpha Thermo Fisher Scientific spectrometer equipped with a monochromated Al K-alpha X-ray Source and a Flood Gun to avoid charging of the sample. The electron energy analyzer was operated with a pass energy of 50 eV, and every location was scanned ten times.

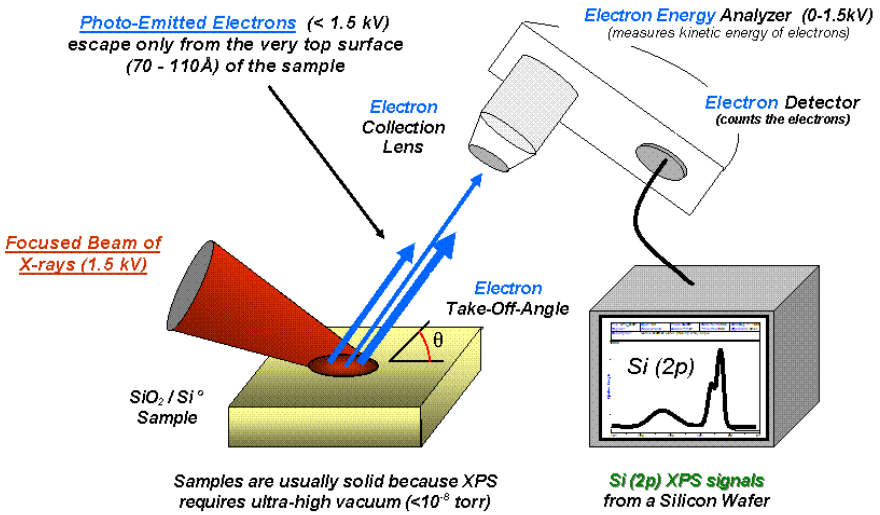

Figure 28. Scheme of XPS instrument

1.4.3 HPLC

To identify and quantify all the chemical compounds present in solution, the analytical technique high performance liquid chromatography is chosen. It relies on degas-unit and two pumps to pass a solvent called "*mobile phase*" (e.g. water, acetonitrile, methanol etc.) and sample mixture through a column referred to as a "*stationary phase*" filled with a solid adsorbent material, is typically a granular material made of solid particles (e.g. silica, polymers, etc.). Each component in the sample interacts slightly differently with the adsorbent material, causing different flow rates for the different components and leading to the separation of the components as they flow out the column. HPLC is different from the traditional "low pressure" liquid chromatography because operational pressures are significantly higher while ordinary LC relies on the force of gravity to pass the mobile phase through the column. Due to small sample amount (10 to 100 μl) separated in HPLC, the typical column dimensions are 2.1-4-6 mm diameter and, 30-250 mm length moreover, they're made of smaller adsorbed particles (2-50 μm in average particle size) which gives to HPLC higher ability to distinguish between compounds when separating mixtures. The temperature plays an important role in the separation process by influencing the interaction taking place between sample components and adsorbent. Due to degree of interaction taking place between the sample components and the adsorbent, each sample to elutes at different time, this time is called retention time of the

compound. The detector generates a signal proportional to the amount of the sample components emerging from the column, allowing in this way the quantitative analysis.

The analyses are carried out using Shimadzu HPLC system and are performed using 0.006 M H_2SO_4 in ultra-pure water as eluent with a flow of 0.6 ml/min. The injection system is an autosampler and the injection volume is 10 μl. The column used is Aminex HPX-87H to allow the separation of the products of interest. The system is characterized of two detectors: UV/VIS and RID. The column compartment was thermostated at 65 °C while the Refractive Index Detector was kept at constant temperature of 40 °C.

Keeping the same conditions of analysis, quantification and identification in the reaction mixture is carried out by comparing the retention time of each standard with the substrates obtained from the reaction. Moreover, the determination of the response factor (RF) with the preparation and the analysis of the calibration curve leads to quantify the concentration of each product detected in the liquid phase and to know the conversion and the yield of each molecule.

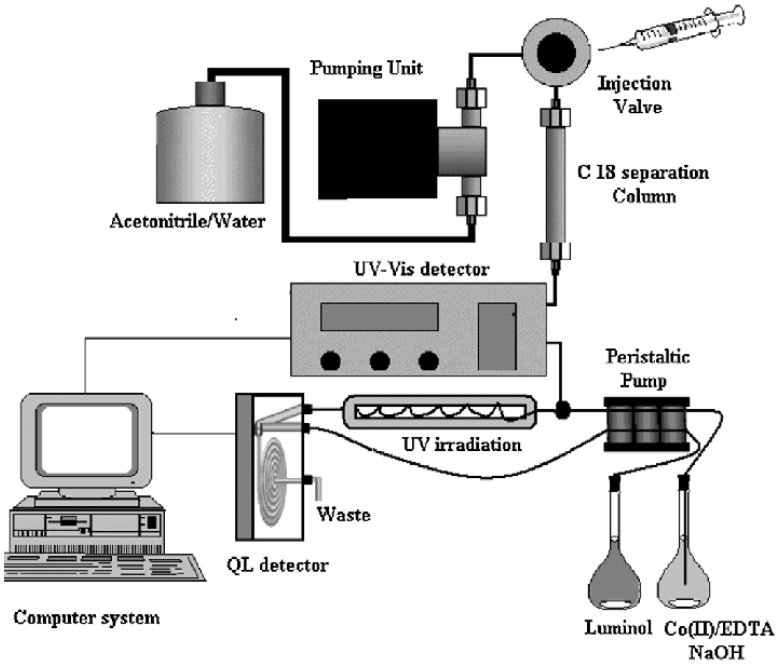

Figure 29. Scheme of the HPLC

From the initial concentration of Maltose Monohydrate (0.02921 mol/L) the scale of concentrations for five standards is established, as it is showed in Table 2.

C0 maltose (%)	1.00
C0 maltose (mol/L)	0.02921414
Cstd lowest (mol/L)	0.000146071
Cstd highest (mol/L)	0.02921414

Standard	Desired C *(mol/L)*
STD 1	0.0001
STD 2	0.005
STD 3	0.01
STD 4	0.02
STD 5	0.03

Table 2. Calibration Data

The mother solution containing the samples of interest is prepared. As reported in Table 4, the theoretical concentration is 0.1 mol/L and the volume is 50 ml. The theoretical mass for each sample to use for the mother solution is calculated according to this formula:

$$g_{th} = \left[\frac{\left(C_{th} * \frac{V_{sol}}{1000}\right) * PM}{Purity}\right]$$

The actual mass' column is referred to what is effectively weighted, and, from that, the actual concentration is calculated with the following formula:

$$C_{act} = \left[\frac{\frac{(g_{act} * Purity)}{PM}}{\frac{V_{sol}}{1000}}\right]$$

Components	MM (*g/mol*)	Purity
Maltose	342.3	1
Glucose	180.156	1
Sorbitol	182.17	1
1-2 Propandiol	76.09	1
Ethanol	46.07	0.97
Propanol	60.0952	1
Ethylenglycol	62.07	1
Formaldehyide	30.031	0.37

Acetaldehyde	44.05	099
Lactic Acid	90.08	1
Acetic Acid	60.052	1
HMF	126.11	0.99

Table 3. Mother Solution's Data

Theoretical C (*mol/L*)	**Volume (mL)**	**Theoretical mass g_{th} (*g*)**	**Actual mass g_{act} (*g*)**	**Actual Concentration of each compound C_{act} (*mol/ml*)**
0.1	50	1.74573	1.715	0.0982397
		0.9188	0.905	0.09849851
		0.929	0.912	0.098163
		0.38806	0.381	0.09818095
		0.24222	0.236	0.09743059
		0.30649	0.32	0.1044095
		0.31656	0.328	0.10361483
		0.41394	0.414	0.1000143
		0.22692	0.24	0.10576217
		0.45941	0.467	0.10165256
		0.30627	0.306	0.09991341
		0.64966	0.637	0.09805165

Table 4. Mother Solution's Data

Considering the desired concentration already reported in Table 2 and 10 ml as final volume for each standard, the volume to take from the mother solution is calculated as can be seen in the following Table.

Standard	**Desired C (mol/L)**	**Final Volume V_f (mL)**	**Volume taken V_t (mL)**
STD 1	0.0001	10	0.01
STD 2	0.005	10	0.5
STD 3	0.01	10	1
STD 4	0.02	10	2
STD 5	0.03	10	3

Table 5. Standard's Data

The final concentration of each compound in each standard is calculated:

$$C_f = \left(\frac{C_{act} * V_t}{V_f}\right)$$

Final Concentration (mol/ml)					
Standard	Maltose	Glucose	Sorbitol	1-2 Propanediol	Ethanol
STD 1	9.82397E-05	9.84985E-05	9.8163E-05	9.81809E-05	9.7E-05
STD 2	0.004911985	0.004924926	0.00490815	0.004909047	0.00487
STD 3	0.00982397	0.009849851	0.0098163	0.009818095	0.00974
STD 4	0.019647941	0.019699703	0.019632599	0.019636189	0.01949
STD 5	0.029471911	0.029549554	0.029448899	0.029454284	0.02923

Table 6. Final Concentration of each compound in each standard

Final Concentration (mol/ml)					
Standard	Propanol	Ethylene Glycol	Formaldehyde	Acetaldehyde	Lactic Acid
STD 1	0.0001044	0.00010361	0.000100014	0.00010576	0.000101653
STD 2	0.0052205	0.00518074	0.005000715	0.00528811	0.005082628
STD 3	0.010441	0.01036148	0.01000143	0.01057622	0.010165256
STD 4	0.0208819	0.02072297	0.02000286	0.02115243	0.020330512
STD 5	0.0313229	0.03108445	0.03000429	0.03172865	0.030495768

Table 7.Final Concentration of each compound in each standard

Final Concentration (mol/ml)		
Standard	Acetic Acid	HMF
STD 1	9.99134E-05	9.80517E-05
STD 2	0.00499567	0.004902583
STD 3	0.009991341	0.009805165
STD 4	0.019982682	0.019610331
STD 5	0.029974023	0.029415496

Table 8.Final Concentration of each compound in each standard

The HPLC areas for each compound in each standard are reported below.

HPLC Areas					
Standard	Maltose	Glucose	Sorbitol	1-2 Propanediol	Ethanol
STD 1	590507	305194	314107	70526	0
STD 2	353925	185821	183483	45164	0
STD 3	610880	334797	324855	82371	22496
STD 4	1513267	826130	798146	217490	54176
STD 5	2024501	1105314	1071392	286196	70153

Table 9. HPLC Areas of each compound in each standard

HPLC Areas					
Standard	Propanol	Ethylene Glycol	Formaldehyde	Acetaldehyde	Lactic Acid
STD 1	39626	69012	28155	14092	44651
STD 2	36810	35882	14385	11008	20901
STD 3	50323	60535	87376	21420	44785
STD 4	125459	148834	87376	71010	117559
STD 5	190797	200289	121936	92577	166898

Table 10. HPLC Areas of each compound in each standard

HPLC Areas		
Standard	Acetic Acid	HMF
STD 1	38938	223146
STD 2	16758	132336
STD 3	38814	233527
STD 4	108392	633952
STD 5	145152	881905

Table 11. HPLC Areas of each compound in each standard

As last, the response factors are calculated with linear regression and the calibration curves are plotted.

RF	
Components	RF
Maltose	70631959
Glucose	38443252.2
Sorbitol	37367598.8
1-2 Propanediol	9996015.3
Ethanol	2502198.8
Propanol	5995535.61
Ethylene glycol	6617023.34
Formaldehyde	4456404.89
Acetaldehyde	2964697.45
Lactic Acid	5460964.72
Acetic Acid	4912555.62
HMF	30154632.3

Table 12. Response Factors

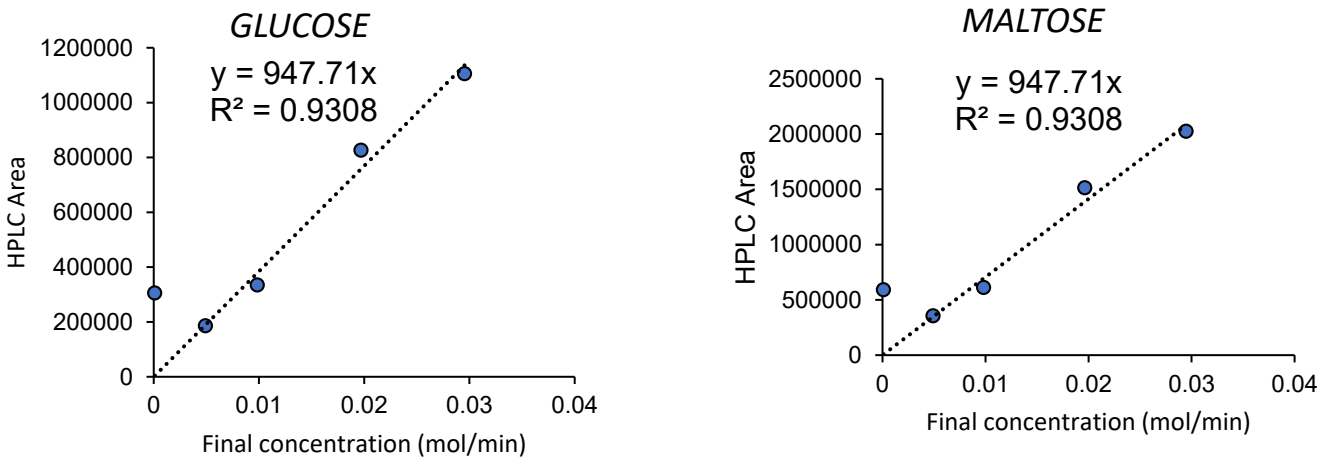

Figure 30. Calibration Curves

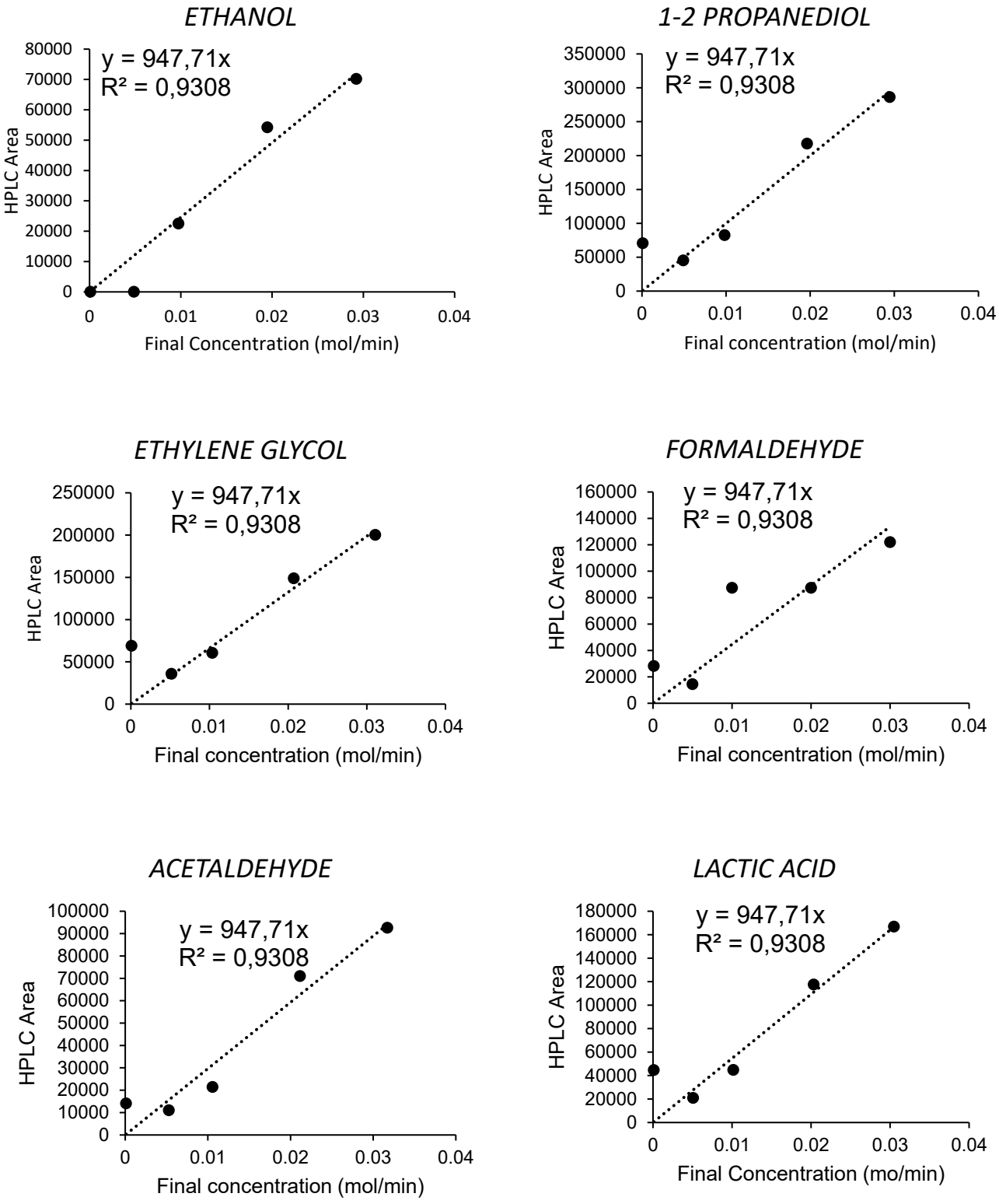

Figure 31. Calibration Curves

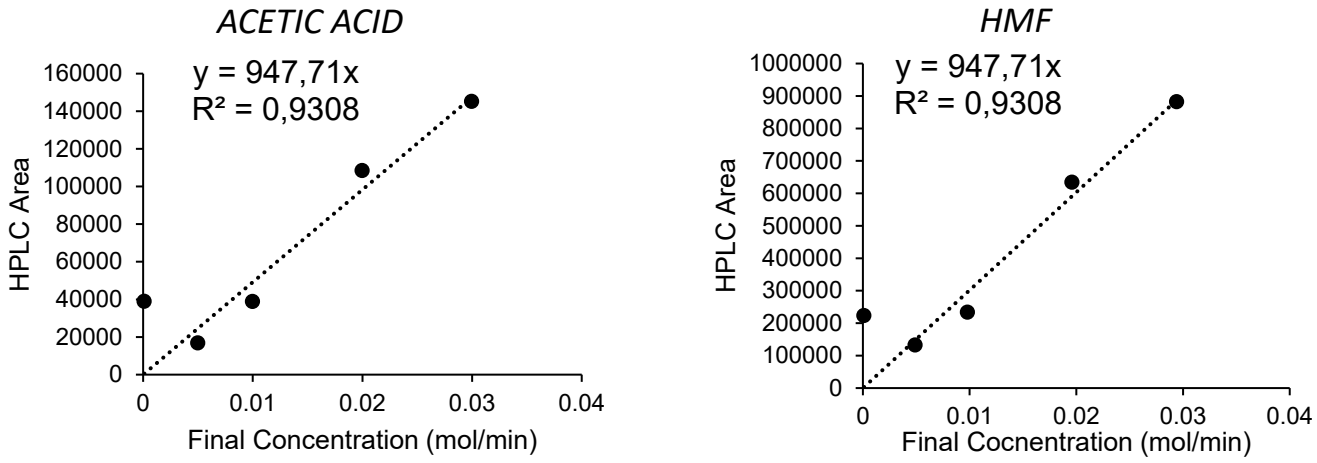

Figure 32. Calibration Curves

3.4.3 GC

Gas chromatography is an analytical technique used to separate and detect the chemical components of a sample micture to determine their presence/absence and their quantities. These chemical components are usually organic molecules or gases, they need to be volatile and thermally stable so they don't degrade in the GC system. Gas chromatographs are usually linked to a mass spectometer to enable the identification of chemical compounds.

The GC uses a carrier gas in the separation which represents the mobile phase, it transports the sample molecules through the system, without reacting with them. The sample is introduced to the GC with an autosampler, it is injected in the GC inlet through a septum which enables the injection of the sample mixture without losing the mobile phase. The inlet is connected to the analytical column which contains the stationary phase coated on the inside walls. The column is held in the colun oven which is heated during the analysis to elute the less volatile components. The outlet of the column is inserted to the detector which responds to the chemical components eluting from the column to produce a signal. The latter is recorded by the acquisition software on a computer to obtain the chromatogram.

After injection into the GC inlet, the chemical components of the sample mixture are first vaporized, if they aren't already in the gas phase. For low concentration samples the whole vapour cloud is transferred into the analytical column by the carrier gas in a splitless mode; for high concentration samples only a portion of the sample is transferred to the analytical column

in split mode, the remaining part is flushed from the system through the split line to prevent overaloading of the analytical column.

Once in the analytical column, the samples are separated by their different interaction with the stationary phase therefore, when selecting the type of column to use, the volatility and functional groups of the analytes should be considered to match them to the stationary phase.

The final step is the detection of the analyte molecules when they elute from the column. There are many GC detectors for example, the FID (flame ionization detector) responds to C-H bonds and the TCD (thermal conductivity detector) catches gases like Argon, Nitrogen, Hydrogen, CO_2 and so on.

Once the reaction is finished the GC leaves on the computer .txt files that are analyzed through a pyhton code then, a the FID and the TCD readings are separated and reported in a single Excel File and the calculations for the analysis are made.

First, the areas are calculated considering the calibration areas. The calibration is done analyzing at the GC a Linde gas tank containing a wide range of hydrocarbons as well as N_2, H_2 and CO_2. The calibration gas composition, the average areas and the volume percentage agiven by Linde are reported in Table 13.

a)

TCD		
Component	Vol %	Avg. Area
Hydrogen	14.00	22.677126
Carbon Dioxide	4.01	58.111
Nitrogen	70.15	1.147812
Carbon Monoxide	6.00	93.280

b)

FID		
Component	Vol %	Avg. Area
Methane	3.97	789.197
Ethylene	0.03	11.836
Ethane	0.41	157.628
Propylene	0.20	115.966
Propane	0.41	233.593
iso-Butane	0.01	7.173
iso-Butene	0.01	4.839
1-Butene	0.07	57.570
Butane	0.31	0
trans-2-Butene	0.07	0
Cis-2-Butene	0.05	290.738
iso-pentane	0.01	9.718
Pentane	0.31	292.837

c)

TCD N_2 Calibration		
Experiment Series	Vol %	Avg. Area
1-8	100	1.718.051
17	100	1.631.325
18-22	100	1.511.723

Table 13. Calibration gas composition and calculated average areas for (a) the TCD, (b) the FID and (c) the N2 calibration area.

After the calibration, different sets of calculation are made:

1) The Refernce Factors for each compound are calculated, with the data obtained from the calibration, according to this equation

$$RF = \frac{Area\ of\ compound\ X}{\%\ X\ compound}$$

So, a certain X gas is injected with a known concentration (% X), from which the area can be obtained and the RF can be calculated as indicated by the equation.

2) The composition of the product X (%) is obtained according to the following equation:

$$\%\, X = \frac{Area\ of\ compound\ X}{RF}$$

3) Then the composition of the product X (%) respect ot the other producs detected, is calculated

$$\%\, X\ respect\ to\ the\ detected\ products = \frac{\%\, X}{Sum\ of\ all\ the\ detcted\ products\ (\%)}$$

4) The total flow rate (ml/min) is also calculated

$$Total\ flow\ rate\ \left(\frac{ml}{min}\right) = \frac{ml/\,min\, N_2}{\%\, N_2}$$

5) From the total flow rate, the flow rate of each compound can be obtained

$$X\ \left(\frac{ml}{min}\right) = \%\, X * Total\ flow\ rate\ \left(\frac{ml}{min}\right)$$

6) From the flow rate, the molar flow rate can be obtained by applying $PV = nRT$, so the following equation is applied

$$X\ \left(\frac{mol}{min}\right) = \frac{P * (ml/\,min)\, X}{RT}$$

It wasn't possible to talk in terms of conversion and selectivity because, in order to obtain the selectivity of each compound in gas phase, during the overall time of the reaction, it would have been necessary to know the concentration of the maltose, during the reaction. The experimental setup, because of the downstream high dead volume and mixing problems, didn't allow sampling during the experiments, thus not allowing the determination of the amount of converted reagent. for this reason it was decided to collect the liquid phase at the end of the

reaction and to demonstrate the production of compounds in the gas phase in terms of molar percentage.

Other important information are collected in the following table

Feedflow load	**1%**
Maltose Monohydrate Concentration	0.03 mol/L
Reactor Solution Flow Rate	3.5 g/h
Molatose Monohydrate Flow Rate	5.83E-04 g/min
Hydrogen Flow Rate	3.89E-05 mol H/min

Table 14. Feed flow conversion.

4. Results and Discussion

This section describes the results obtained, starting from the characterization of the fresh catalysts by TEM and XPS techniques, followed by the catalytic performance of the different catalysts prepared for APR experiments, ending with the characherization of the spent catalysts with the same techniques and the liquid phase analysis.

4.1 Characterization of fresh catalysts

4.1.1 TEM Pt-series

The Pt series catalysts was characterized by TEM microscopy (Figure 33) to evaluate size, particle size distribution and dispersion of the active phase on the support. Despite TiO_2 crystallites which obstacles the correct analysis of the images, the presence of nanoparticles without aggregates as well as good dispersity of the metal nanoparticles was observed for all samples prepared. In particular, for the best catalyst of this series in terms of hydrogen production (as described in the following chapter), Pt:Cu (3:1)/TiO_2, the particle size and mean particle size of Pt was also calculated and the related histogram is reported in Figure 34. An average diameter of 2.1 nm was observed confirming a good size-control of the preparation method employed.

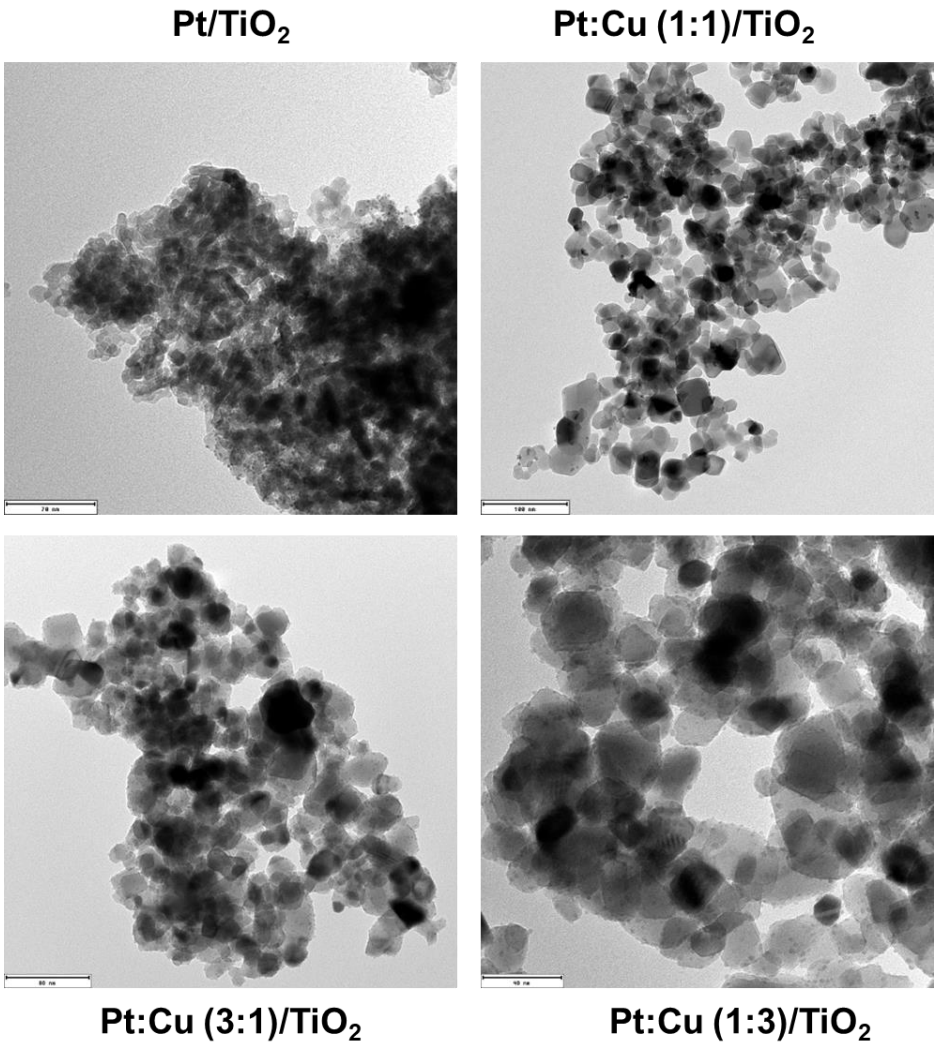

Figure 33. TEM images of Pt-Cu series with different atomic composition (1:0; 1:1; 1:3; 3:1)

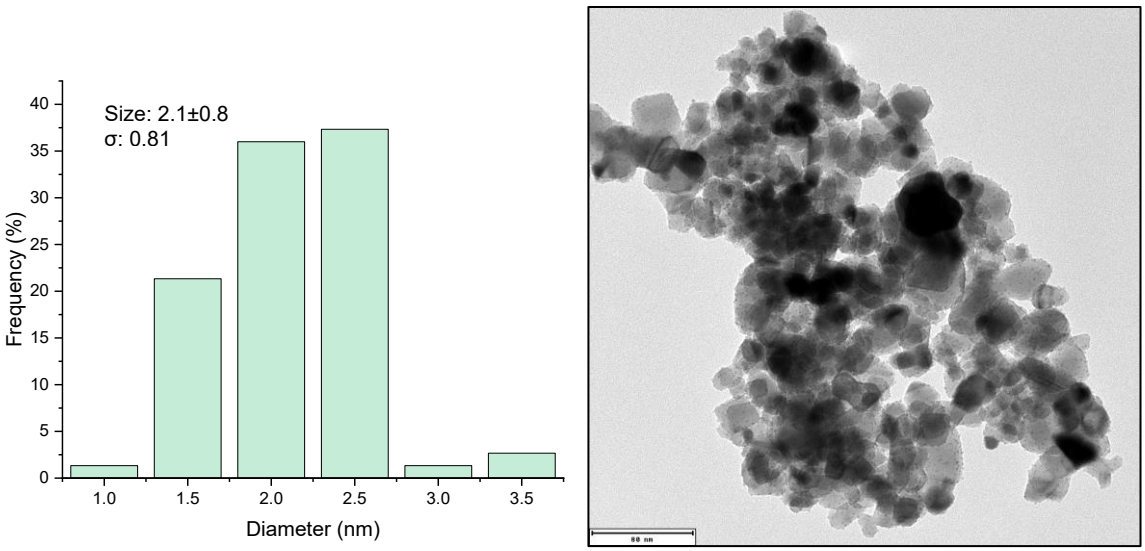

Figure 34. TEM distribution of Pt:Cu (3:1)/TiO_2

4.1.2 TEM Pd-series

Thes synthesis fo Pd-Cu catalysts was carrid out. The results showed for the Pd-series were in agreement with the ones made for the Pt-series catalysts. Despite the presence of support's crystallites, the presence of nanoparticles without aggregates, as well as good dispersity of the metal nanoaprticles was observed for all samples prepared, as shown in Figure 35. Unfortunately, in the case of Pt:Cu(1:3) and Pt:Cu(3:1) samples some difficulty to acquire good images have been found, maybe depending on some errors made in the sample preparation. For the sample prepared using 1:1 atomic reatio of the two metals, Pd:Cu (1:1), the distribution of particle size was calculated and the related histogram is reported in Figure 36. An average diameter of 2.6 nm was observed confirming a good size-control of the preparation method employed.

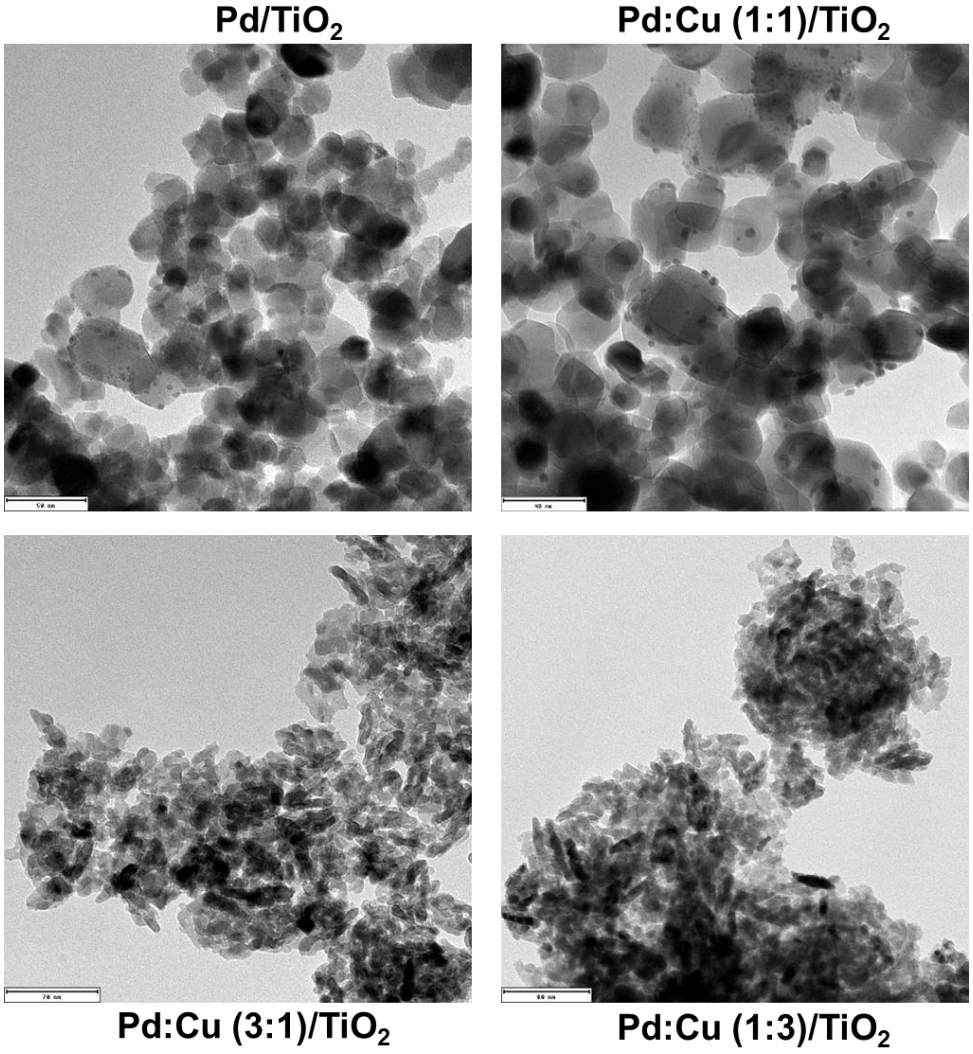

Figure 35. TEM images of Pt:Cu/TiO2 series with different atomic composition (1:0; 1:1; 1:3; 3:1).

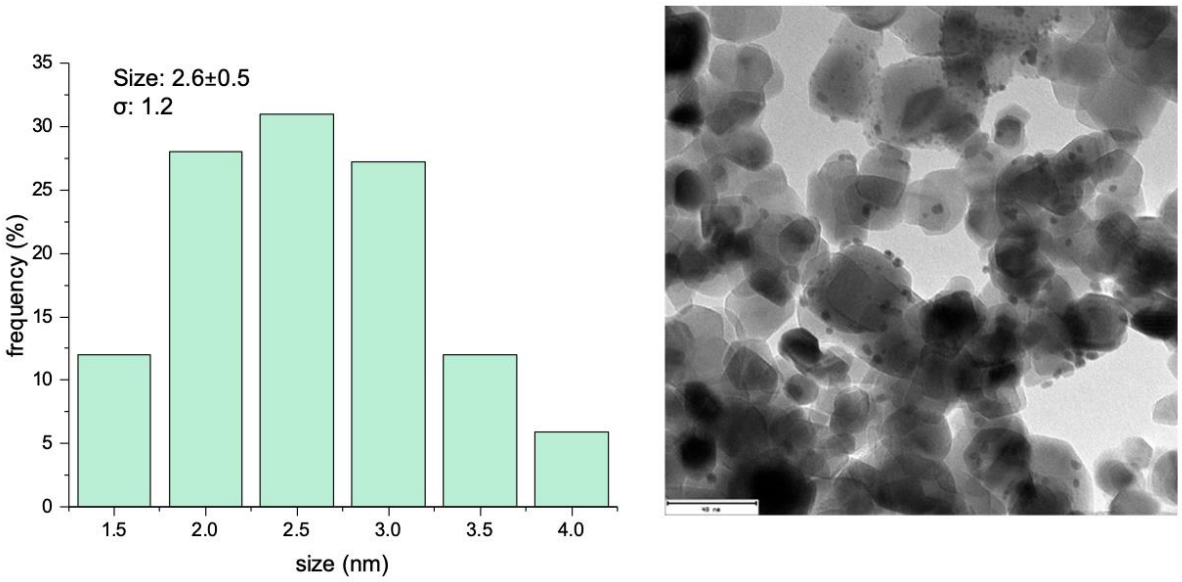

Figure 36. TEM distribution of Pd:Cu (1:1) spent.

4.1.3 XPS analysis

To evaluate the surface composition of metal species loaded on the support and their oxidation states, XPS analysis was carried out and the XPS spectra for each series is reported in Figure 37. Before analyzing the spectra obtained from the analysis, it's fundamental to report the binding energy of the metals under study, found in literature[97] [98] :

Element	Spectral Line	Binding Energy
Pt	$4f_{5/2}$	74.23
Pt	$4f_{7/2}$	70.61
PtO	$4f_{5/2}$	74.2
PtO	$4f_{7/2}$	74.5
Cu	$2p_{1/2}$	952.56
Cu	$2p_{3/2}$	932.62
CuO	$2p_{1/2}$	953.7

[97] Evgeny I. Vovk et al., 'XPS Study of Stability and Reactivity of Oxidized Pt Nanoparticles Supported on TiO_2', *The Journal of Physical Chemistry C* 121, no. 32 (17 August 2017): 17297–304, https://doi.org/10.1021/acs.jpcc.7b04569.

[98] Chun-Kwei Wu et al., 'Quantitative Analysis of Copper Oxide Nanoparticle Composition and Structure by X-Ray Photoelectron Spectroscopy', *Chemistry of Materials* 18, no. 25 (1 December 2006): 6054–58, https://doi.org/10.1021/cm061596d.

CuO	$2p_{3/2}$	933.40
Pd	$3d_{5/2}$	335.10
Pd	$3d_{3/2}$	339.30
PdO	$3d_{5/2}$	335.90
PdO	$3d_{3/2}$	342.40

Table 15. XPS binding energy in literature

Regarding the Pt-Cu series, the copper content and the BE observed at 951.5 and 932.5 eV are related to metal Cu, at $2p_{1/2}$ and $2p_{3/2}$ spin-orbital coupling respectively. The presence of metal copper is confirmed by the literature which showed Cu $2p_{1/2}$ = 952.56 eV and Cu $2p_{3/2}$ = 932.62 eV as binding energie values.. Moreover, for monometallic Cu sample the presence of oxide form can be recognize due to a broad signals and a slight shift towards higher binding energy found at 953.8 eV and 934.8 eV, for CuO $2p_{1/2}$ and CuO $2p_{3/2}$, respectivly. These results are in line with the binding energy value found in literature as shown in the table 15. This behaviour was not observed for the bimetallic system, probably the co-presence of Pt species enhance copper stability in terms of metal oxidation. Instead for the metal Pt doublet signals attributed to Pt $4f_{5/2}$ and Pt $4f_{7/2}$ species at 73 and 70 eV have been showed, , still finding correlation with the data present for metallic platinum in the Table 16 (Pt $4f_{5/2}$ = 74.23 eV and Pt $4f_{7/2}$ = 70.61 eV). The overlapped spectra highlighted a signal shift towards higher BE (Pt $4f_{5/2}$ = 75 eV and Pt $4f_{7/2}$ = 72 eV) due to the increase of the atomic amount of copper in the bimetallic systems that causes the modification of electronic structure derived from the alloy formation.[99] In addition, also in this case a broad peak can be attributed to the presence of PtO species, found at 75 eV and 73.9 for Pt $4f_{5/2}$ and Pt $4f_{7/2,}$ respectively, being, also in this case in accordance with the literature.[100] In overall, by XPS results and the literature found, the presence of bimetallic species in zero valent oxidation state can be observed. Fuhtermore, the oxidized species observed on the support can justify the reduction step with hydrogen before starting the maltose reaction.

[99] Ivan Khalakhan et al., 'On the Interpretation of X-Ray Photoelectron Spectra of Pt-Cu Bimetallic Alloys', *Journal of Electron Spectroscopy and Related Phenomena* 246 (January 2021): 147027, https://doi.org/10.1016/j.elspec.2020.147027.
[100] Vovk et al., 'XPS Study of Stability and Reactivity of Oxidized Pt Nanoparticles Supported on TiO_2'.

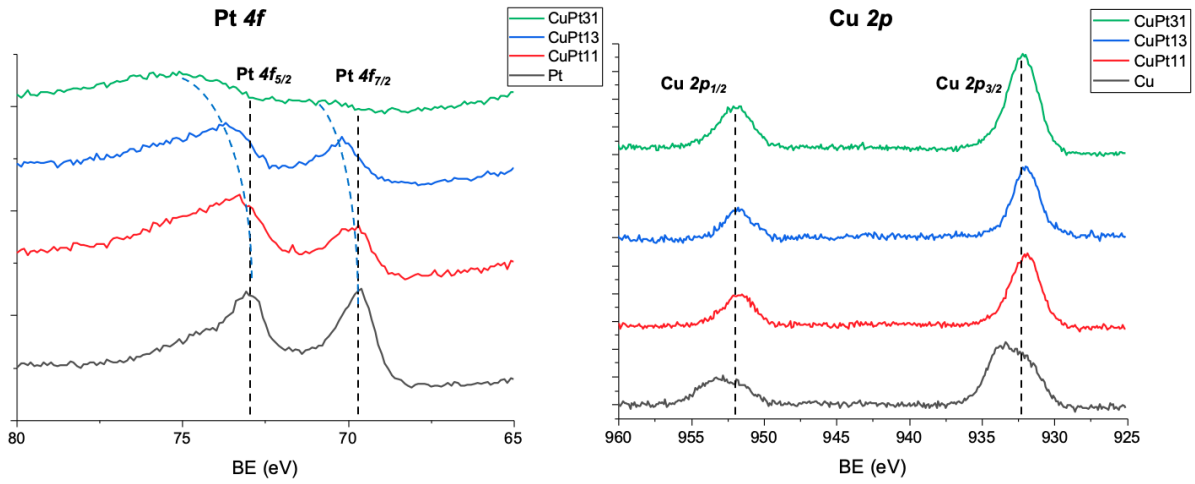

Figure 37. XPS spectra of Pt:Cu/TiO2 series with different atomic composition (1:0; 1:1; 1:3; 3:1)

Regarding the Pd-Cu series, illustrated in Figure 38, the copper highlighted the same behaviour explained in the previous paragraph, in fact the copper content and the BE observed at 951.5 and 932.5 eV are related to metal Cu, at $2p_{1/2}$ and $2p_{3/2}$ spin-orbital coupling respectively and its presence is confirmed by the literature which showed Cu $2p_{1/2}$ = 952.56 eV and Cu $2p_{3/2}$ = 932.62 eV as binding energie values. Also in this case, the presence of copper oxide was observed only for monometallic system and increasing the amount of co-metal in the active phase, the oxidation was limited. Therefore, more metallic state was present. By analysing the spectra, typical binding energy attributed to zero valent palladium nanoparticles peaks at 335 and 339 eV related to Pd $3d_{5/2}$ and $Pd3d_{3/2}$ spin-orbit coupling respectively were observed. The broad peaks can be attributed to the presence of PdO, but in opposite with the Pt series, any kind of change in the Pd peaks in terms of shifting can be evaluated. [101]

[101] Liang Jun Wang et al., 'Palladium Nanoparticles Functionalized Graphene Nanosheets for Li-O2 Batteries: Enhanced Performance by Tailoring the Morphology of Discharge Product', n.d.

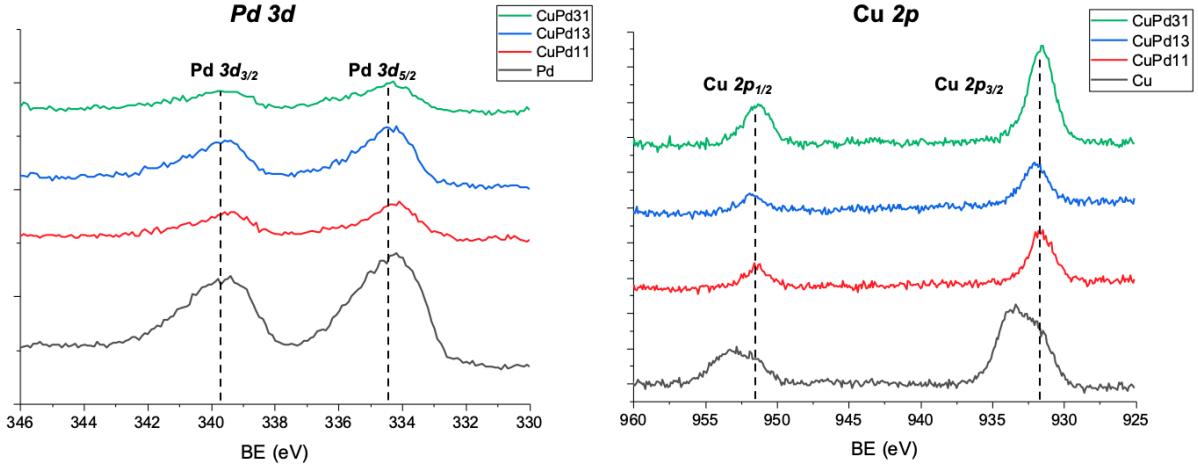

Figure 38. XPS spectra of Pd-Cu-series with different atomic composition (1:0; 1:1; 1:3; 3:1).

4.2 APR experiments

The data concerning the H_2 production and the presence of hydrocarbons have been reported in terms of percentage of each compound respect to the other products in gas phase, during the time of the reaction. During the discussion, it's fundamental to always have in mind, the ramified reaction mechanism concerning the Aqueous Phase Reforming, which follows these steps:

1. Maltose Monohydrate is dehydrogenated on the active metal surface giving as result intermediate products before the C-C and C-O bonds' cleavage.
   1.1 Cleavage of C-C bond with the formation of H_2 and CO.
   1.2 H_2O and CO reacts through the WGS to produce CO_2 and H_2O.
   1.3 The CO left and the CO_2 produced react with H_2 to produce Hydrocarbons (mainly alkanes) and water through the Fischer-Tropsch reactions.
2. Hydrogenation reactions that lead to the C-O bond cleavage producing alcohols, catalyzed by the active metal catalyst.
3. Direct Dehydrogenation of Maltose Monohydrate forming organic acids which, through the catalyst, produce alkanes through decarboxylation reactions.

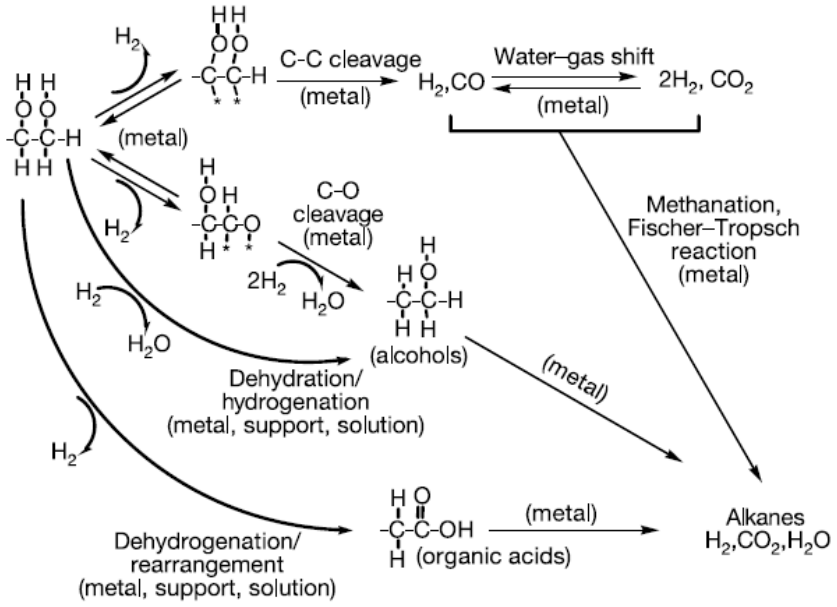

Figure 39. Reaction pathways for production of H_2 by reactions of oxygenated hydrocarbons with water. (Asterisk represents a surface metal site).

In this section, the catalytic performance of Pd and the Pt series is reported, followed by a critical comparison between the two. As it has been already said, the y axis reports the percentage of the compound X with respect to the other products in gas phase; on the x axis there's the reaction time. It's important to anticipate that, in the following graphs, there is for the first 50 minutes of the reaction, a growing curve as it were a heating ramp. Actually, the time zero corresponds to the time at which the oven arrived at 225 °C, so the reason why there's this growing curve, is because of the high dead volume after the reactor in the experimental setup due to that the H_2 arrives to the GC only after 50 minutes.

All the experiments were performed loading 200 mg of catalyst and, after the reactor tube is placed in the setup, the reduction with 30 ml/min of H_2 flow was performed for 2 hours. Then the APR reaction was started, using 10 ml/min of N_2 as carrier gas, sending the feedstock with 0.006 ml/min of flow rate with a pressure of 44 bar at 225° C, for 6 hours. The gas products were detected by the GC instrument which sent the result to the connected computer, the main products expected were *methane, propane, butene and carbon dioxide*.

4.2.1 Palladium Series

4.2.2 Pd/TiO_2

As shown in figure 38 of in the previous section, the APR process is made of several reactions. Overall, the process can be simplified in a set of reactions that produce hydrogen and others that consume hydrogen. The former are the ones that from maltose produce more oxidated intermediates, which can further react through hydrogenolysis and hydrogenation reactions. These consumes hydrogen to generates alkanes and alkenes such as, methane, ethane. propane and butene. The presence of these products, at the end of the reaction, indicates the in-situ consumption of hydrogen produced, which leads to a reduction of the overall final amount of hydrogen produced.

The following table and graph (Table 16 and Figure 40), relative to the reaction conducted using Pd/TiO_2, indicate the molar percentages on the total of the products detected in gas phase, as function of the reaction time.

Pd/TiO_2

Time	$\%X_i$ respect to the detected products in the gas phase				
	H_2	**CH_4**	**C_2H_6**	**C_3H_8**	**cis-2-C_4H_8**
0	88%	0%	0%	0%	1%
22	72%	0%	0%	0%	1%
44	64%	5%	3%	1%	1%
66	60%	6%	3%	1%	1%
88	61%	6%	3%	1%	1%
110	61%	6%	3%	1%	1%
132	61%	6%	3%	0%	0%
153	61%	5%	3%	0%	1%
175	61%	5%	3%	0%	0%
196	61%	5%	3%	0%	0%
218	61%	5%	3%	0%	0%
239	61%	5%	2%	0%	0%

Table 16. Percentage of the product Xi found in the reaction, respect to the other products detected, in the gas phase.

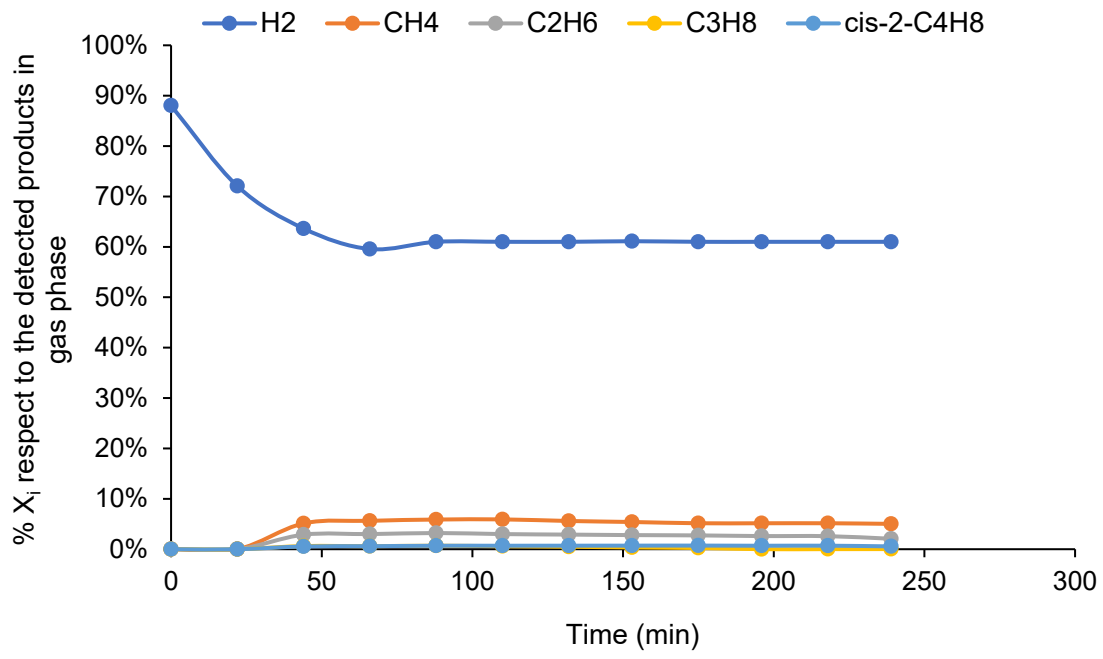

Figure 40. Gas Phase Products, in terms of molar %, of the APR with Pd/TiO_2 catalyst

In this graph is possible to observe that, the blue curve, related to the H_2, decreases in the first 50 minutes of the reaction while, the curves of the by-products, at the same time, increases. This is the demonstration of what happens in the reaction mechanism of the APR: the H_2 produced at the beginning is consumed to produce the secondary products, by undesired consecutive reactions. It is possible to hypothesize that, a significant amount of the H_2 produced is consumed in-situ to produce alkanes and alkenes like, methane, ethane, propane and butene. It seems that the Pd is a metal capable, not only of promoting the hydrogen production at this reaction condition, but also to promote the undesired consecutive reactions. However, the system seems stable, without showing signs of deactivation in the first five hours of reactions, except for the last hour. The main by-products observed in gas phase were methane and ethane obtained, probably, from hydrogenation reactions of alcohols like methanol and ethanol.

The sum of the molar percentages was less than 100% because, both in Table 17 and in Figure 39 it hasn't been included the amount of CO_2 because it can be produced from reactions that co-produce Hydrogen, like in the case of the WGS and it can be, later,

involved in reactions that consume hydrogen as the Fischer-Tropsch. In overall, the presence of CO_2 doesn't indicate the net production or consumption of H_2.

4.2.3 Pd:Cu (3:1)/TiO_2

The following table and graph (Table 17 and Figure 41), relative to the reaction conducted using Pd:Cu (3:1)/TiO2, indicate the molar percentages on the total of the products detected in gas phase, as function of the reaction time.

Pd:Cu (3:1)/TiO_2

Time	%X_i respect to the detected products in the gas phase				
	H_2	**CH_4**	**C_2H_6**	**C_3H_8**	**cis-2-C_4H_8**
0	0%	0%	0%	0%	0%
24	75%	0%	0%	0%	0%
47	75%	0%	0%	0%	0%
71	74%	0%	0%	0%	0%
94	74%	0%	0%	0%	0%
117	74%	0%	0%	0%	0%
141	74%	0%	0%	0%	0%
164	74%	0%	0%	0%	0%
187	74%	0%	0%	0%	0%
210	74%	0%	0%	0%	0%
233	73%	0%	0%	0%	0%
255	73%	0%	0%	0%	0%
278	73%	0%	0%	0%	0%
300	73%	0%	0%	0%	0%
322	71%	0%	0%	0%	0%
343	68%	0%	0%	0%	0%

Table 17. Percentage of the product Xi found in the reaction, respect to the other products formed, in the gas phase.

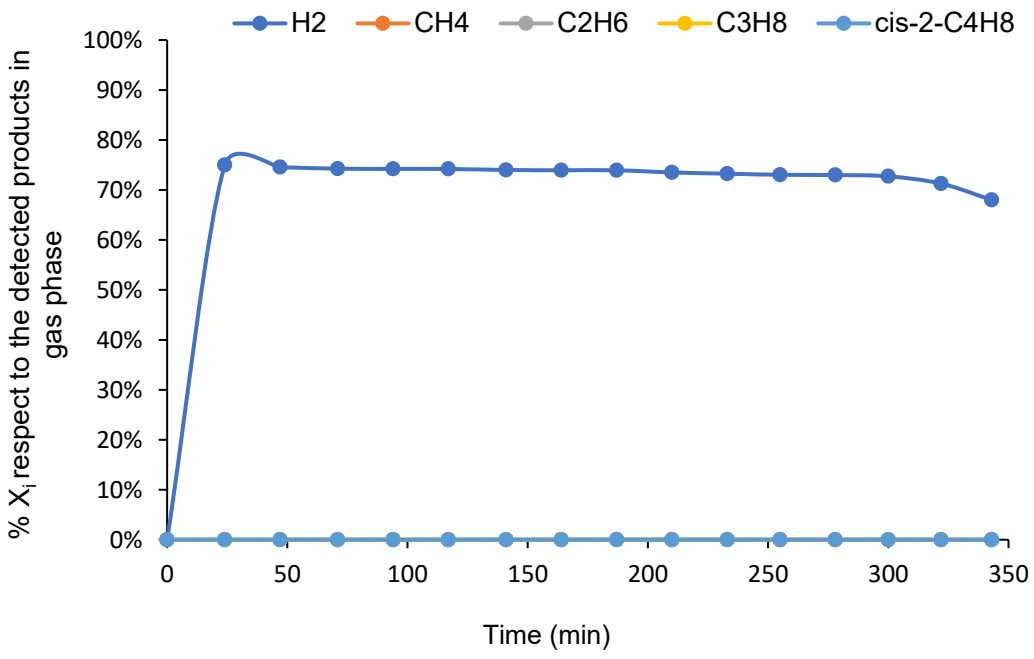

Figure 41. Gas Phase Products, in terms of molar %, of the APR with Pd:Cu (3:1)/TiO2 catalyst

In the case of the reaction done with Pd:Cu (3:1), which presents 25% of Cu, it is possible to assess that the by-products, deriving from consecutive reactions, like methane, ethane, propane and butene were not formed. It seems that the addition of copper was effective in inhibiting the undesired consecutive reactions, avoiding the in-situ consumption of hydrogen. It is also confirmed by the hydrogen production which molar percentage stabilized around 75%, about 10% more than what happened in the reaction conducted under monometallic Pd. Also in this case, obvious signs of deactivation had not been detected for the first five hours of reaction, expect for the last hour. However, the addition of copper to the active metal was effective in the inhibition of the undesired reactions without influencing the catalytic activity connected to the hydrogen production, for the first five hours of the experiment.

4.2.4 Pd:Cu (1:1)/TiO_2

The following table and graph (Table 18 and Figure 42), relative to the reaction conducted using Pd:Cu (1:1)/TiO2, indicate the molar percentages on the total of the products detected in gas phase, as function of the reaction time.

Pd:Cu (1:1)/TiO_2

Time	%X_i respect to the detected products in the gas phase				
	H_2	**CH_4**	**C_2H_6**	**C_3H_8**	**cis-2-C_4H_8**
0	8%	0%	0%	0%	0%
21	84%	0%	0%	0%	0%
42	83%	0%	0%	0%	0%
63	84%	0%	0%	0%	0%
85	84%	0%	0%	0%	0%
106	84%	0%	0%	0%	0%
127	83%	0%	0%	0%	0%
148	84%	0%	0%	0%	0%
169	83%	0%	0%	0%	0%
191	82%	0%	0%	0%	0%
212	82%	0%	0%	0%	0%
233	81%	0%	0%	0%	0%
254	82%	0%	0%	0%	0%
275	83%	0%	0%	0%	0%
296	83%	0%	0%	0%	0%
317	84%	0%	0%	0%	0%
338	82%	0%	0%	0%	0%
359	79%	0%	0%	0%	0%

Table 18. Percentage of the product Xi found in the reaction, respect to the other products detected, in the gas phase.

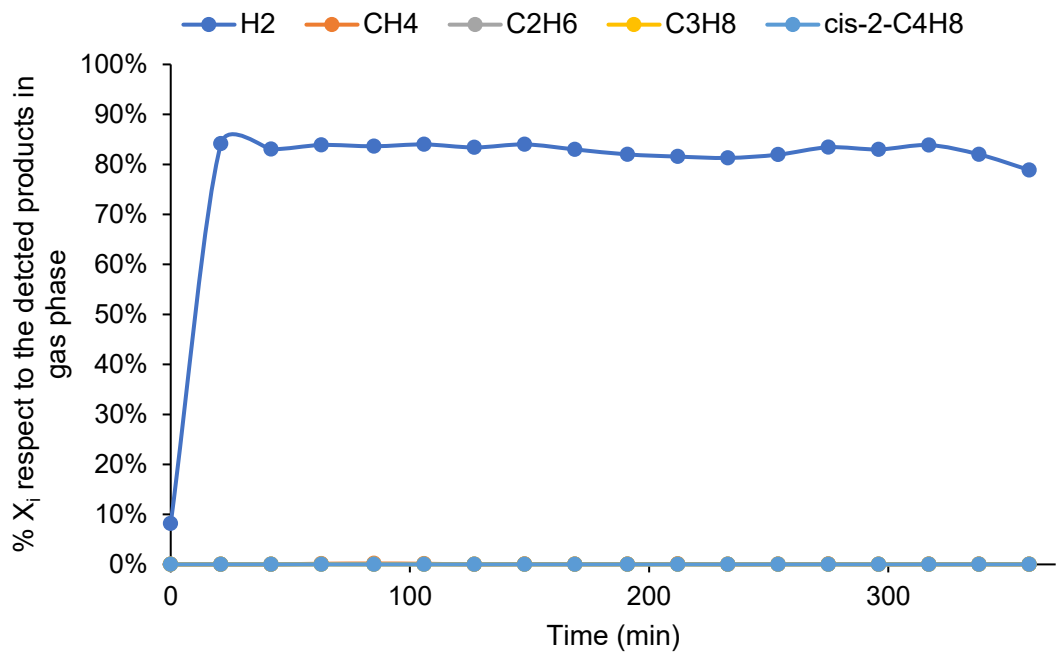

Figure 42. Gas Phase Products, in terms of molar %, of the APR with Pd:Cu (1:1)/TiO_2 catalyst.

In the case of the reaction done with Pd:Cu (1:1) which presents 50% of Cu, it is possible to assess that the by-products, deriving from consecutive reactions, like methane, ethane, propane and butene didn't formed. It seems that the addition of copper was effective in inhibiting the undesired consecutive reactions, avoiding the in-situ consumption of hydrogen, again. It is also confirmed by the hydrogen production which molar percentage stabilized around 85 %, higher than using Pd/TiO_2 and even higher than the Pd:Cu (3:1), in fact the difference between the two cases is about 10%. Concerning the deactivation, it wasn't detected for the first five hours of reaction, except for the last hour. However, the addition of copper to the active metal was effective in the inhibition of the undesired reactions without affecting the catalytic activity connected to the hydrogen production, for the first five hours of the experiment.

4.2.5 Pd:Cu (1:3)/ TiO_2

The following table and graph (Table 19 and Figure 43), relative to the reaction conducted using Pd:Cu (1:3)/TiO2, indicate the molar percentages on the total of the products detected in gas phase, as function of the reaction time.

Pd/TiO_2

Time	%X_i respect to the detected products in the gas phase				
	H_2	**CH_4**	**C_2H_6**	**C_3H_8**	**cis-2-C_4H_8**
0	0%	0%	0%	0%	0%
22	74%	0%	0%	0%	0%
43	71%	0%	0%	0%	0%
64	72%	0%	0%	0%	0%
85	72%	0%	0%	0%	0%
106	72%	0%	0%	0%	0%
127	72%	0%	0%	0%	0%
148	71%	0%	0%	0%	0%
169	71%	0%	0%	0%	0%
191	71%	0%	0%	0%	0%
212	71%	0%	0%	0%	0%
233	71%	0%	0%	0%	0%
254	71%	0%	0%	0%	0%
275	66%	0%	0%	0%	0%
299	63%	0%	0%	0%	0%

Table 19. Percentage of the product Xi found in the reaction, respect to the other products detected, in the gas phase.

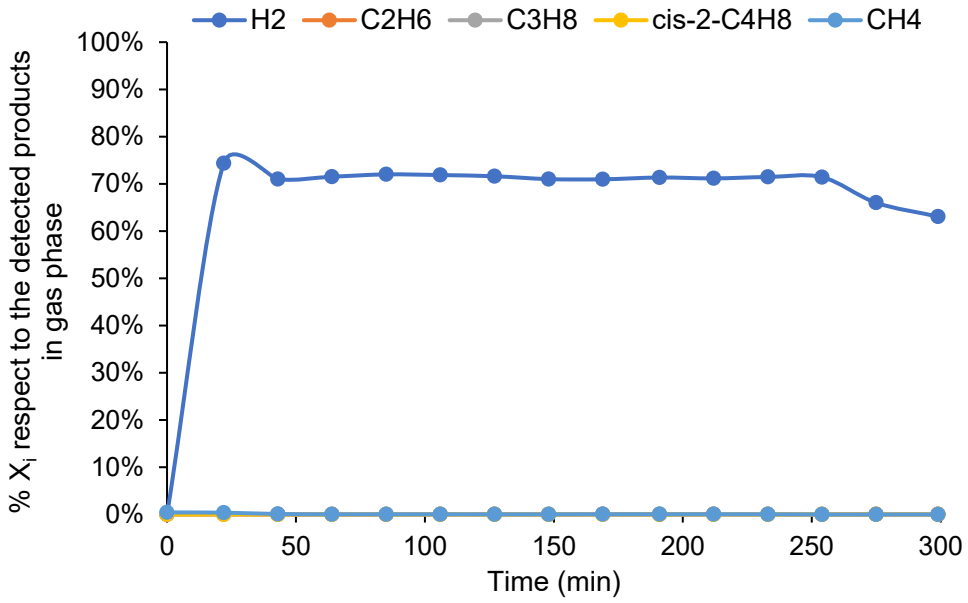

Figure 43. Gas Phase Products, in terms of molar %, of the APR with Pd:Cu (1:3)/TiO2 catalyst

Even in the reaction done with Pd:Cu (1:3) so, increasing by the 75% the amount of Cu, by-products (methane, ethane, propane and butene) deriving from consecutive reactions, didn't t form. Also in this case copper has the ability to inhibit the undesired consecutive reactions, avoiding the in-situ consumption of hydrogen. This thesis is also supported by the hydrogen production which molar percentage stabilized around 70%, with a 15% of difference in the hydrogen production with the Pd:Cu (3:1). It happens probably because the platinum active sites are screened by the considerable amount of copper added. The deactivation wasn't detected for the first four hours of reaction, except for the last hour. However, the addition of copper to the active metal is effective in the inhibition of the undesired reactions without inhibiting the catalytic activity.

4.2.6 Comparison of H_2 production between all the catalysts in the Pd-series

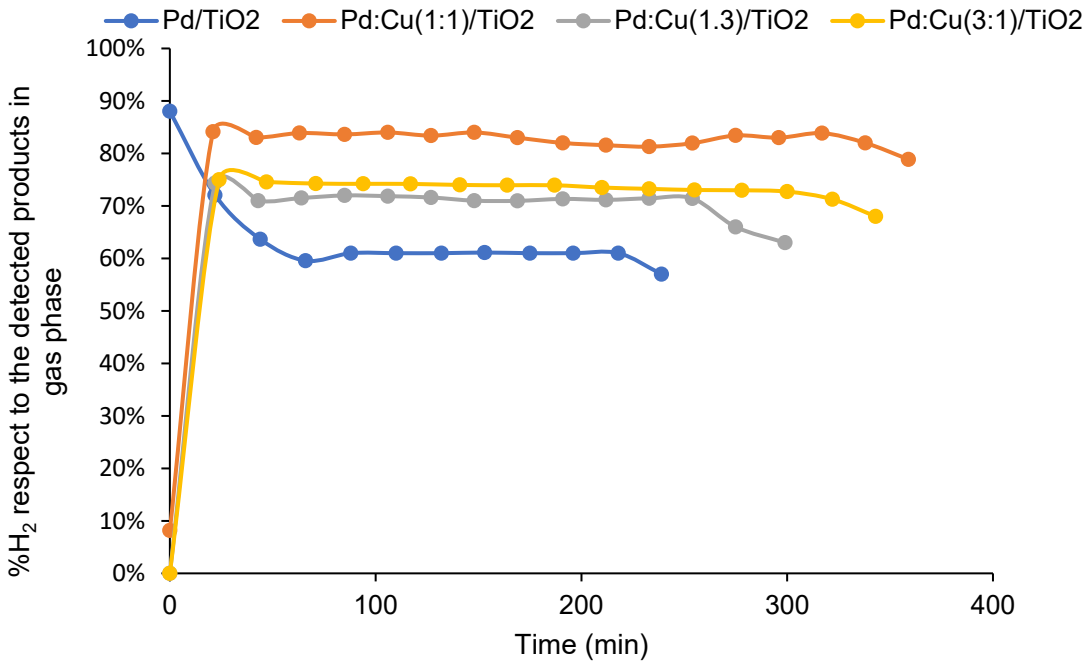

Figure 44. Comparison of the molar % of H_2 obtained from Pd-series catalyst as function of the reaction time.

The reaction catalyzed by Pd/TiO_2 is the only one that favoured the production of hydrocarbons as displaced in the reaction network of the APR. Looking at the graph related to the molar percentage of hydrogen produced in reactions cataltzed by the Pd-catalysts, it can be assessed that the reaction under the monometalic Pd catalyst was the worst from the hydrogen production point of view, because eventhough it was the most active one in its production, it was also the most active in the side reactions that, to happen, consume hydrogen. Increasing the amount of copper by 25% so, in the case of Pd:Cu (3:1), side reactions didn't t take place and the hydrogen produced was higher than the monometallic one. For the bimetallic catalyst made with 50% of copper, increasing even more the amount of the co-metal, Pd:Cu (1:1) the overall scenario became even better, since the hydrogen production for this case was the highest, still properly inhibiting the undesired reactions. Increasing the co-metal by the 75%, in the case of Pt:Cu (1:3) it seemed that the active sites of Pd were screened by copper or the Pd-loading was too low because there was a low molar percentage of hydrogen. Moreover, increasing at this level the amount of the co-catalyst, a less active system, during time, was obtained in fact it deactivates early. It can be probably due to two reasons: first, in this reaction conditions the

copper metal can oxidize leading to the formation of the copper oxide, which leads to a decrease of its activity; second, it has the tendency of adsorbing strongly reaction intermediates on its surface, which block the active sites.

These results suggest that the optimal catalyst is Pd:Cu (1:1)/TiO_2. All the catalysts reported Figure 44 showed deactivation.

4.2.1 Platinum series

4.2.2 Pt/TiO_2

The following table and graph (Table 20 and Figure 45), relative to the reaction conducted using Pt/TiO_2, indicate the molar percentages on the total of the products detected in gas phase, as function of the reaction time,

Pt/TiO_2

Time	$\%X_i$ respect to the detected products in the gas phase				
	H_2	**CH_4**	**C_2H_6**	**C_3H_8**	**cis-2-C_4H_8**
0	21%	0%	0%	0,0%	0%
21	70%	0%	0%	0,0%	0%
42	100%	0%	0%	0,0%	0%
84	90%	15%	0%	23,0%	0%
105	82%	28%	10%	20,7%	0%
127	71%	19%	9%	19,8%	0%
148	66%	18%	8%	18,8%	0%
170	60%	18%	8%	17,8%	0%
191	59%	17%	8%	16,9%	0%
213	58%	16%	8%	15,4%	1%
234	56%	14%	7%	13,9%	1%

256	54%	13%	7%	12,4%	0%
277	53%	12%	7%	11,0%	1%
299	52%	11%	7%	9,5%	1%
321	51%	9%	7%	8,0%	0%
342	50%	9%	7%	7,4%	2%
364	49%	9%	6%	0,1%	0%
359	79%	0%	0%	0%	0%

Table 15. Percentage of the product X_i found in the reaction, respect to the other products detected in the gas phase.

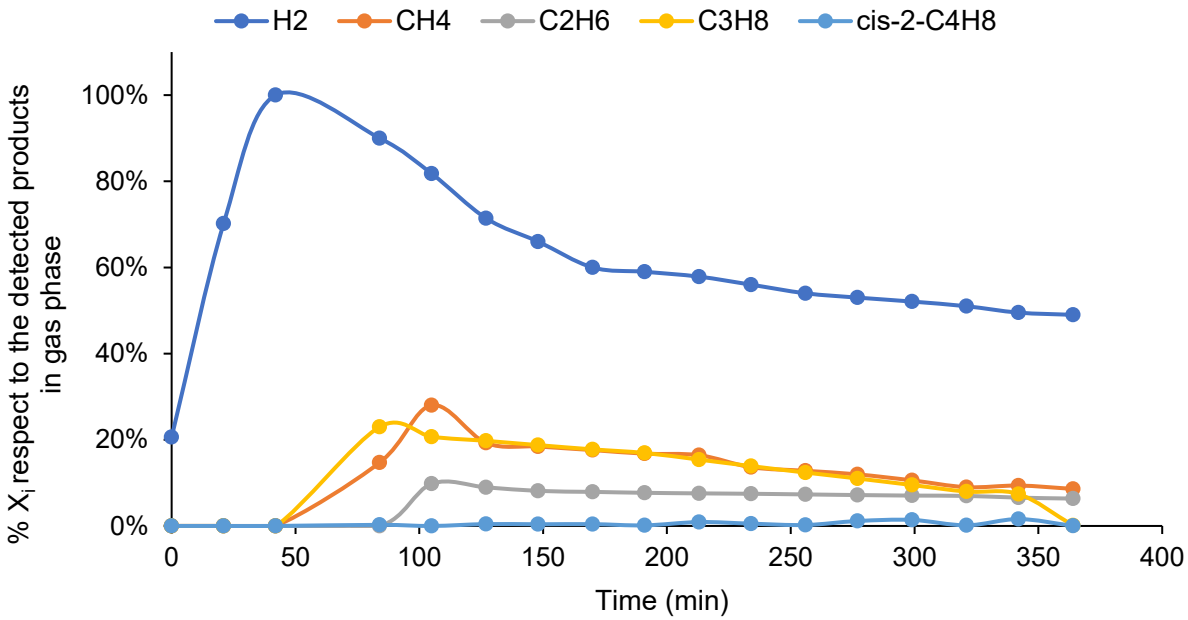

Figure 45 Gas Phase Products, in terms of molar %, of the APR with Pt/TiO2 catalyst

In this graph is possible to observe that, the blue curve related to the H_2, is quite high in the first two hours of the reaction and then it starts to decrease. Also in this case, the molar percentage of side products like, methane, ethane, propane and butene was detected and, in particular when the curve related to the hydrogen started to decrease, the curves related to the side products started to increase. This is the demonstration of what happens in the reaction mechanism of the APR: the H_2 produced at the beginning is consumed to produce the secondary products, by the undesired consecutive reactions. Also in this case, as it happened for Pd-monometallic catalyst, a significant amount of the H_2 produced is consumed in-situ to produce alkanes and alkenes. So, also Platinum is a metal capable of

generating hydrogen and of promoting the undesired consecutive reactions. The main by-products observed in gas phase were methane and propane obtained, probably, from hydrogenation reactions of alcohols like methanol and propanol. On the contrary of what happened with Pd/TiO2, this catalyst was less active in fact it can be seen a gradual deactivation, during the reaction time, probably, it was caused by the oxidation of the active metal under the reaction conditions or because of the surface of the catalysts can absorb strongly the intermediates formed, blocking the active sites. In overall, the amount of H_2 produced in terms of molar percentage was around 60%.

4.2.3 Pt:Cu (3:1)/TiO2

The following table and graph (Table 21 and Figure 46), relative to the reaction conducted using Pt:Cu (3:1)/TiO_2, indicate the molar percentages on the total of the products detected in gas phase, as function of the reaction time.

Pt:Cu(3:1)/TiO_2

Time	%X_i respect to the detected products in the gas phase				
	H_2	**CH_4**	**C_2H_6**	**C_3H_8**	**cis-2-C_4H_8**
0	0%	0%	0%	1%	0%
21	0%	0%	0%	0%	0%
42	35%	0%	0%	0%	0%
63	99%	0%	0%	0%	0%
84	97%	0%	0%	0%	0%
105	97%	0%	0%	0%	0%
126	98%	0%	0%	0%	0%
147	98%	0%	0%	0%	0%
168	98%	0%	0%	0%	0%
189	97%	0%	0%	0%	0%
210	97%	0%	0%	0%	0%

231	96%	0%	0%	0%	0%
252	97%	0%	0%	0%	0%
273	97%	0%	0%	0%	0%
294	96%	0%	0%	0%	0%
315	97%	0%	0%	0%	0%
336	96%	0%	0%	0%	0%
357	96%	0%	0%	0%	0%

Table 21. Percentage of the product Xi found in the reaction, respect to the other products detected in the gas phase.

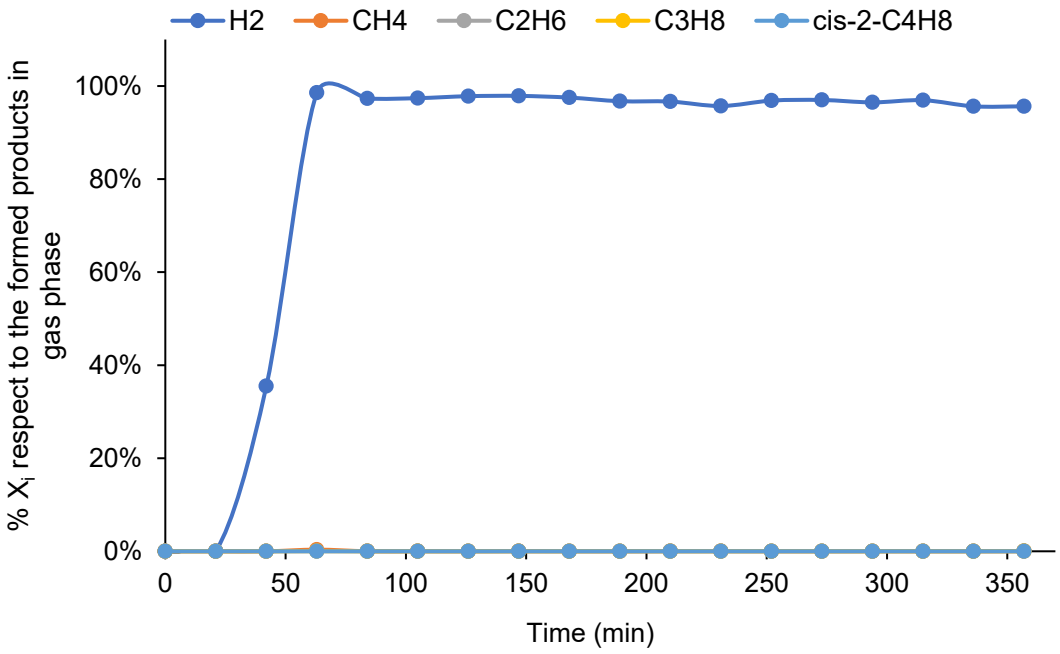

Figure 46. Gas Phase Products, in terms of molar %, of the APR with Pt:Cu(3:1)/TiO_2 catalyst

In the case of the reaction done with Pt:Cu (3:1) which presents 25% of Cu, it is possible to assess that the by-products, deriving from consecutive reactions, like methane, ethane, propane and butene didn't formed. It seems that the addition of copper, also in this series of catalyst, was effective in inhibiting the undesired consecutive reactions, avoiding the in-situ consumption of hydrogen. It is also confirmed by the considerable hydrogen production which molar percentage stabilized around 96%, about 30% more than what happened in the reaction conducted under monometallic Pt. The addition of copper, as co-

metal, seems to have a stabilizing effect on the system, avoiding its the deactivation during time, on the contrary of what shown in the case of the Pt/TiO_2.

.

4.2.4 Pt:Cu (1:1)/TiO2

The following table and graph (Table 22 and Figure 47), relative to the reaction conducted using $Pt:Cu(1:1)/TiO_2$, indicate the molar percentages on the total of the products detected in gas phase, as function of the reaction time.

$Pt:Cu(1:1)/TiO_2$

Time	%X_i respect to the detected products in the gas phase				
	H_2	**CH_4**	**C_2H_6**	**C_3H_8**	**cis-2-C_4H_8**
0	4%	0%	0%	0%	0%
22	24%	0%	0%	0%	0%
43	22%	0%	0%	0%	0%
65	22%	0%	0%	0%	0%
87	23%	0%	0%	0%	0%
109	22%	0%	0%	0%	0%
131	23%	0%	0%	0%	0%
153	22%	0%	0%	0%	0%
175	22%	0%	0%	0%	0%
197	22%	1%	0%	0%	0%
219	22%	0%	0%	0%	0%
241	22%	0%	0%	0%	0%
263	23%	0%	0%	0%	0%
273	97%	0%	0%	0%	0%
294	96%	0%	0%	0%	0%

315	97%	0%	0%	0%	0%
336	96%	0%	0%	0%	0%
357	96%	0%	0%	0%	0%

Table 22. Percentage of the product Xi found in the reaction, respect to the other products detected, in the gas phase.

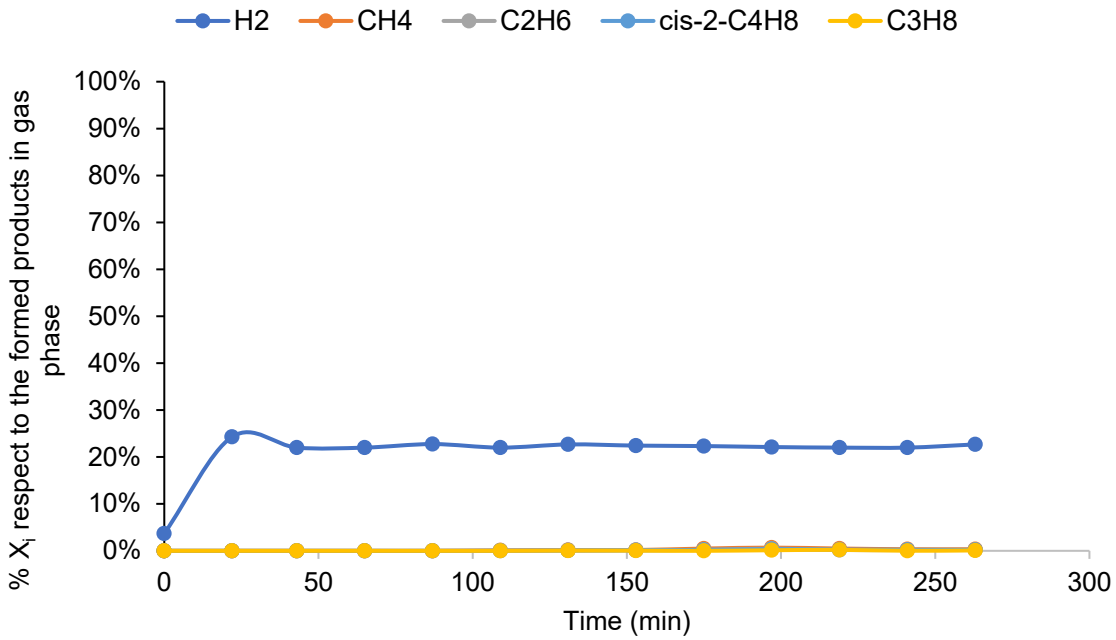

Figure 47. Gas Phase Products, in terms of molar %, of the APR with Pt:Cu(1:1)/TiO_2 catalyst

In the case of the reaction done with Pd:Cu (1:1) which presents 50% of Cu, the by-products, deriving from consecutive reactions, like methane, ethane, propane and butene didn't formed. Also in this case, it seems that the addition of copper is effective in inhibiting the undesired consecutive reactions. However, unlike what has been seen for Pd:Cu (1:1), the amount of hydrogen produced was quite low, around the 20% in terms of molar percentage, less than 70% respect to the previous case. In the light of the trend obtained in the case of Pd:Cu (1:1), the same trend was expected and since it didn't happen, problems related to the synthesis of the material, to the performance of the catalytic test or due to some leaks in the system, are assumed.

4.2.5 Pt:Cu(1:3)/TiO2

The following table and graph (Table 23 and Figure 48), relative to the reaction conducted using Pt:Cu (1:3)/TiO_2, indicate the molar percentages on the total of the products detected in gas phase, as function of the reaction time.

Pt:Cu(1:3)/TiO_2

Time	%X_i respect to the detected products in the gas phase				
	H_2	**CH_4**	**C_2H_6**	**C_3H_8**	**cis-2-C_4H_8**
0	0%	0%	0%	0%	0%
22	23%	0%	0%	0%	0%
43	73%	0%	0%	0%	0%
65	89%	1%	0%	0%	0%
88	90%	1%	0%	0%	0%
110	93%	1%	0%	0%	0%
132	88%	0%	0%	0%	0%
153	89%	0%	0%	0%	0%
175	87%	0%	0%	0%	0%
197	87%	1%	0%	0%	0%
219	84%	0%	0%	0%	0%
240	84%	0%	0%	0%	0%
262	85%	0%	0%	0%	0%
283	84%	0%	0%	0%	0%
305	86%	0%	0%	0%	0%
326	84%	0%	0%	0%	0%
347	82%	0%	0%	0%	0%
357	96%	0%	0%	0%	0%

Table 23. Percentage of the product Xi found in the reaction, respect to the other products detected, in the gas phase.

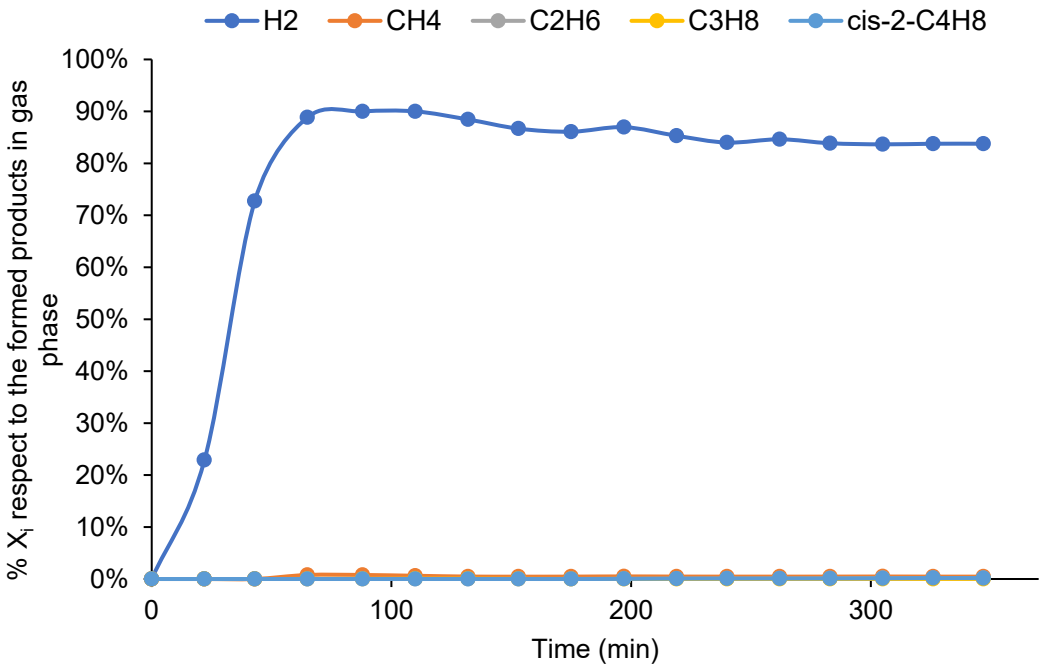

Figure 35. Gas Phase Products, in terms of molar %, of the APR with Pt:Cu(1:3)/TiO2 catalyst.

Increasing the amount of copper up to 75%, in the case of Pd:Cu (3:1), intermediates expected like, methane, ethane, propane and butene deriving from the consecutive reactions were not formed. This showed that copper has the ablity to inhibit the undesired consecutive reactions, avoiding the in-situ consumption of hydrogen. It is also demonstrated by the high hydrogen production which molar percentage stabilized around the 80%, 15% less than what obtained from the Pt:Cu (3:1) catalyst of the series, but still quite high. The less amount of hydrogen produced was probably due to the fact that high amount of copper screened the active sites of platinum. This catalyst showed a constant deactivation trend during the five hours of the reaction, but the addition of Cu was still effective for inhibiting the undesired reaction, leading to quite high amount of hydrogen.

4.2.6 Comparison of H_2 production between all the catalysts in the Pt-series

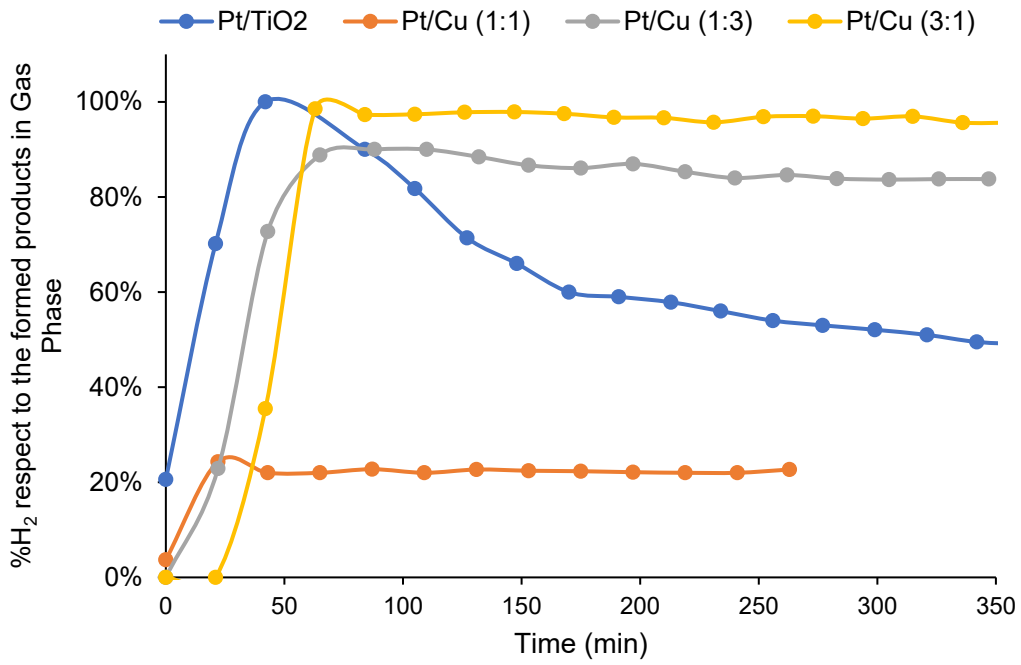

Figure 36. Comparison of the molar % of H_2 obtained from Pt-series catalyst as function of the reaction time.

The reaction catalyzed by Pt/TiO_2 was the only that allowed side reactions, which led to the formation of hydrocarbons, beside the production of hydrogen that was around the 60%. However, this system was more prone to deactivation. Comparing the different molar percentage of hydrogen, obtained catalyzing the process with different catalyst of the Pt-series, and excluding the Pt:Cu (1:1) catalyst since some problems in the setup or in the synthesis of the material are hypothesized, the catalyst showing the worst catalytic perfomance was the monometallic one. The addition of low atomic copper amount (3:1) allowed to inhibit effectively the secondary reactions, without decreasing too much the amount of the noble metal and so, without lowering the production of hydrogen. As it happened for the Pd:Cu (1:3), the addition of high atomic copper amount led to a decrese of the amount of the noble metal, the active phase, showing a decrease in the hydrogen production. These results suggest that the optimal catalyst, excluding Pt:Cu (1:1)/TiO_2, is the Pt:Cu (3:1)/TiO_2.

The effect of reaction temperature was studied and the best catalyst of this series was also tested at different temperatures besides 225 °C, at 200 °C and 175 °C.

Also in this case, all the three experiments performed at the three different temperatures were conducted loading 200 mg of catalyst and, after the reactor tube in the setup is placed, the reduction with 30 ml/min of H_2 flow is conducted for 2 hours. Then the APR reaction is performed, using 10 ml/min of N_2 as carrier gas, sending the feedstock with 0.006 ml/min of flow rate with a pressure of 44 bar at 225° C/200 °C/175 °C, for 6 hours. The gas products were detected by the GC instrument which sends the result to the connected computer, the main products expected were *methane, propane, butene and carbon dioxide*. The following table and graph (Table 25 and graph 49), relative to the reaction conducted using Pt:Cu (3:1)/TiO_2, at 225 °C/200 °C/175 °C, indicate the molar percentages of hydrogen on the total of the products detected in gas phase, as function of the reaction time, at different temperatures.

Pt:Cu (3:1) – 225 °C		**Pt:Cu (3:1) – 200 °C**		**Pt:Cu (3:1) – 175 °C**	
Time	%H_2	Time	%H_2	Time	%H_2
0	0%	0	7%	0	0%
21	0%	21	95%	21	94%
42	35%	42	95%	42	95%
63	99%	62	99%	63	94%
84	97%	83	99%	84	93%
105	97%	104	99%	105	94%
126	98%	124	99%	126	95%
147	98%	145	99%	146	95%
168	98%	166	98%	167	95%
189	97%	187	98%	188	96%
210	97%	207	97%	209	96%
231	96%	228	97%	230	95%
252	97%	249	97%	251	93%
273	97%	270	97%	271	93%

294	96%	291	94%	292	91%
315	97%	311	93%	313	88%
336	96%	332	93%	334	88%

Table 24. Hydrogen percentage, respect to the other products in gas phase, for the best catalyst at 225° C, 200 °C and 175 °C

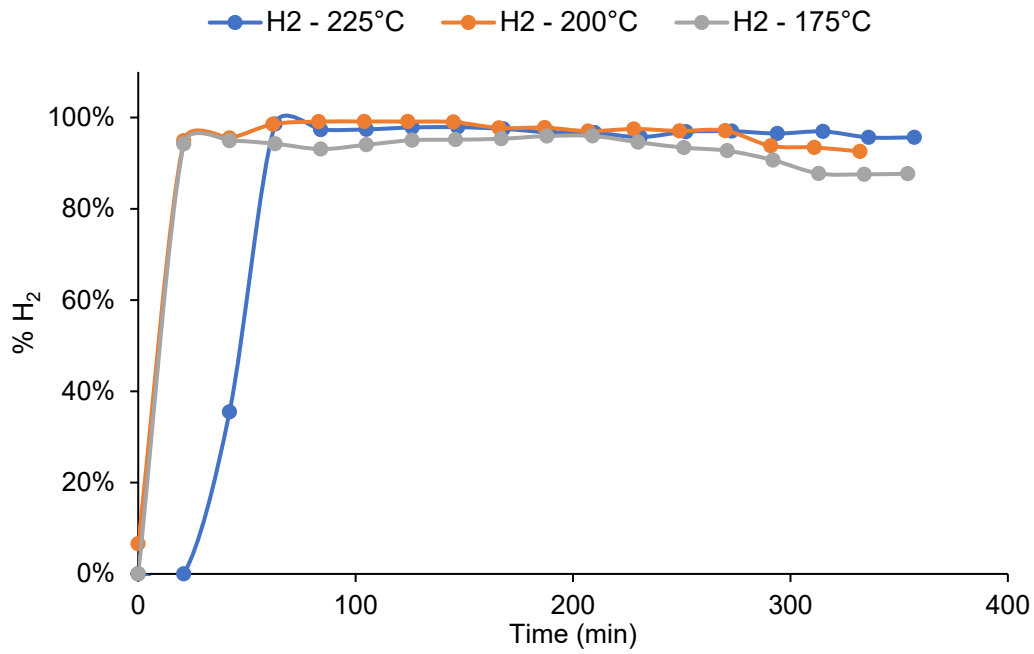

Figure 50. Hydrogen percentage, respect to the other products in gas phase, for the best catalyst at 225° C, 200 °C and 175°C.

From this comparison, what can be said is that once the stationary state was reached, the three different reactions at three different temperatures had an analogous behaviour, suggesting that, even at lower temperatures, the catalyst was still performing properly, as it was confirmed by the amount of hydrogen produced. It can be seen a marked deactivation at lower temperatures, probably because, at these temperatures, the reaction intermediates are difficult to detouch from the catalyst surface, so that they can react eachother producing heavy compounds blocking the active sites.

4.3 HPLC

The HPLC anlaysis is important to analyse the products formed in liquid phase and it is essential to complete the comprehension of the reaction mechanism, to fournish more data which can confirm or not the hypothesis made for the gas phase. Because of problems related to the setup, the high dead volume at the end of the reactor which causes problems of backmixing of the reaction products, and for the lack of time, it was not possible to conduct a detailed analysis of the liquid phase, along the reaction time. Reliable results couldn't be obtained on the time profile of the reaction of the liquid phase products. It has been decided so, to collect the entire liquid phase at the end of the reaction, to have an idea of the produced species in the liquid phase. However, in Table 25 the main products obtained from the liquid phase analysis are shown and, based on their presence, it can be done, in the next studies, a more precise and complete HPLC analysis.

SELECTIVITY				
Catalyst	**Glucose**	**Lactic Acid**	**Acetic Acid**	**HMF**
Pt	**1.17**	**18.83**	**6.30**	**1.06**
Pt:Cu (1:1)	**6.89**	**10.43**	**11.60**	**3.39**
Pt:Cu (3:1)	**0.64**	**1.77**	**0.00**	**0.00**
Pt:Cu (1:3)	**1.43**	**7.29**	**0.00**	**2.09**
Pd	**2.70**	**11.83**	**0.00**	**0.00**
Pd:Cu (1:1)	**0.54**	**0.00**	**0.00**	**0.00**
Pd:Cu (3:1)	**183**	**10.41**	**0.00**	**3.40**
Pd:Cu (1:3)	**2.03**	**5.91**	**0.00**	**2.82**

Table 25. Selectivity of the main products found in liquid phase through HPLC analysis.

4.4 Spent characterization

The best catalysts for each series (Pt:Cu 1:3 and Pd:Cu 1:1) were characterized with TEM and XPS after the APR reaction.

4.4.1 TEM analysis

4.4.2 TEM Pt-series

The catalytic activity of Pt:Cu (3:1) that has exhibited the best catalytic performance in terms of hydrogen production as described previously, was investigated at different temperatures (225, 200 and 175 °C) and the spent catalysts was recovered and characterized. In spite of the high temperature and the acqueous phase flow, TEM images showed the absence of aggregate phases as therefore the presence of small nanoparticles.

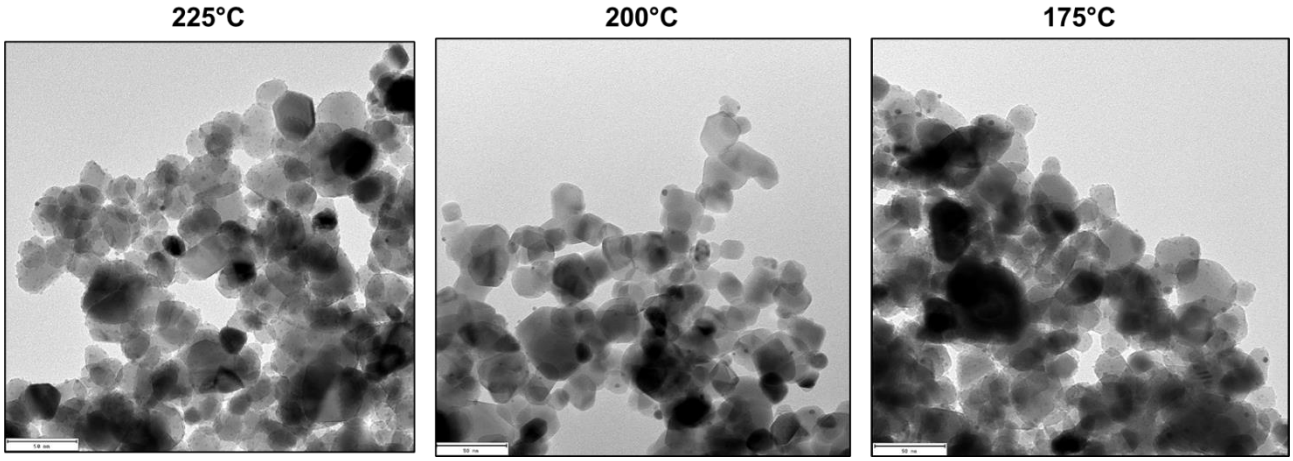

Figure 51. TEM images of spent Pt:Cu (3:1)/TiO_2 after the reactions conducted at different temperatures 225, 200 and 175 °C.

To compare the particle size of the catalyst before and after the reaction, particle size distribution was calculated for the sample at 225 °C and the fresh one. (Figure 52). By analysing the two particle size distributions, no significant change was observed in terms of nanoparticles size confirming the absence of nanoparticles aggregation.

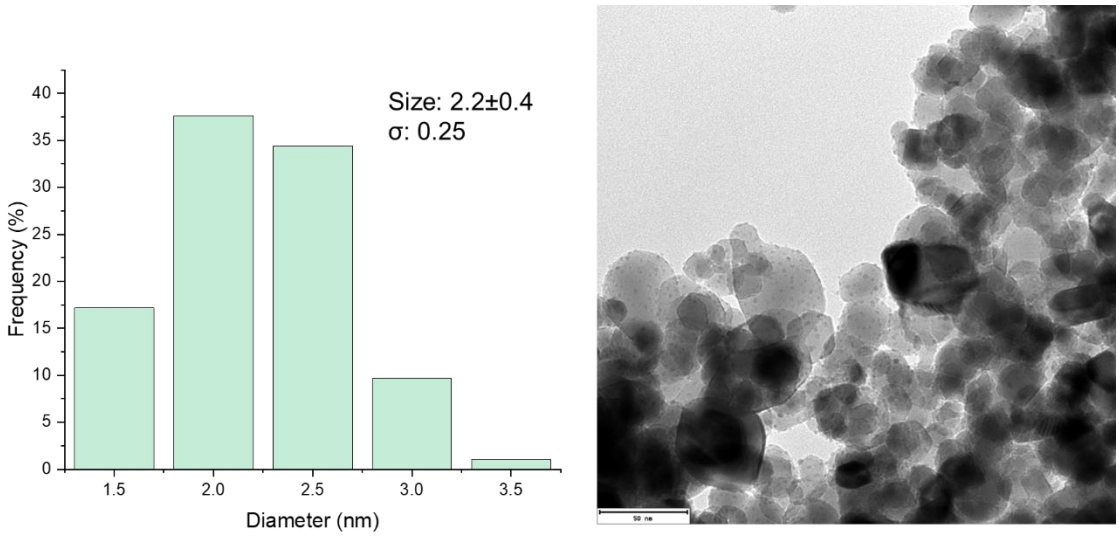

Figure 52. TEM distribution of Pt:Cu (3:1) spent (225 °C).

4.4.3 TEM Pd-series

To compare the particle size of the catalyst before and after the reaction, particle size distribution for the best sample Pd:Cu (1:1) after the reaction was calculated. By analyzing the two particle size distribution, a change in terms of nanoparticle size by 1 nm was observed, this probably is connected to the deactivation found in the APR experiments in the last hours of the reactions.

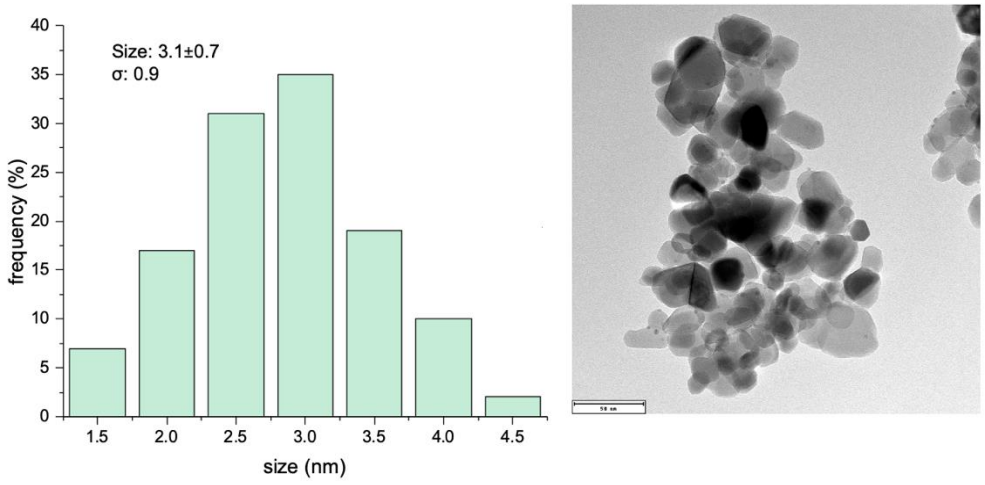

Figure 53. TEM distribution Pd:Cu (1:1) spent

4.4.4 XPS analysis.

Taking in consideration the binding energy of the metals under study, found in in literature and shown in Table 26,

Element	Spectral Line	Binding Energy
Pt	$4f_{5/2}$	74.23
Pt	$4f_{7/2}$	70.61
PtO	$4f_{5/2}$	74.2
PtO	$4f_{7/2}$	74.5
Cu	$2p_{1/2}$	952.56
Cu	$2p_{3/2}$	932.62
CuO	$2p_{1/2}$	953.7
CuO	$2p_{3/2}$	933.40

Table 26. XPS binding energy found in literature (Pt and Cu-species)

the XPS spectra for the fresh and spent bimetallic catalysts are presented below. The copper spectra, after the reaction, did not exhibit the broad peak related to the co-presence of oxide and metal species, as it happened in the fresh characterization, because of the co-presence of Pt species that enhances copper stability in terms of metal oxidation. This highlights that the acqueous phase flow and the reaction conditions didn't oxidized the metal form and so, even during the reaction, the Pt still enhances the copper stability. Instead, the broad signals of Pt-spectra ($4f_{5/2}$ = 74.2) revealed the co-presence of PtO with the metal one, being perfectly in line with the literature results. Probably, the Pt phase is more subjected to an alteration during the reactions.

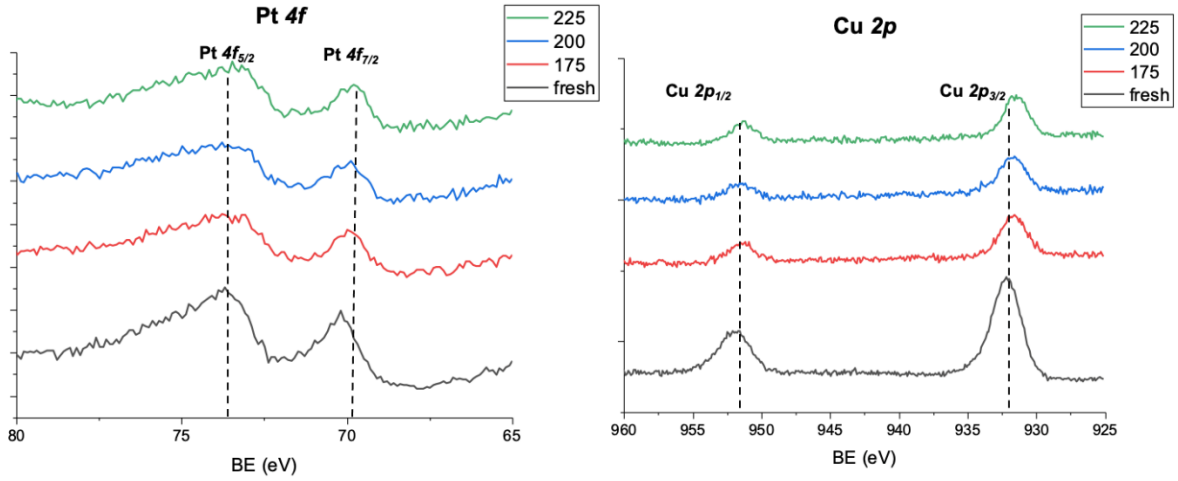

Figure 54. XPS spectra of Pt:Cu (3:1) fresh and spent at different temperatures (225, 200 and 175 °C)

Always having in mind the data of BE found in literature and summed up in the following table, the XPS analysis for Pd:Cu (1:1) fresh and spent catalysts can be discussed.

Element	Spectral Line	Binding Energy
Cu	$2p_{1/2}$	952.56
Cu	$2p_{3/2}$	932.62
CuO	$2p_{1/2}$	953.7
CuO	$2p_{3/2}$	933.40
Pd	$3d_{5/2}$	335.10
Pd	$3d_{3/2}$	339.30
PdO	$3d_{5/2}$	335.90
PdO	$3d_{3/2}$	342.40

Table 27. XPS binding energy found in literature (Pd and Cu-species)

For Pd:Cu (1:1) significant change was observed beetween fresh and spent catalysts. The binding energy found in literature of Pd $3d_{5/2}$, Pd $3d_{3/2}$ and Cu $2p_{1/2}$, Cu $2p_{3/2}$ are 335.10 eV, 339.30 eV and 952.56 eV, 932.62 eV rispectively. So, starting from these data and looking at the spent catalyst signal, it can be observed that oxidized form of Pd and Cu are present, in fact a shift of the spectral peak towards higher BE can be observed (Pd $3d_{5/2}$ = 335.90 eV; Pd $3d_{3/2}$ = 341 eV; Cu $2p_{3/2}$ = 933 eV; Cu $2p_{1/2}$ = 954 eV). This results are in line with the literature,

since the signal related to the PdO and CuO are around those values.[102] [103] In this case, the analysis could justfy a partial deactivation of the catalysts at the end of the reaction, as shown in the APR experiments section.

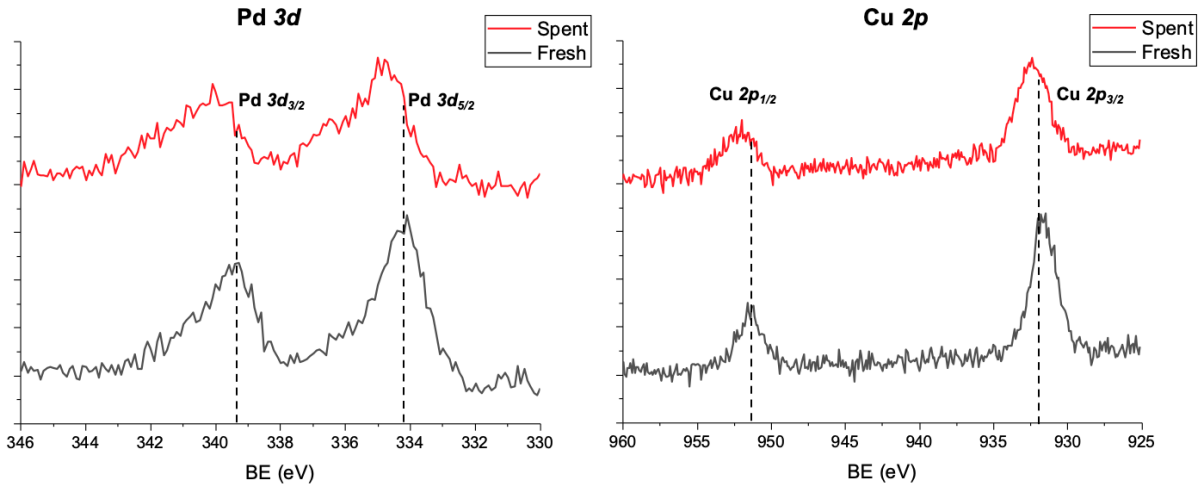

Figure 55. XPS spectra for Pd:Cu (1.1) fresh and spent

5. Conclusion

In this work it has been studied how the use of nanostructured bimetallic catalysts (Pd-Cu, Pt-Cu) can influence the production of hydrogen and of the other byproducts expected from the Aqueous Phase Reforming reaction of maltose monohydrate. The catalysts have been obtained using the sol-immobilization method for producing supported nanoparticles with mean particle size of 2-3 nm and narrow particle size distribution.

From the gas phase analysis, it was confirmed thet the APR reaction mechanisms consists of reaction producing hydrogen and reactions which consume hysrogen. . The former are the ones that from maltose produce more oxidated intermediates, which can further react through hydrogenolysis and hydrogenation reactions that consumes hydrogen to generates alkanes and alkenes such as, methane ethane propane and butene. The presence of these products, at the end of the reaction, indicates the in-situ consumption of hydrogen produced, which leads to a reduction of the overall final amount of hydrogen produced. Depending on the catalyst used to

[102] Vovk et al., 'XPS Study of Stability and Reactivity of Oxidized Pt Nanoparticles Supported on TiO $_2$'.
[103] Wu et al., 'Quantitative Analysis of Copper Oxide Nanoparticle Composition and Structure by X-Ray Photoelectron Spectroscopy'.

perform the reactions, different are the outcomes concerning both the hydrogen production and the by-products reactions. The main outcome is that the monometallic catalysts, both the Pd/TiO_2 and the Pt/TiO_2 are the most active in terms of hydrogen production but also the less selective since they both produce hydrogen around the 60% and they both present the formation of side products, particularly in the case of platinum. It means that, probably, more than 60% of hydrogen in terms of molar percentage is formed, but a part of it is consumed to form products like methan, ethane, propane and butene. On the other hand, Pt-Cu bimetallic catalysts made with a copper amount of 25 %, 50 %, and 70%, 1:3, 1:1 and 3:1 atomic ratios repectively, cause a sort of inhibition towards the main side reaction, avoiding the formation of methane, ethane, propane, butane and other by-products. The same behavior was demonstarted for the Pd-Cu bimetallic catalysts, unlike the Pd:Cu (1:1), for which a similar trend to the one of Pt:Cu (1:1) was expected. In fact, this catalyst showed that, as the other catalysts, the undesired consecutive reactions didn't take place, but it also showed the 20% of molar percentage of hydrogen, respect to the detected products, which is very low respect to the other catalysts also considering that the inhibition of the undesired reactions, should increase the hydrogen amount produced. So, in overall, it can be assesed that copper as co-metal in the bimetallic catalysts with Pt and Pd as active sites, with atomic ratio 3:1 for Pt and 1:1 and 3:1 for Pd, exhibits an inhibitory behvaiour, which can favour high production of hydrogen (96%, 85% and 75% respectively). But, exciding with the atomic amount of Cu, Pt:Cu (1:3) and Pd:Cu (1:3) the side reactions were still inhibited, confirming the role of copper, but the hydrogen production decreased, meaning that the Pd and Pt active sites are screened by the high amount of atomic copper present in the structure of the catalyst. The analysis of the liquid phase would have been fundamental to confirm this behaviour, unfortunatly it was not possible to finish it because of the time and the lack of avalability of the instrument. However, the main products with their selectivity have been reported to demonstrate that the analysis found the expected product reported in literature.

Concerning the charaterization, the TEM of the spent of the best Pt-catalyst of the series demonstarates that there isn't deactivation caused by the formation of aggregates, when compared with the fresh catalyst size distribution. The XPS analysis for the Cu-spectra shows that there isn't co-presence of oxide and metal species while, for the Pt-spectra showed a broad peak related to PtO and Pt, it means that, probably the Pt-phase is more subjected to some alteration during the reaction. However, the deactivation of the catalyst cannot be observed in the first five hors of reactions, mening that the formation of the platinum oxide didn't influence the catalytic activity, being also in line with the unaffected Pt particle size.

In the case of Pd-series, the TEM characterization after the reaction, showed an increase of particle size of about 1 nm, compared to the fresh catalyst particle size. The XPS showed for the best Pd:Cu (1:1) catalyst of the series significant changes between the fresh and spent catalyst. In fact, the catalyst after the reaction present a spectral peak towards higher binding energy. Both the TEM and XPS characterization of the spent catalyst allow to sustain what happened in the gas phase for the Pd-series, which was a slight deactivation in the last hours of the reaction. In conclusion, it can be assessed that bimetallic catalysts made of Pt:Cu and of Pd:Cu can improve the aqueous phase reaction in terms of hydrogen production and inhibition of consecutive undesired reactions, which lowered the amount of hydrogen produced in-situ. The best atomic ratios are 1:1 and 3:1 for Pd and 3:1 for Pt, since increasing the copper amount up to 75%, decreases the activity of the platinum and palladium, decreasing the amount of hydrogen produced even if the 3:1 atomic ratio is able to inhibite the undesired reactions. The characterization techniques prove to be fundamental to confirm the catalytic activity and the results of the reaction, closing the discussion of what was observed. Complete HPLC analysis would have been fundamental to better understand the entire reaction mechanism and, for this reason, it is strongly suggested in future studies.

6. Future studies

The experimental protocol followed was proposed by the Industrial Catlaysis Laboratory of the TU Delft but, in order to complete the discussion of this experimental work and compare it with the already available studies, it will be necessary to go more in deeper in terms of characterization, liquid and gas phase analysis and catalytic perfomance. In fact, necessary would be to repeat the analysis with Pt:Cu (1:1)/TiO_2 to confirm or not if the behavior is similar to the analogous platinum bimetallic catalyst and, as consequence, characterize again the material to have more information on what happen on its surface. Moreover, the analysis of monometallic Cu would be necessary to confirm or not the behaviour of bimetallic catalysts made with different amount of copper, it will allow to look for similarities and to put more attention on the copper catalyst behavior in this kind of reaction.

For what concenrns the catalysts, since the metals allow a consistant production of hydrogen, it will be interesting to use the same metals but changing the support. In this way it would be possible to study the different metal-support interaction and understand if some supports can have significant role in the reaction.

The catalytic performance of all the experimnts can be thorough by changing the amount of catlayst and so analysing the effect of the contact time, to assess if it improves or not the results. It would be interesting to see if an increase of liquid flow rate helps to reduce the high amount of dead volume present in the experimental setup. It would be also interesting to study the long-term stability of the catalysts and check the number of cycles that each catalys could perform.
Since it was not possible to calculate the selectivy and the conversion of each product in gas phase, because it was not possible to assess the final concentration of the starting reagent, it is suggested to try to assess the final concentration of maltose and speaking in terms of conversion. This, also to make more comparable results with the avaialble literature. Coupled with a perfect gas phase analysis, fundamental will be the HPLC analysis to find a correlation with the data obtained in both phases, and to compare the reults with the only article present in the literature whose authors faced with the liquid phase.[104] Also in this case it would be foundamental speaking in terms of maltose conversion to assess how much of the initial feedstock is converted into the main products expected in the liquid phase. The products that should be found are lactic acid, formaldehyde, acetic acid, ethylen glycol, 1-2 propanediol, acetaldehyde, ethanol, propanol and HMF. As analysed in the section related to the HPLC, half of these products were found after the APR experiments, highlighting how useful will be the proper liquid phase analysis in understanding the behaviour of each catalysts in this reaction, depending which products they favours or not. It is also very useful because, some of this products, if produced, can be also considered alternative compounds and not byproducts as some of them could be implemented in other fields or used as potential fuels, like in the case of HMF.
GC-MS and HPLC analysis are fundamental to build up the reaction network since, as demonstrated, these techniques are really helpful in understanding how the evolution of the intermediates happens. Additionally to the general characterization would be also useful to go more in detail using high advanced characterization, in particular for bimetallic catalyst, using techniques such as HAADF, which produces Z-contrast images, and allows to detect variations in the atomic number of atoms in the sample. Another useful technique would be XAFS to probe and chemical structure of the material at an atomic scale.
Moreover, some modification of the setup are suggested in order to eliminate or, at least, reduce the high amount of dead volume at the end of the reactor, that delays the injection at the GC and to avoid the backmixing along the lines of the reactor that doesn't allow the right time resolution, to make more representative data.

[104] Oliveira et al., 'Enhanced H2 Production in the Aqueous-Phase Reforming of Maltose by Feedstock Pre-Hydrogenation'.